

Improving Treatments for Peritoneal Metastasis Originating from Colorectal Cancer

Dissertation

zur

**Erlangung der naturwissenschaftlichen Doktorwürde
(Dr. sc. nat.)**

vorgelegt der

Mathematisch-naturwissenschaftlichen Fakultät

der

Universität Zürich

von

Linda Huynh-Russo

von/aus

Glattfelden, ZH

Promotionskommission

Prof. Dr. Maries van den Broek (Vorsitz)

Prof. Dr. Lubor Borsig

Prof. Dr. Michael Scharl

PD. Dr. Anurag Gupta (Leitung der Dissertation)

Prof. Dr. Kuno Lehmann (Leitung der Dissertation)

Zürich, 2024

Table of content

I. Abbreviations	4
II. Summary	6
III. Zusammenfassung	8
1. Introduction	10
1.1 Cancer.....	10
1.2 Epidemiology.....	12
1.3 Hallmarks of Cancer	13
1.4 Tumorigenesis of Colorectal cancer.....	15
1.5 Consensus Molecular Subtypes (CMS Classification) of colorectal cancer	17
1.6 Immunology and immune response against cancers	17
1.7 Metastasis from Colorectal cancer.....	22
1.8 Peritoneal metastasis characterization	24
1.9 Treatment options for peritoneal metastasis	25
2. Aims of the thesis	33
3. Material and Methods	34
4. Results	44
4.1 Cytotoxic drug screening on CRC cell lines.....	44
4.2 Combination of Oxaliplatin and ATRi enhances cytotoxicity in human CRC cell lines	46
4.3 The combination of Oxaliplatin and ATRi shows enhanced cytotoxicity on Patient-derived PM organoids	51
4.4 Combination of Oxaliplatin and ATRi enhanced protein levels of DNA damage marker γ H2AX and lowered protein levels of pCHK1	54
4.5 Combination of Oxaliplatin and ATRi leads to immunogenic changes on CRC cell lines	55
4.6 The combination treatment prevents Oxaliplatin-mediated upregulation of MHC class I and PD-L1 in patient-derived PM organoids and in murine CRC cell lines	61
4.7 Oxaliplatin in combination with ATRi facilitates enhanced recognition of tumor cells by antigen-specific CD8+T cells <i>in vitro</i>	64
4.8 Development of PM mouse model	65
4.9 Enhanced control of PM lesions in PM mouse model upon combination treatment	66
4.10 Characterization of mouse PM tumor microenvironment (TME)	67
4.11 PM lesion in PM mouse model are controlled in a CD8+ T-cell-dependent manner after combination treatment.....	72
4.12 Combination treatment promotes antigen-specific CD8+ T-cell effector function ..	73
4.13 The therapeutic effect of ATRi is mediated by reduced PD-L1 expression	79

4.14 Blockade of PD-1 provides greater control of PM lesions	81
5. Discussion.....	84
6. Figures and Tables	93
7. References.....	95
8. Acknowledgements	99
9. Curriculum vitae.....	100

I. Abbreviations

APC	Antigen presenting cell
ATM	Ataxia telangiectasia mutated
ATR	Ataxia telangiectasia and Rad3 related
CAF	Cancer associated fibroblasts
CAR-T	Chimeric antigen receptor T cells
CD	Cluster of differentiation
CEA	Carcinoembryonic antigen
CHK1	Checkpoint kinase 1
CIMP	CpG island methylation phenotype
CIN	Chromosome instability
CMS	Consensus Molecular Subtype
CRC	Colorectal cancer
CRS	Cytoreductive surgery
CTLA4	Cytotoxic T-lymphocyte-associated protein 4
CXCL	Chemokine (C-X-C motif) ligand
DAMP	Damage-associated molecular pattern
DSF	Disease free survival
DC	Dendritic cell
eATP	Extracellular adenosine triphosphate
EGF	Epidermal growth factor
EGFR	Epidermal growth factor receptor
EMT	Epithelial–mesenchymal transition
EpCAM	Epithelial cell adhesion molecule
ER	Endoplasmic reticulum
ERK	Extracellular signal-regulated kinase
FOLFIRI	Folinic acid, Fluorouracil, Irinotecan
FOLFOX	Folinic acid, Fluorouracil, Oxaliplatin
FOLFOXIR	Folinic acid, Fluorouracil, Oxaliplatin, Irinotecan
GCSF	Granulocyte colony-stimulating factor
GM-CSF	Granulocyte macrophage colony-stimulating factor
HGF	Hepatocyte growth factor
HIPEC	Heated intraperitoneal chemotherapy
HMGB1	High mobility group box 1
HSC	Hematopoietic stem cells
HSP	Heat shock protein
H2AX	Histone H2A variant
ICD	Immunogenic cell death
IFN- γ	Interferon-gamma
IGF-1	insulin-like growth factor 1
IL	Interleukin
i.p.	Intraperitoneal
IVIS	in vivo imaging system
KO	Knock out
LAG3	Lymphocyte-activation gene 3
LCMV	lymphocytic choriomeningitis virus
MACS	Magnetic-activated cell sorting
MCSF	Macrophage colony-stimulating factor
MDSC	Myeloid-derived suppressor cell
MEK	Mitogen-activated protein kinase kinase
MHC	Major histocompatibility complex
MMP	matrix metalloproteinase
MSI	Microsatellite instable
MSN	Moesin
MSS	Microsatellite stable
NER	nucleotide excision repair
NET	Neutrophil extracellular traps

NK	Natural Killer cells
OS	Overall survival
OT-I	Transgenic mice with an anti-OVA specific T-cell receptor
OVA	Ovalbumin
PARP	Poly (ADP-ribose) polymerase
PCI	Peritoneal cancer index
PDGF	Platelet-Derived Growth Factor
PD-1	Programmed cell death 1
PD-L1	Programmed death ligand 1
PFS	Progression free survival
PIPAC	Pressurized intraperitoneal aerosol chemotherapy
PM	Peritoneal metastasis
RAF (BRAF)	rapidly accelerated fibrosarcoma
RAS (NRAS, KRAS)	Rat sarcoma virus
ROS	reactive oxygen species
TAM	tumor-associated macrophage
TCR	T-cell receptor
TGF- β	Transforming growth factor-beta
TIM-3	T cell immunoglobulin and mucin domain 3
TIGIT	T cell immunoglobulin and ITIM domain
TME	Tumor microenvironment
TNF α	Tumor Necrosis Factor alpha
Treg	T-regulatory cell
TSG	Tumor suppressor gene
TSIP	Tumor spheres with inverted polarity
VEGF	Vascular endothelial growth factor
WHO	World Health Organization
WT	Wildtype
5-FU	5-fluororacil

II. Summary

Peritoneal metastasis (PM) is an advanced-stage disease, spreading through direct dissemination of cancer cells from different primary tumors that include colon, gastric, ovarian and appendix cancers. PM arising from colorectal cancer (CRC) through a non-haematogenous route demonstrate significant differences in terms of clinical behavior, prognosis and overall survival (OS) when compared to hematogenous dissemination into the liver or lungs. First line treatment for patients harboring PM is systemic chemotherapy that includes combinations of 5-FU, Folinic acid, Oxaliplatin, and Irinotecan. Depending on the molecular signature of the tumor, patients receive further targeted drugs against VEGF or EGFR. A subset of PM patients may qualify for additional local therapy that includes cytoreductive surgery (CRS) to remove macroscopic cancer lesions that is followed by a heated intraperitoneal chemotherapy (HIPEC) lavage to eradicate residual cancer cells. In case of unresectable cancer lesions, patients might receive local treatment through an alternative approach in form of pressurized intraperitoneal chemotherapy (PIPAC). These local treatments seem to be beneficial approaches prolonging survival of PM patients compared to systemic therapy. Our previously generated data suggests that the benefit of local treatment (HIPEC) is primarily mediated by CD8+ T-cell activation within the tumor microenvironment. Nevertheless, more than 70% of patients relapse within 2-5 years affecting long-term survival. Especially, patients harboring PM lesions recurred faster and showed a shorter overall survival (OS) after recurrence compared to patients with other metastatic sites such as the liver. The reason for this high relapse rate might be due to inefficient treatments or due to PM tumor biology.

Therefore, in this study, we have explored the therapeutic potential of existing drugs and drug combinations to induce tumor-specific immunity against PM lesions. Overall, we sought to find a PM-specific treatment modality that can be offered to the majority of PM patients. To do so, we first investigated the cytotoxic potential of different drugs and drug combinations as well as we examined drug-induced immunogenic changes on CRC cell lines and patient-derived PM organoids. Our data revealed that the combination of Oxaliplatin with ATR (Ataxia telangiectasia and Rad3 related, protein involved in DNA damage repair) inhibitor resulted in enhanced cytotoxicity on different CRC cell lines and patient derived PM organoids. Furthermore, we observed that the combination treatment leads to the expression and secretion of both pro- and anti-immunogenic molecules. Interestingly, pro-immunogenic signals, such as secretion of immunogenic cell death (ICD) marker HMGB1 and

extracellular ATP as well as blocking of Oxaliplatin induced PD-L1 upregulation, resulted in enhanced recognition of tumor cells by antigen-specific CD8+ T-cells after the combination treatment *in vitro*. Using our PM mouse model, we demonstrated the greatest tumor control when mice were treated with Oxaliplatin + ATRi. Furthermore, we revealed that the combination treatment induced increased CD8+ T-cell effector functions (IFN- γ and Granzyme B secretion) and CD8+/T-regulatory cell ratio to control PM lesions. Furthermore, as observed *in vitro*, ATRi blocked Oxaliplatin induced PD-L1 upregulation promoting CD8+ T-cells functions *in vivo*. Finally, adding immune checkpoint PD-1 blocking antibody to our treatments provided enhanced control of PM.

Overall, this study suggested that relying solely on cytotoxic effects of chemotherapeutic agents is ineffective against PM. By using Oxaliplatin in combination with ATRi we were not only able to enhance tumor cell killing but induced immunogenic changes that promoted protective immunity. Therefore, we propose a new PM-specific treatment i.e. the combination of Oxaliplatin+ ATRi \pm anti-PD-1 immunotherapy. We hope that this proposed combination can be evaluated in PM-associated clinical trials.

III. Zusammenfassung

Peritoneale Metastasen (PM) ist eine fortgeschrittene Krankheit, die durch verschiedene Primärtumore wie Kolon-, Magen-, Eierstock- und Bilddarmkarzinome entstehen. Die Behandlung von Patienten mit metastasierendem Kolonkarzinom besteht in der Regel aus systemischer Chemotherapie, die Medikamente wie 5-FU, Folsäure, Oxaliplatin und Irinotecan umfasst. Je nach molekularer Signatur kann auch ein monoklonaler Antikörper gegen VEGF oder EGFR eingesetzt werden. Ein kleiner Teil der PM-Patienten qualifiziert sich möglicherweise für eine zusätzliche lokale Chemotherapie, bei der sichtbare Tumorknoten operativ entfernt werden (CRS) und die Bauchhöhle mit einer erhitzten Chemotherapie-Lösung ausgespült wird (HIPEC), um verbliebene Krebszellen zu zerstören. In einigen Fällen, in denen eine Resektion nicht möglich ist, kann ein alternativer Ansatz der lokalen Chemotherapie in Form eines Aerosols (PIPAC) angewendet werden.

Studien haben gezeigt, dass Patienten, die mit CRS/HIPEC behandelt wurden, im Vergleich zu Patienten, die nur systemische Chemotherapie erhielten, eine bessere Überlebensrate aufweisen. Darüber hinaus haben unsere eigenen Studien gezeigt, dass Patienten mit einer höheren Anzahl von CD8+ T-Zellen im PM-Tumor signifikant längere Überlebenszeiten haben. Dennoch erleiden mehr als 70% der Patienten, die CRS/HIPEC erhalten haben, innerhalb von 2-5 Jahren einen Rückfall, was die Langzeitüberlebensrate beeinträchtigt. Insbesondere Patienten mit Metastasen ausschliesslich in der Bauchhöhle haben eine kürzere Zeit bis zum Rückfall und eine geringere Überlebensrate im Vergleich zu Patienten mit Lebermetastasen. Dies könnte auf eine ineffiziente Behandlung oder die Biologie der PM zurückzuführen sein.

Unser Ziel ist es, eine Behandlungsmöglichkeit zu finden, die für möglichst viele PM-Patienten wirksam ist. Zu diesem Zweck haben wir die Zytotoxizität verschiedener Medikamente an Zelllinien und PM-Organoiden von Patienten getestet. Dabei haben wir festgestellt, dass die Kombination von Oxaliplatin und ATR-Inhibition zu einer verstärkten Zytotoxizität führt. Darüber hinaus haben wir beobachtet, dass diese Kombination die Expression und Sekretion von immunstimulierenden und immuninhibierenden Molekülen beeinflusst. Zu den immunstimulierenden Molekülen gehören die Sekretion von HMGB1, extrazelluläres ATP und die Blockierung der durch Oxaliplatin induzierten PD-L1-Expression. Diese Signale führten zu einer erhöhten antigen-spezifischen Erkennung von CD8+ T-Zellen.

In unserem Maus-PM-Modell konnten wir zudem nachweisen, dass die Kombinationstherapie das Tumorstadium am stärksten einschränkte. Darüber hinaus führte die kombinierte Behandlung zu einer erhöhten Aktivität von CD8+ T-Zellen (durch IFN- γ und Granzyme B Sekretion) und einem erhöhten Verhältnis von CD8+ zu regulatorischen T-Zellen. Weiterhin konnten wir in unserem Maus-Modell feststellen, dass die Hemmung von ATR, wie bereits bei den Zelllinien beobachtet, zur Herunterregulierung von PD-L1 führte. Schliesslich haben wir unsere Behandlung zusätzlich mit dem Immun-Checkpoint-Inhibitor PD-1 kombiniert, was zu einer verstärkten Kontrolle des Tumors führte. Die Ergebnisse dieser Arbeit zeigen, dass der zytotoxische Effekt von Chemotherapien allein nicht ausreichend ist, um das Krebswachstum effizient zu kontrollieren. Die Kombination von Oxaliplatin und ATR-Inhibitor führte nicht nur zu verstärkter Zytotoxizität, sondern förderte auch die tumorspezifische Immunität. Diese Daten legen nahe, dass die Kombination von Oxaliplatin, ATR-Inhibitor und anti-PD-1-Immuntherapie zusammen mit zukünftigen Untersuchungen als spezifische Behandlung für PM in klinischen Studien evaluiert werden kann.

1. Introduction

1.1 Cancer

Cancer is a disease that can arise in any tissue and organ of our body. Most of the cancer originate from epithelial tissues, giving rise to what are commonly known as carcinomas. This particular form of cancers accounts for almost 80% of cancer-related deaths. Carcinomas are classified into two distinct subgroups: squamous cell carcinomas refer to tumors originating from an epithelial sheet, which functions to seal cavities and channels or line surfaces to safeguard underlying tissue.

Adenocarcinomas are tumors that originate from specialized epithelial cells that produce substances to defend themselves and release them into ducts and cavities (5).

In addition to carcinomas, there are many categories of non-epithelial malignancies, including sarcomas. These cancers originate from mesenchymal cells including fibroblasts, adipocytes, osteoblasts, myocytes, chondrocytes and endothelial cells. Sarcomas are less common than carcinomas, occurring in only 1% of individuals. Hematopoietic cancers, which belong to a distinct category of non-epithelial malignancies, originate from the hematopoietic lineage. This category is classified into two subtypes, namely leukemia and lymphoma. In leukemia, cancer cells move freely through the circulation, while when cancer cells aggregate into a solid mass in lymph nodes, they are termed as lymphomas. The cells implicated in hematopoietic malignancies are erythrocytes, plasma cells as well as T- and B-lymphocytes. This cohort is accountable for around 7% of cancer-related deaths. The last group of non-epithelial cancers are neuroectodermal tumors. These tumors originate from several types of cells found in both the central and peripheral nervous system, such as astrocytes, oligodendrocytes, Schwann cells, arachnoidal cells and granular cells. These groups contribute to around 2.5% of cancer-related deaths(5).

Carcinomas

<u>Adenocarcinoma</u>	<u>Squamous cell carcinoma</u>	<u>Other types of carcinoma</u>
Lung	Skin	Small-cell lung carcinoma
Colon	Nasal cavity	Large-cell lung carcinoma
Breast	Oropharynx	Hepatocellular carcinoma
Pancreas	Larynx	Renal cell carcinoma
Stomach	Lung	Transitional-cell carcinoma (from urinary bladder)
Esophagus	Esophagus	
Prostate	Cervix	
Endometrium		
Ovary		

Sarcomas

Osteosarcoma
Liposarcoma
Leiomyosarcoma
Rhabdomyosarcoma
Malignant fibrous histiocytoma
Fibrosarcoma
Angiosarcoma
Chondrosarcoma

Neuroectodermal malignancies

Glioblastoma multiforme
Astrocytoma
Meningioma
Schwannoma
Retinoblastoma
Neuroblastoma
Ependymoma
Oligodendroglioma
Medulloblastoma

Hematopoietic malignancies

Acute lymphocytic leukemia (ALL)
Acute myelogenous leukemia (AML)
Chronic lymphocytic leukemia (CLL)
Chronic myelogenous leukemia (CML)
Multiple myeloma (MM)
Non-Hodkin's lymphoma (NHL)
Hodgkin's lymphoma (HL)

Cancers not fitting in major classification (due to switching tissue lineage)

Melanomas
Teratomas

Table 1: Examples of Cancer Subtypes (adapted from The Biology of Cancer, 2. Edition, Chapter 2: The Nature of Cancer, Robert A. Weinberg) (5)

1.2 Epidemiology

Based on data from the World Health Organization (WHO), around 19.3 million new cases of cancer were detected in the year 2020, with an expected death toll of over 10 million. These astonishing statistics establish cancer as the second most prevalent cause of mortality globally (2). Overall, due to aging and growth of the population as well as changes in dominant risk factors, the WHO estimates until 2060 more than 18 million cancer-related deaths worldwide (11). Currently, the incidence of developing cancer before the age of 75 years is 20.2%, whereas men have a 19% higher incidence rate than women (2, 11). However, these rates can vary depending on the exposure to risk factors, world region and high-quality cancer

prevention and early detection. Overall, the top ten cancer types for both sexes account for more than 60% of newly diagnosed cancer cases and more than 70% of cancer-related deaths (2) Lung cancer has the highest prevalence among all cancer kinds, accounting for 14.3% of cases in men. Prostate cancer and colorectal cancer follow closely behind, with incidences of 14.1% and 10.6%, respectively. Lung cancer is responsible for 21.5% of cancer-related deaths in men, followed by liver cancer at 10.5% and colorectal cancer at 9.3%. The incidence of breast cancer is highest among women, with a rate of 24.5%, followed by colorectal cancer at 9.4% and lung cancer at 8.4%.

Additionally, breast cancer (15.5%) is the

primary cause of mortality in women, along with lung cancer (13.7%) and colorectal cancer (9.7%) (2).

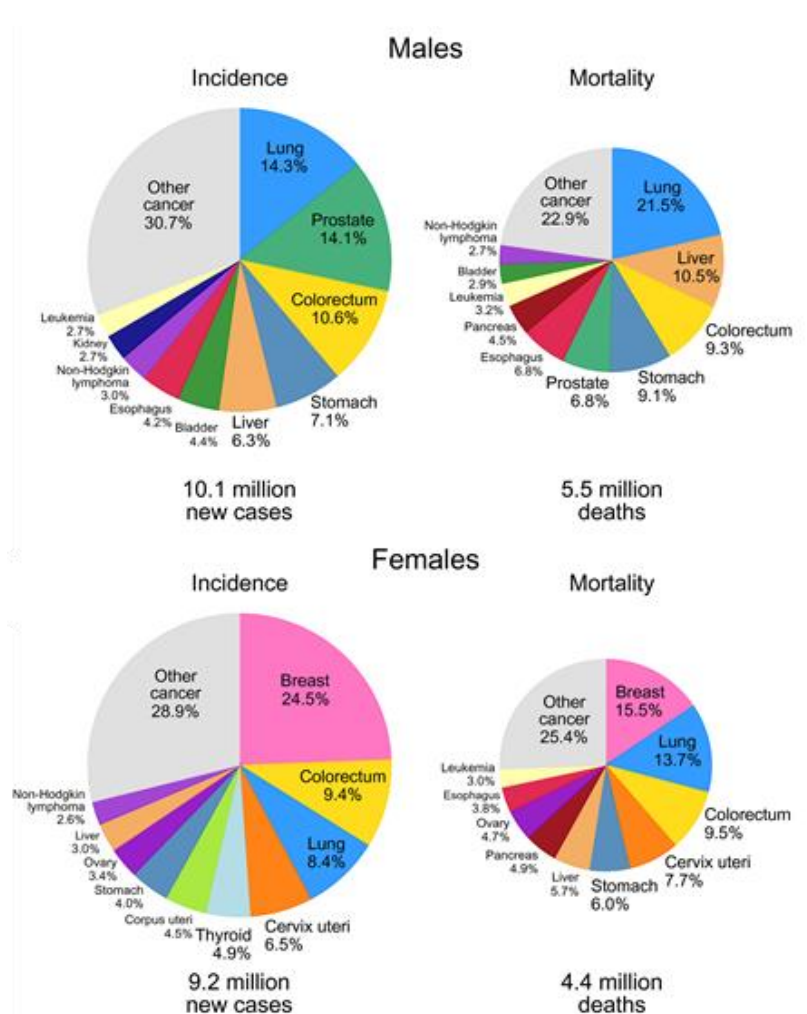


Figure 1: Pie chart of incidence and death for top ten most common cancers in males and females. Each area represents the proportion of the total number. Adapted illustration, source: (2)

1.3 Hallmarks of Cancer

The ability of cancer cells to show uncontrolled cell proliferation and spread across the body is a simplified aspect of explaining this deadly disease. Recent research has shown that cancer growth is a highly complex process involving multiple pathways and other cell types. In 2000, D. Hanahan and R.A. Weinberg defined six functional malfunctions or hallmarks in cancer cells that differ from normal cells. These hallmarks included the ability of sustaining proliferative signaling, evading growth suppressors, resisting cell death, enabling replicative immortality, inducing vasculature and activating invasion and metastasis. These hallmarks are acquired during the multistep tumor development process showing disease's complexity. In recent decades, major progress has been made in cancer research resulting in a better understanding of the disease development processes. Therefore, D. Hanahan and R.A. Weinberg recently updated the list of cancer hallmarks. In the extended list, they have included two enabling characteristics, namely the genomic instability and the tumor-promoting inflammation. Furthermore, they also described two additional emerging hallmarks, the deregulation of cellular energetics and the evasion of immune destruction, which are crucial during tumor development (12). Later, four additional hallmarks were described that are broadly relevant across all human cancers. These include the prospective features of unlocking phenotypic plasticity, non-mutational epigenetic reprogramming, polymorphic microbiomes and senescent cells (8). Overall, the hallmarks listed in the diagram below are just tip of an iceberg as every hallmark is further complicated by many sub-pathways that either work in unison or in a multistep process often making targeted and/or non-targeted treatments ineffective.

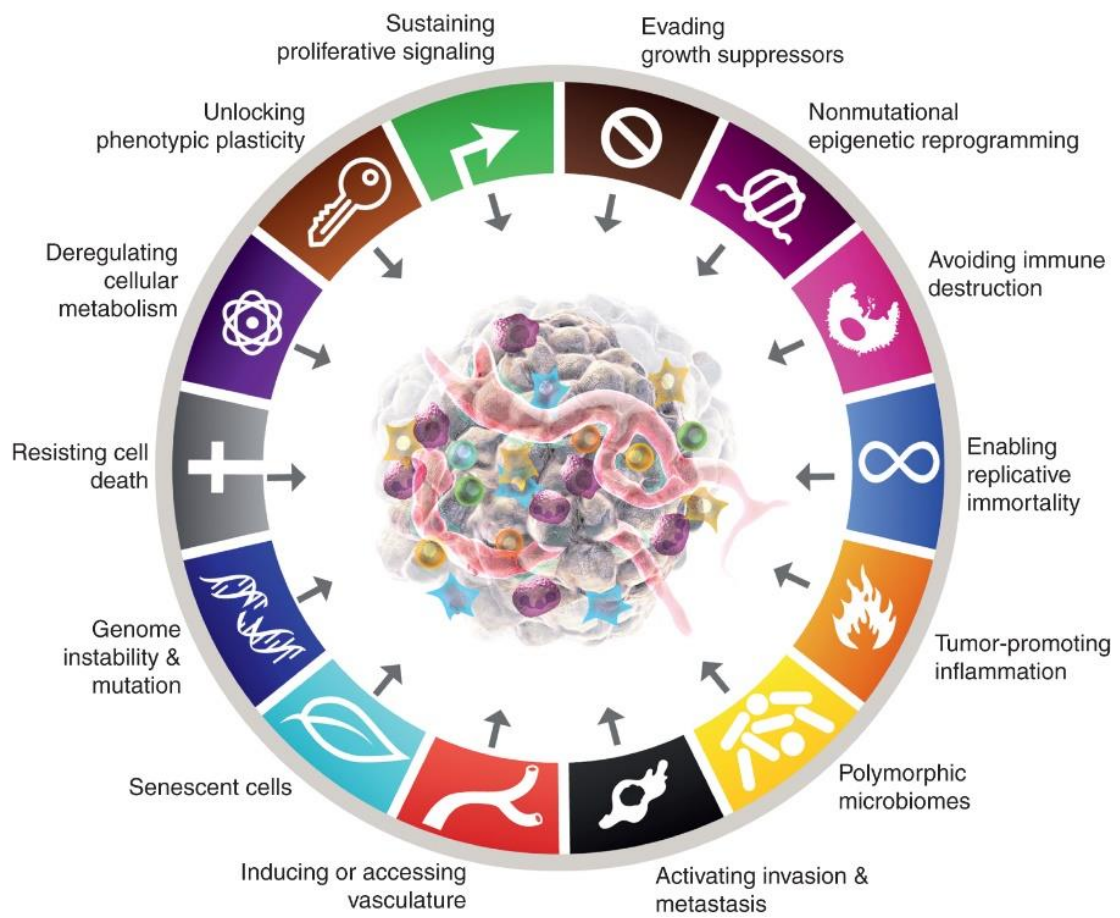


Figure 2: Most recent version of Hallmarks of Cancer. Graphic has been adapted from Hanahan and Weinberg, illustrating 14 Hallmarks that demonstrate properties of cells to become neoplastic. Image Source : (8)

1.4 Tumorigenesis of Colorectal cancer

Tumorigenesis is the pathological process that describes steps involved in transforming a normal cell into neoplastic cells through polyclonal or monoclonal cell proliferation. Cancer development is a multi-step process including, the acquisition of various alterations at different molecular and cellular levels (13). Moreover, environmental as well as hereditary factors influence the dynamics of cancer development. In addition, lifestyle-related factors such as smoking, excessive drinking, obesity, unhealthy diet and physical inactivity could expedite cancer formation (14, 15).

Cancer initiation in any organ is somewhat similar, starting with the accumulation of specific mutations; however the sequence in which they are acquired may vary from organ to organ. This thesis describes tumorigenesis of colorectal cancer that can also be extended to other epithelial cancers.

Colorectal cancer is the second most common cause of cancer-related death worldwide (2).

According to a statistical study performed in 2017, the 5-year and 10-year survival rate of CRC is 65% and 58%, respectively. Furthermore, the overall incidence of CRC is increasing in people younger than 50 years, whereas the incidence in individuals older than 50 years seems to decrease (16).

Already in 1990, Fearon and Vogelstein described the tumorigenesis process of colorectal cancer (CRC). The so-called adenoma-carcinoma pathway majorly contributed to the understanding of the multi-step tumor development and suggests that at least five mutations are required to induce transformation (17). The adenoma-carcinoma transformation is characterized by increased chromosome instability (CIN), chromosomal numerical alteration (aneuploidy) and structural alterations (deletions, insertions, amplifications, loss of heterozygosity). For CRC this includes mutations in APC, TP53, KRAS and SMAD4 leading to accelerated cell proliferation and resistance to apoptosis (5, 8, 14). CRC arising from the adenoma-carcinoma transformation occurs in 70-90% of patients and represents the major sporadic (=“non-hereditary”) subset of CRC. However, a small subset of sporadic CRC patients (10-20% of patients) develop CRC through the serrated neoplasia pathway. Compared to the traditional adenoma-carcinoma pathway, the serrated neoplasia pathway harbors next to the RAS mutation additional RAF mutations and epigenetic instability leading to a CpG island methylation phenotype (CIMP) that affects tumor suppressor gene silencing (12, 14, 18). Furthermore, if the latter occurs in promotor regions of mismatch repair genes (MLH1, MSH2, MSH6

and PMS2) the resulting consequence is an expansion of microsatellite regions, thus forming Microsatellite instable (MSI) tumors (14, 19).

In addition to sporadic subtypes of CRC, 10-20% of all patients genetically inherit CRC. Hereditary CRC can be divided into two different forms: a polyposis and a non-polyposis condition. Based on histology, the polyposis syndrome is further categorized in adenomatous, hamartomatous, serrated and mixed conditions, depending on the mutated genes. Furthermore, due to the increased number of polyps, this condition is easily diagnosed. A greater challenge is identifying the non-polyposis condition, the Lynch syndrome. The Lynch syndrome is characterized by small numbers of adenomatous polyps that have a high risk to develop CRC but also endometrial, ovarian and stomach cancer. The high risk is based on a dysfunction of the mismatch repair pathway leading to an accelerated adenoma to carcinoma transformation. Depending on which gene is affected by a mutation (MLH1, MSH2, MSH6, PMS2, EPCAM), individuals with a pathogenic variant need to undergo colonoscopy every 1 to 2 years beginning at the age of 20-25 years (14, 20).

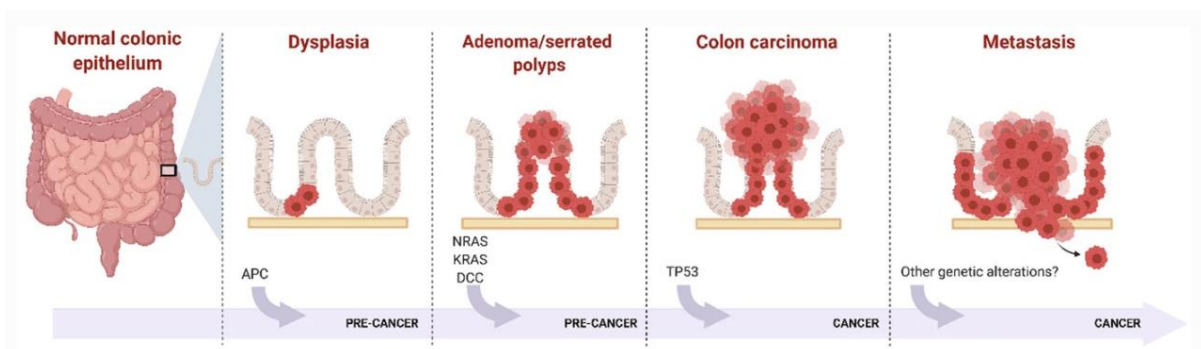


Figure 3: The adenoma-carcinoma sequence of sporadic or serrated CRC. Tumorigenesis in CRC include known driver mutations, such as alterations in APC, NRAS, KRAS, DCC, TP53 and other genetic alterations that can differ from tumor to tumor. This multistep process leads to development of neoplastic cells that expand until they invade surrounding tissue and form metastases. Adapted illustration, source: (6)

1.5 Consensus Molecular Subtypes (CMS Classification) of colorectal cancer

In 2015, a collaboration between different research groups across the world developed a new classification system for CRC based on transcription profile analysis, molecular and biological features and clinical outcomes. Based on their analysis they detected four robust consensus molecular subtypes (CMS) for CRC (21).

CMS1 tumors are associated with highly defective DNA mismatch repair genes (MSI tumors), hypermutation and hypermethylation, increased BRAF mutations, high immune infiltration and strong activation of the immune evasion pathway. About 14% of all CRC belong to the CMS1.

CMS2 represents the greatest part with 37%. CMS2 tumors are associated with canonical, epithelial cancers that harbor increased chromosomal instability due to high copy number gains in oncogenes or copy number losses in tumor suppressor genes (TSG). Furthermore, they show high WNT and MYC activation and mutations in KRAS and TP53.

CMS3 represents epithelial metabolic dysregulated tumors, which make up 13%. MSI tumors overlap with this subtype, whereas in this group tumors show an increased frequency of CpG methylation phenotype (CIMP) but intermediate levels of hypermethylation. Genetic mutations in KRAS and SMAD4 are the most common.

CMS4 is associated with aggressive mesenchymal tumors that show increased stromal invasion, high TGF- β levels, activation of angiogenesis and matrix remodeling pathways and are often resistant to commonly used chemotherapies. These tumors, are therefore, prone to metastasize and thus have the worst overall survival and relapse free survival. 23% of all CRC tumors belong to CMS4 (21, 22). Around 13% of all CRC cannot be categorized within the CMS classification.

1.6 Immunology and immune response against cancers

The immune system protects our body from disease-causing agents like pathogens, viruses, bacteria and fungi but also from toxins and removes unhealthy and damaged cells. Diverse immune cells are produced from pluripotent hematopoietic stem cells (HSCs) within the bone marrow. HSCs can give rise to a variety of immune cells that include red blood cells (erythrocytes), platelets and the two white blood cell subgroups (leukocytes) termed lymphoid and myeloid cells. The immune cells can be classified as part of the innate or adaptive immune system. Cells associated with the innate immune system are the first line of defense of the body as they respond within seconds to hours against

foreign germs or substances entering the body. Immune cells from the innate immunity include amongst others Macrophages, Granulocytes, Dendritic cells and Natural Killer (NK) cells. An alternative type of the innate immune system is the complement system. This arm consists of plasma proteins that recognize antibody-covered cells or germs. Furthermore, the innate immune responses are thought to be unspecific or antigen-independent; thus, providing limited control of an infection and causing inflammation. If the innate immune system cannot stop a pathogen, the adaptive immune system comes into play. Cells from the adaptive immunity include T-lymphocytes and B-lymphocytes that are capable of antigen-specific immunity. The innate and adaptive immune systems work closely together as cells from the innate immune system are involved in the activation of a specific immune response. In contrast, soluble factors such as cytokines and antibodies released from cells of the adaptive immune system are known to regulate the immune activities of innate immune cells (5, 23). A key component of the adaptive immune response are T-lymphocytes. After their production in the bone marrow, T-lymphocytes migrate to the thymus for maturation. Thereby, they start to express unique and specific antigen receptors (termed T-cell receptor (TCR)) and undergo positive or negative selection to ensure that they mainly recognize and react against foreign molecules, not self-peptides. The TCR consists of highly polymorphic α - and β -glycoprotein chains responsible for the variety of T-cell clones recognizing a plethora of antigens (peptides that may provoke an immune response) that are bound to major histocompatibility complexes (MHC). Two types of MHC molecules exist: MHC class I is expressed on almost every nucleated vertebrate cell and presents degraded cytosolic self-proteins. MHC class II is expressed on antigen presenting cells (APC), such as dendritic cells or macrophages, in order to present molecular fragments that were taken up by these cells(5, 23). Upon correct antigen binding, T-cells are activated, proliferate and differentiate into T-cells with different effector functions. T-cells are divided into two major categories: the T-helper cells and cytotoxic T-cells. T-helper cells are characterized by CD4+ surface expression and activation through MHC class II molecules presented by APCs. Upon activation, T-helper cells release a variety of cytokines like IFN- γ , IL-2 and TNF- α that activate B-cells, cytotoxic T-cells and macrophages. Cytotoxic T-cells express CD8+ on their surface and are activated via MHC class I molecules expressed on antigen presenting cells such as DCs that are able to cross-present antigens to CD8+ T cells via MHC class I molecules. Thereby, cytotoxic T-cells can induce an antigen-specific killing of infected or cancer cells by either secretion of IFN- γ and TNF- α , direct release of perforin and

granzymes or by binding to Fas receptor to induce apoptosis. In order to achieve optimal T-cells activation, three distinct signals are necessary: first MHC-TCR interaction; second, additional co-stimulation signal between B7 family (like CD80 or CD86) and CD28 receptor family members and third cytokine stimulation including IL-12 and Type I IFN cytokines. In order to maintain immune homeostasis, the adaptive immune response is controlled by a subset of differentiated CD4+ T cells known as T-regulatory cells. T-regulatory cells are characterized by additional CD25+ surface expression and FoxP3+ nuclear expression and are responsible for suppressing the immune response by inhibiting T-cell proliferation and cytokine production. Dysfunction of T-regulatory cells may result in uncontrolled immune reactions and autoimmune disease (5, 23).

Already in 1909, Paul Ehrlich suggested the role of the immune system in controlling cancer development without exactly knowing the molecular and cellular aspects of immunity. In recent decades, enormous progress has been made in the field of immunology and immuno-oncology. Thereby a concept of cancer immunoediting has been proposed to explain the interaction of the immune system with cancer development. The concept presents three phases known as the “three E’s”: Elimination, Equilibrium and Escape. In the best-case scenario, during the elimination phase, the innate and adaptive immune systems work in harmony to induce an anti-cancer response resulting in the eradication of the transformed cells already at their initial stage. At this stage, cells of the innate immune system like NK cells, NK T-cells or macrophages recognize transformed cells due to phenotypic changes like expression of stress ligands and released damage-associated molecular pattern (DAMP) molecules. Nevertheless, certain tumorigenic cells may survive the elimination phase through acquired additional mutations that allow them to reduce immunogenicity and become more resistant to immune killing. In this case, the second phase, the equilibrium, is reached where cancer cells remain undetected for days to years in a dormant-like state until they escape immune control. Once cancer cells enter the escape phase, they form clinically apparent cancer. The immune escape is usually achieved via various evasion strategies allowing cancer cells to grow in an immunologically competent environment. In this stage, cancers show immunosuppressing microenvironment via recruiting suppressive cells like myeloid-derived suppressor cells (MDSC), T-regulatory cells and type 2 macrophages that release cytokines and molecules like TGF- β , IL-10, 2,3-dioxygenase (IDO), arginase-1 and cyclooxygenase-2 (COX-2). Furthermore, cancer cells alter their antigenicity by reducing MHC components and stress ligands, get resistant to the death-receptor signaling pathway

(Fas receptor), increase production of anti-apoptotic proteins like BCL-2 or express inhibitory molecules like PD-L1 or Galectin-9. Successful escape can lead to uncontrolled tumor growth (9, 24).

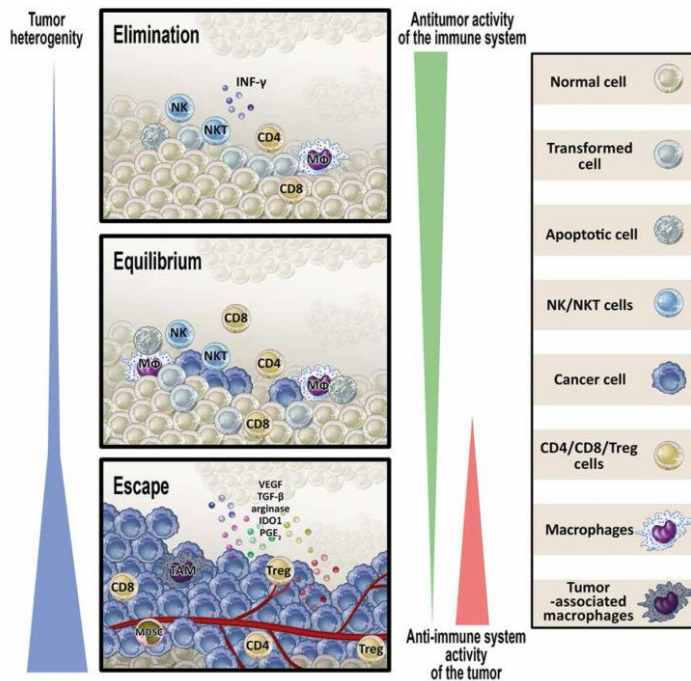


Figure 4: Illustration of cancer immunoeediting hypothesis of the “three E’s”: Elimination, equilibrium, and escape. This hypothesis describes the relation between cancer development and the immune system. During the first phase, the elimination, transformed cells are attacked by the immune system. However, Certain cells survive and enter the second phase, the equilibrium where they stay dormant-like and remain undetected. In the last stage, the escape, cancer becomes clinically apparent and develops evasion strategies to avoid immune detection. Image Source : (9)

Despite the different evasion strategies of cancer cells, clinical observations showed that treatment with various anti-tumor agents can temporarily re-stimulate the immune system. Typically, cells undergo cell death without eliciting an immune response (tolerogenic). However, especially in cancer settings, certain therapy strategies can induce an immunogenic cell death (ICD) that subsequently stimulates a tumor-specific immune reaction and thus favor clinical outcomes. In the context of CRC, this was shown using the platinum-based chemotherapy Oxaliplatin. However, not every anti-cancer treatment induces ICD. Clinically available ICD inducers include certain chemotherapeutics (Oxaliplatin, Anthracyclines, Cyclophosphamide), irradiation, targeted anticancer agents (bortezomib, crizotinib), photochemotherapy, photodynamic therapy and oncolytic virotherapy (25). The ability of these agents to induce ICD and a subsequent adaptive immune reaction involves three main concepts: antigenicity, adjuvanticity and permissive microenvironment. Antigens presented on the surface of healthy cells do not induce an immune reaction. Whereas malignant cells harbor altered peptides due to mutations and post-translational modification like tumor neoantigens or oncofetal antigens display sufficient antigenicity to alarm the immune system. Furthermore, it was shown that treatment agents upregulate the expression of MHC class I and II molecules on the cancer surface

leading to enhanced antigenicity. Moreover, upon treatment stress pathways are activated that result in the release of different DAMPs. This includes the expression of ecto-Calreticulin, Annexin A1, ER chaperones like HSP70 and the release of ATP, CXCL10 and HMGB1. Intracellular DAMPS include cytosolic DNA that stimulates the cGAS-STING pathway that lead to the release of type I interferon cytokines. The expression and the release of these molecules attract the infiltration of immune cells, like dendritic cells to trigger their maturation and to promote subsequent priming of T-cells in order to efficiently kill the cancer cells in a similar approach as during the elimination phase mentioned above (25, 26).

T-cell activation results in clonal expansion and acquisition of effector functions to induce cancer-specific killing. After cancer control, more than 90% of T-cells die via apoptosis. The remaining T-cells further differentiate into T memory cells to build protective immunity. This protective immunity remains even after the antigen withdraws and allows the immune system to react faster upon re-stimulation via a known antigen than naïve T-cells. However, observation in HIV-infected patients and experiments performed in an *in vivo* mouse model experiencing a chronic infection with lymphocytic choriomeningitis virus (LCMV) suggested an additional subset of T-cells that upon activation, persistent antigen exposure and attenuation of effector function demonstrated a dysfunctional, less active phenotype. Today, these T-cells are broadly termed exhausted T-cells. This type of dysfunctional T-cells is also observed in cancer settings. However, the T-cell exhaustion is a complex process that is not fully understood. So far, the description of some characteristics of exhausted T-

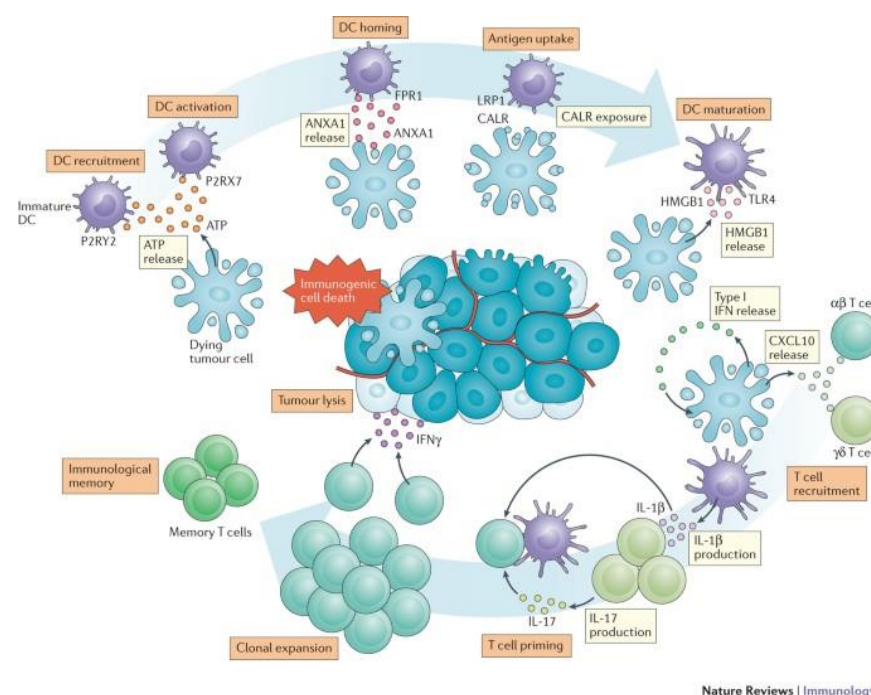


Figure 5: Certain anti-tumor agents, like Oxaliplatin, are immunogenic cell death (ICD) inducers. Thereby cancer cells die and release or express damage-associated molecular patterns (DAMPs), such as calreticulin (CALR), ATP, type I Interferon, CXCL10, HMGB1 or annexin A1. These DAMPs stimulate the recruitment and maturation of immune cells, like dendritic cells, which subsequently activate T-cells to induce a cancer-specific reaction. A certain subset of activated T-cells further differentiate to memory T-cells. Image source: (4)

cells is accepted, whereas a clear definition and how they develop in detail is still controversial (27). Such characteristics are an increased expression of inhibitory receptors such as PD1, TIM-3, LAG-3, CTLA4, TIGIT, a decrease of cytokine production like IL-2, IFN- γ , TNF- α , Granzyme B and nuclear expression of T-bet, TOX, EOMES and BLIMP1(28, 29).

1.7 Metastasis from Colorectal cancer

Invasion and metastasis refer to the process of cancer cells leaving their primary site, moving to a distant organ and successfully colonizing to form a second cancer. Metastasis is considered an advanced stage disease and is fatal to an individual. The most common site for CRC metastases is the liver. Up to 60% of all patients develop liver metastasis within 5 years (30). Metastasis in the liver is formed according to the classical invasion-metastatic cascade. First, cancer cells lose their cell-cell adhesion and start to invade the surrounding tissue. This involves the epithelial-mesenchymal transition (EMT) that is characterized by the transition from epithelial cells to a mesenchymal phenotype to enhance motility and invasiveness. The key component of the EMT is E-cadherin, a transmembrane adhesion protein expressed by epithelial cells to maintain cell polarity and to ensure cell-cell adhesion. Repressors acting directly or indirectly on the promotor of E-cadherin like SNAIL, ZEB1, AP4, SOX2 and TWIST are responsible for its downregulation. Loss of E-cadherin is precursory to the upregulation of mesenchymal markers such as N-cadherin, vimentin and fibronectin. Furthermore, various growth factors such as TGF- β , EGF and HGF induce the production of matrix metalloproteinase (MMPs) to degrade components of the extracellular matrix in order to facilitate invasion. Another important aspect required to successfully reach the circulatory system is the growth of new blood vessels from pre-existing vessels (angiogenesis), which is mediated by proangiogenic factors such as members of the VEGF family. Having managed the intravasation to the circulatory system, cancer cells are protected physically by platelets and neutrophils. In addition, to support extravasation, platelets release TGF- β and PDGF to re-induce the transformation to an epithelial state and neutrophils form extracellular traps helping the cancer cells to adhere to endothelial cells. After extravasation, cancer cells are either killed, enter a state of dormancy or successfully invade the new tissue forming macroscopic tumors (30, 31). The formation of CRC metastasis is not only restricted to the circulatory route. 25% of CRC patients get metastasis through direct dissemination of cancer cells

directly to the peritoneum. Formation of peritoneal metastasis presents a poor prognosis and poor overall-survival (OS) compared to liver metastasis (32, 33).

The peritoneum consists of two layers: the parietal layer covers the abdominal wall and the pelvis, whereas the visceral layer surrounds the organs. The peritoneum comprises a single layer of mesothelial cells sitting on the basal membrane. The stroma below consists of various cells like fibroblasts, macrophages, endothelial cells, and extracellular matrix components like collagen, glycoproteins and proteoglycans. Furthermore, peritoneal organs are additionally covered by the greater omentum, a visceral fat coat protecting the organs from inflammation (34). In addition to CRC, other gastrointestinal cancers such as gastric cancer and pancreatic cancer as well as ovarian cancer are also known to metastasize to the peritoneum (30, 32).

Metastasis formation of cancer cells into the peritoneum involves EMT, where the transcription factor TWIST is the main repressor for E-cadherin. Other possible mechanisms involve the spontaneous detachment of cancer cells from primary tumors, increased interstitial fluid pressure, surgery-induced tumor spills or post-operative infections due to anastomotic leakage (30). Cancer cells disseminate from the primary tumor as single cells into the peritoneum forming tumor spheres with inverted polarity (TSIPs) (35). Thereafter, TSIP move around the abdominal cavity, where they adhere to the mesothelial cell layer, are trapped within omentum immune aggregates or are caught by neutrophil extracellular traps (NETs). The mesothelium expresses various adhesion molecules (ICAM-1, PECAM-1, VCAM-1, EPCAM), proteoglycans (CD44) and mucins (MUC16) that facilitate adhesion of cancer cell clusters. Furthermore, pro-inflammatory cytokines such as TNF- α , IL-6, IL-1 β and IFN- γ induce mesothelium cell contraction resulting in exposed basement membrane favoring the invasion of cancer cells. Having reached the sub-peritoneal space, cancer or stromal cells secrete MMPs and growth factors to further facilitate invasion and migration. Specifically, insulin-like growth factor 1 (IGF-1) was found to be overexpressed in peritoneal metastasis from CRC (30, 36, 37).

1.8 Peritoneal metastasis characterization

Using transcriptomic analysis, a Dutch study classified over 80% of PM as CMS4 type. Furthermore, a high similarity was noted between matching patient samples of PM and CRC at epithelial, stromal and immune cell levels. Nevertheless, several pathways and genes were enriched in PM compared to the primary tumor including TGF- β , angiogenesis, and frequency of stromal fibroblasts, monocytes and macrophages. Meanwhile, APC, MYC and KRAS mutations were less frequent in PM. This study showed differences from liver metastasis, where lesions showed increased heterogeneity compared to primary tumor and mainly belonged to CMS2 type. Further analysis revealed that most patients with high PCI (Peritoneal cancer index) scores are classified as CMS4 and that these patients presented worse OS survival (22, 38).

In order to support the finding that peritoneal spread is closely associated with CMS4, various cell lines were screened genetically and examined for their ability to form PM. This analysis confirmed that CMS4 primary tumors metastasize to the peritoneum. In addition, these cell lines had a differential expression of moesin (MSN). MSN belongs to the ERM family and acts as cross-link between transmembrane proteins such as CD44 or EGFR and the actin cytoskeleton, thus playing a role in adhesion and migration. MSN is already expressed in CMS4 primary tumor and compared to liver metastasis MSN was highly expressed in PM (22).

Even though most patients harboring PM are classified as CMS4, disease progression, treatment response and outcome differ from patient to patient. This led to a deeper analysis of CMS4 patients resulting in three additional CMS4 subtypes that vary in molecular and clinical properties. CMS4 subgroup A represents the highest frequency of KRAS mutation and high expression of oxidative phosphorylation, myc and reactive oxygen species (ROS). CMS4 subgroup B originates mainly from mucinous primary tumors, thereby possessing an increased expression of genes encoding for secretion mucins like MUC2, MUC5AC, MUC5B and MUC6. Furthermore, in this subgroup KRAS and TP53 mutations are less frequent. Finally, subgroup C is predominantly located at the omentum and represents the subgroup with the highest expression of EMT genes and increased levels of TGF- β and KRAS. Moreover, CMS4 subgroup C signifies the highest immune- and stroma cell infiltration and inhibitory molecule expression like PD-1, PD-L1, CTLA4, TIM-3 and TIGIT thereby creating an immunosuppressive microenvironment (22, 38).

PM tumor microenvironment (TME) also plays an important role in disease progression. In the peritoneal cavity, lymph nodes and the greater omentum have a significant presence of immune cells like macrophages, T-cells, NK-cells and dendritic cells. Furthermore, approximately half of the immune cells are positive for class II major histocompatibility complex important for antigen presentation. Cytokines and growth factors such as IL-1, IL-6, prostaglandin E2, GCSF, GM-CSF and MCSF create a pro-inflammatory environment. Nevertheless, the TME in the diseased peritoneum is known to be immunosuppressive. There is evidence that PM is associated with a high frequency of cancer associated fibroblasts (CAFs) located in the subperitoneal space. CAFs are driven by TGF- β , TNF- β and IGF-1 promoting an immunosuppressive environment and thus promoting tumor progression. Another important cellular component in the PM TME is tumor-associated macrophages (TAMs). TAMs support the formation of metastasis by releasing factors such as VEGF, MMPs, TNF- α and IL-10 (36, 39, 40).

1.9 Treatment options for peritoneal metastasis

In the past decades, treatment strategies for PM have evolved dramatically. Treatment strategies are chosen depending on the molecular and pathological features of the tumor. Systemic chemotherapy is the most preferred treatment option for metastatic CRC. In 2004, the MOSAIC trial showed the advantage of combined chemotherapy of 5-FU and Oxaliplatin (FOLFOX) compared to a single chemotherapy application. The chemotherapy treatment was further refined and patients were also treated with the combination of 5-FU and Irinotecan (FOLFIRI) or even with the combination of 5-FU, Oxaliplatin and Irinotecan (FOLFOXIR). Depending on the molecular signature of the tumor, chemotherapy was additionally combined with monoclonal antibodies against VEGF and EGFR. This treatment strategy improved the outcome of CRC patients and patients harboring liver metastasis but was less effective for PM patients (41).

The introduction of cytoreductive surgery (CRS) in combination with hyperthermic intraperitoneal chemotherapy (HIPEC) by Sugarbaker gave new hope to selected PM patients (42, 43). During this procedure, macroscopic tumor lesions are surgically removed and this is followed by a heated chemotherapy lavage of the abdomen to remove residual tumor lesions. Sugarbaker also proposed a scoring system to quantify tumor load in the peritoneum during the operation. The so-called peritoneal cancer index (PCI) ranging from 0-39 is used to describe the initial tumor load and as a tool to pre-

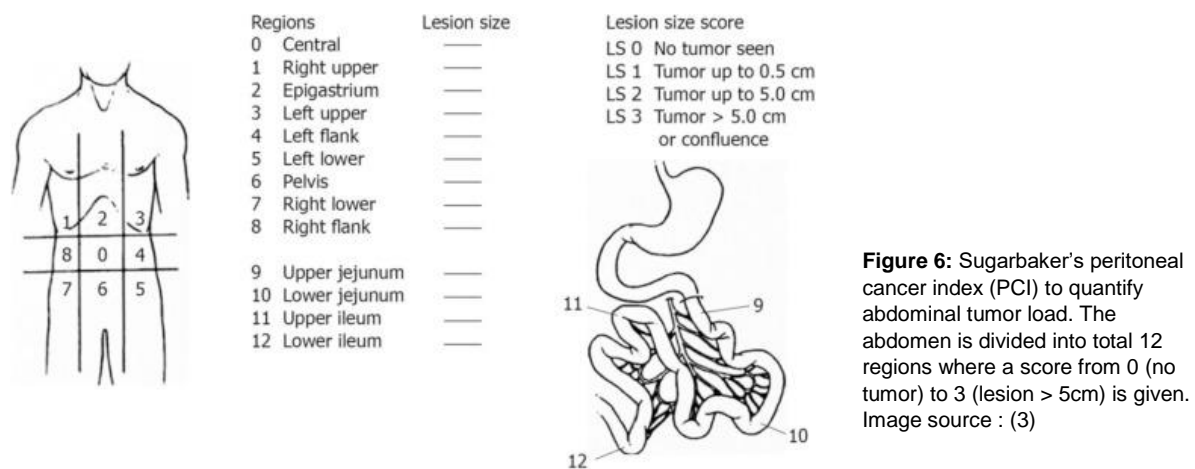
select patients for CRS/HIPEC and to compare outcomes from different clinical centers (44). Since the first CRS/HIPEC procedure in the 1990s, the treatment was further refined, new protocols were established and patient selection improved (37, 41). Only selected patients benefit from the CRS/HIPEC treatment. In order to predict the responsiveness of a patient to CRS/HIPEC, different prognostic factors are considered, including the PCI score, extra-peritoneal metastases, nodal stage and RAS/RAF mutations (45, 46).

Even though the CRS/HIPEC procedure has been performed for more than twenty years, no standardization regarding temperature, treatment duration or type of drug was established for HIPEC. Currently, the most frequently used protocols are Oxaliplatin for 30 minutes at 43°C and MitomycinC/Doxorubicin for 90 minutes at 42°C. Oxaliplatin is a third-generation platinum chemotherapeutic agent that demonstrated cytotoxic properties in a broad range of cancers. Oxaliplatin binds to GC-rich DNA regions, leading to intra- and interstrand crosslinks and DNA-protein crosslinks. The formed adducts prevent DNA transcription and translation resulting in apoptosis induction if not removed by nucleotide excision repair (NER)(47).

Furthermore, Oxaliplatin is known to induce ICD. Unfortunately, resistance to Oxaliplatin is common amongst CRC patients, resulting in disrupted long-term therapy success and recurrence. Many research groups are interested in understanding the causes behind resistance, therefore exploring the mechanisms such as single-cell RNA-sequencing of patient-derived organoids or broad profiling of CRC cell lines to clarify resistance against Oxaliplatin (48, 49). Studies performed on patient-derived organoids also confirmed Oxaliplatin resistance in PM. A study performed by Laoukili *et al.* demonstrated that Oxaliplatin resistance in PM was caused by a high production of glutathione, which could be reversed when the catalytic subunit of glutamate-cysteine ligase (GCLC) was blocked (38). This study, as well as many others, demonstrate that the potential of Oxaliplatin to induce long-term anti-cancer effects only unfolds in combination with other drugs. Mitomycin C is the most frequently used agent for HIPEC procedure, but also in many solid tumors as systemic chemotherapy. Mitomycin C is an alkylating tumor antibiotic extracted from *Streptomyces* that induces DNA cross-linking, resulting in DNA breaks during transcription that leads to cell death. Furthermore, oxygen and radiation therapy were shown to enhance cytotoxicity of Mitomycin C (50, 51). During HIPEC, Mitomycin C is often applied together with Doxorubicin. This combination is known as the “Sugarbaker Regimen”(50). Like Oxaliplatin, Doxorubicin is able to intercalate into DNA, thereby

disrupting transcription and translation. Furthermore, it was shown that Doxorubicin generates free radicals that damage DNA, proteins and the cell membrane (52) as well as is known to be an ICD inducer (25).

Despite of the progress made in recent times in terms of patient selection and regimen development, more than 70% of patients receiving CRS/HIPEC relapse within 2-5 years, affecting the long-term survival of patients. Patients with PM show a significantly shorter OS of only 21 months after recurrence compared to 43 months for liver metastasis. Predictive factors for the recurrence are RAS mutations and positive nodal stage of the primary tumor (33).



Moreover, a French group completed in 2021 the first controlled randomized trial to assess the benefit of CRS/HIPEC (PRODIGE-7). In this trial, 265 patients with stage IV CRC with isolated PM and a PCI score of >25 underwent CRS/HIPEC or CRS alone. The study reported that patients receiving HIPEC after CRS did not demonstrate a significant survival advantage compared to CRS alone (53).

However, this trial had limitations, as the efficacy of HIPEC with other drug combinations was not examined, the survival benefit of HIPEC with 18 months was overestimated and patient selection criteria were poorly defined. For example, patients with a PCI between 11 and 15 showed increased OS after CRS/HIPEC compared to CRS alone. Moreover, in other studies CRS/HIPEC significantly performed better compared to systemic chemotherapy treatment. Complete resection during CRS is definitely of importance for a successful treatment, but the effectiveness of HIPEC is still debatable (43, 53-55).

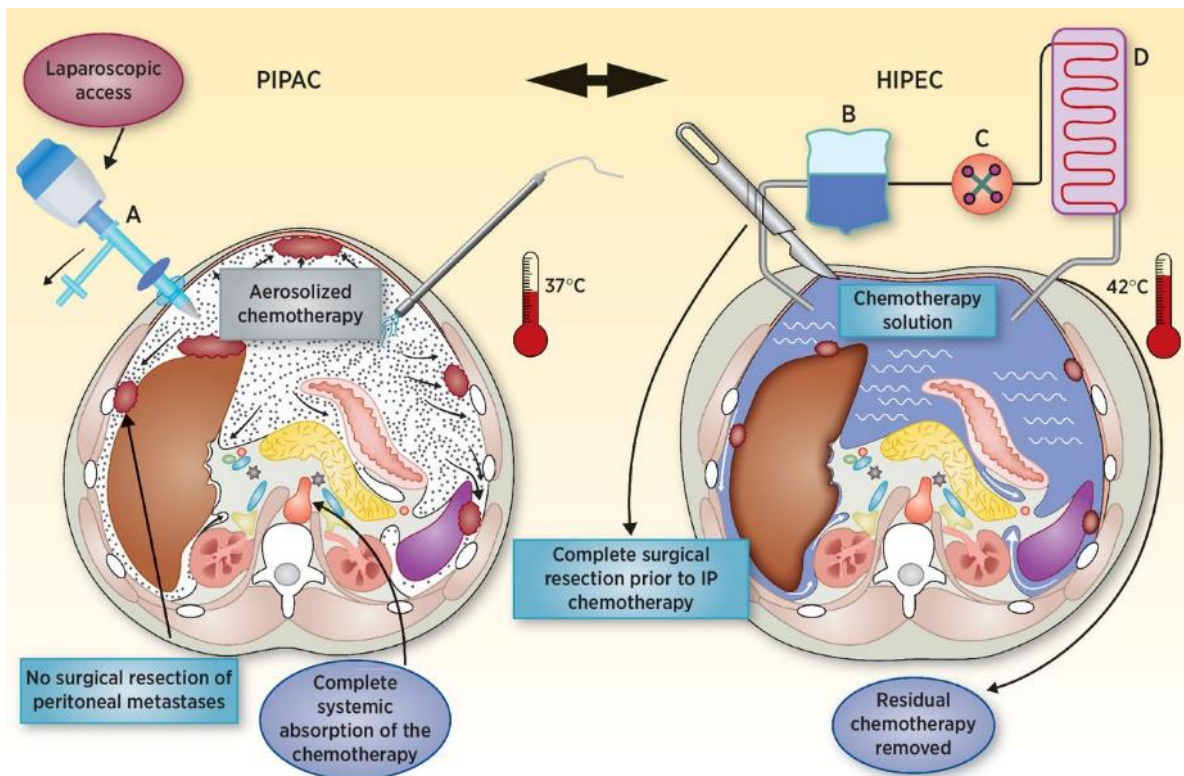


Figure 7: Comparison of local application of chemotherapy. Left: PIPAC. Chemotherapy application in the form of a pressurized aerosol. Treatment occurs laparoscopic, at body temperature and without removing residual chemotherapy. This procedure is repeated approximately every 4 weeks. Right: HIPEC. Prior to treatment macroscopic tumor lesions are removed via CRS. Heated chemotherapy lavage occurs on open abdomen, whereas residual chemotherapy is removed. Patient undergo this procedure normally once. Image Source: (10)

Another local treatment option for PM patients is the laparoscopic application of chemotherapy as pressurized intraperitoneal aerosol (PIPAC). PIPAC is used in advanced stage patients, where resection is not an option anymore. Therefore, PIPAC is performed at intervals of approximately four weeks to keep tumor growth under control (56). However, recent studies demonstrated that repeated PIPAC as neoadjuvant therapy can lead to a qualification for secondary CRS/HIPEC with a curative intent (57).

Another treatment option that has gained importance in general for all types of cancer is the use of immunotherapy. Despite the immunosuppressive TME of PM, recent studies demonstrated the advantage of immunotherapy to activate immune cells within the peritoneal cavity. Furthermore, it was shown that combining immunotherapy and other treatment strategies potentially improve the outcome of PM patients.

So far, three monoclonal antibodies for metastatic CRC have been approved. Bevacizumab targeting VEGF and Cetuximab and Panitumumab targeting EGFR are additionally administered to patients depending on the molecular signature of the tumor. Another monoclonal antibody, which is currently under clinical investigation, is MOC31PE. MOC31PE targets the commonly expressed epithelial cell adhesion molecule (EpCAM). Upon binding, the antibody releases pseudomonas exotoxin A, disrupting cellular processes and induce cell death. During a phase 1 dose-escalation study in 2017, MOC31PE demonstrated promising results. MOC31PE was given intraperitoneally after CRS/HIPEC and was found to be well tolerated even if given in a cytotoxic concentration as it was not absorbed systemically. The 3-year OS in this study was 78% and the median PFS was 21 months.

Catumaxomab is another monoclonal antibody that was already approved in 2009 in Europe for malignant ascites. Catumaxomab is a rat-murine bispecific trifunctional antibody that can target EpCAM, CD3+ T cells and NK cells, inducing the release of pro-apoptotic cytokines like IL-2, IL-12 and TNF- α , resulting in cancer cell death (58, 59).

The most commonly used immunotherapies are immune checkpoint inhibitors that target CTLA4, PD-1 and PD-L1. In 2011, the FDA approved the first immune checkpoint inhibitor for the treatment of melanoma, since then several clinical phase I and II studies have tried immune checkpoint inhibitors on a large variety of cancers including PM arising from various primary tumors. Even though factors such as microsatellite instability, high tumor mutation burden and PD-L1 expression support the use of immune checkpoint inhibitors, only minimal success was observed when this type of drug was used as monotherapy. However, combining immunotherapy with other drugs like STING agonists or CAF inhibitors demonstrated increased therapeutic efficacy in PM mouse models, suggesting that immune checkpoint inhibitors need to be combined with other treatment strategies to achieve a treatment response in PM (58, 59).

Another arm of immunotherapy broadly used are cancer vaccines. Recently, many different cancer vaccines were developed but are still part of different clinical trials for solid tumors, including CRC and PM. Cancer vaccines are based on protein/peptides, DNA/RNA, whole cells or oncolytic viruses. In the case of whole cell cancer vaccines, dendritic cells are often used due to their ability to cross present antigens, which stimulate the immune system to kill cancer cells. Genetically modified oncolytic viral vaccines also activate the immune system but can directly target and kill cancer cells. Protein/peptide cancer vaccines bind tumor specific antigens on MHC to prime T-cells, thus provoking

a specific immune response. DNA/mRNA vaccines encode for antigens or immunostimulatory molecules that are produced upon internalization resulting in a tumor-specific killing. Despite this progress, the heterogeneity of cancer cells and the lack of antigenicity after relapse remain a problem that needs to be solved.

Lastly, the most remarkable achievement of immunotherapy in the past years was the development of personalized CAR-T cells. CAR-T cells are genetically modified T-cells expressing a chimeric receptor allowing antigen-specific binding independent of MHC. This leads to a strong T-cell activation and powerful anti-tumor response. Initially, CAR-T cells demonstrated their efficacy in hematological malignancies. Currently, CAR-T cells are in clinical trials for advanced solid tumors. For metastatic CRC, mouse models and human studies demonstrated a successful treatment response of CAR-T cells targeting the carcinoembryonic antigen (CEA), an antigen that is overexpressed in metastatic CRC. Another target for CAR-T cell therapy in PM is for example the folate receptor alpha. However, despite improving T-cell persistence, it failed to have a sustained anti-tumor response. This indicates that CAR-T cell therapy in the context of PM has potential but needs further refinement (58, 59).

Currently several clinical studies investigate the use of inhibitors interfering with the DNA repair pathway, growth and proliferation pathway as well as multikinase inhibitors for metastatic CRC. They are either examined as monotherapy or combined with chemotherapy or irradiation. Some of these inhibitors were part of this study (Table 3), whereas the most relevant target, ATR, will be described in more detail below.

Inhibitors used in this study	
Targets of DNA damage repair pathway inhibitors	Example of clinical study (Ref.)
ATR	(60)
ATM	(61)
CHK1	(62)
PARP	(63)
Targets of growth and proliferation pathway inhibitors	
ERK	(64)
MEK	(65)
BRAF	(66)
Multikinase inhibitors (target amongst others Raf-1, Braf, VEGF-R, PDGFR- β and FGF-R)	
Sorafenib	(67)
Pazopanib	(68)

Table 3: List of drugs used in this study. Inhibitors interfere either with DNA repair pathway, growth and proliferation pathway or act as multikinase inhibitors. An example for clinical studies performed in CRC or metastatic CRC patients is given for every inhibitor.

Ataxia telangiectasia and Rad3-related (ATR) is a serine/threonine kinase and member of the phosphatidylinositol-3-kinase (PI3K)-related kinase (PIKK) family that also includes ATM, mTOR, DNA-PKcs and SMG1. ATR is activated upon DNA damage and replication stress. Activation is triggered by RPA-coated single-strand DNA, which is recognized by ATRIP which then forms a complex with ATR. This is followed by recruiting other damage regulators such as Rad17, 9-1-1 complex, R1HNO and TopBP1. Subsequently ATR phosphorylates its downstream target CHK1, further regulating DNA replication arrest, replication fork stabilization and DNA repair promotion. Especially in cancers with dysregulated cell cycle, increased replication stress or deficiency in ATM or DNA repair proteins ATR pathway demonstrated to be crucial for survival. Therefore, ATR is a suitable candidate for anti-cancer combination treatments (69, 70).

This was demonstrated already in several studies, like in 2019, where Combès *et al.* published a study establishing that ATR inhibition overcomes Oxaliplatin resistance in CRC cell lines, induces ICD *in vitro* and promotes T-cell depending anti-tumor response *in vivo* (71). Furthermore, it has been shown for osteosarcoma that irradiation induced double strand breaks enhance PD-L1 expression in cancer cells, indicating that PD-L1 upregulation is dependent on ATM/ATR/CHK1 kinases that activate STAT1, STAT3 and IRF1 (72).

So far, several ATR inhibitors (ATRi) were developed and refined by different companies such as Berzosertib (VE-822 by Merck KGaA), Ceralasertib (AZD6738 by AstraZeneca), Gartisertib (VX-803 by Merck), Tuvusertib (M1774 by Merck), Elimusertib (BAY1895344 by Bayer) Camonsertib (RP-3500 by Roche), to mention a few. Some inhibitors have progressed to phase I and II clinical trials for various tumors, as monotherapy or in combination with other DNA damaging agents. In 2021, a clinical phase I study started recruiting patients to investigate the combination of ATRi with FOLFIRI in advanced metastatic CRC patients (NCT04535401) (69).

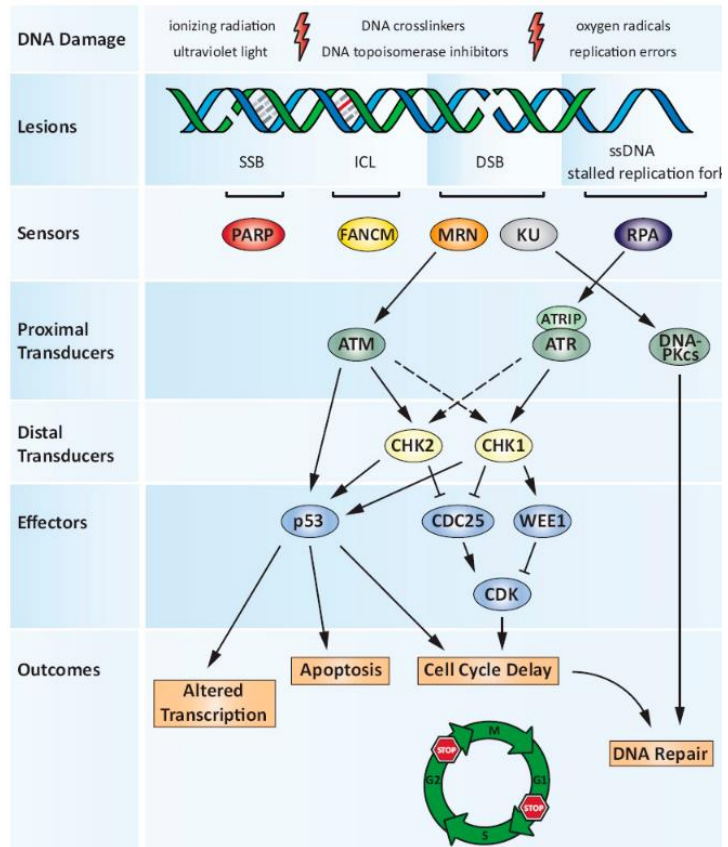


Figure 8: DNA damage response. Endogenous and exogenous sources lead to DNA damage like single-strand breaks (SSD), interstrand crosslinks (ICL), double-strand breaks (DSB) and single-stranded DNA (ssDNA). ATR and ATM are two master transducers that have overlapping but also distinct functions. ATM is mostly responsible for double-strand breaks, whereas ATR responds on a broad range of DNA damage and replication stress. RPA binds to region of single strand DNA thereby recruiting ATRIP and ATR. This results in a phosphorylation cascade that activates CHK1. CHK1 subsequently activates downstream effector proteins that are responsible for cell cycle arrest, DNA repair, altered transcription and apoptosis. Image source : (7)

2. Aims of the thesis

Peritoneal metastasis (PM) is an advanced-stage metastatic disease arising from different primary cancers that include colon, gastric, ovarian and appendix cancers. Direct dissemination of cancer cells into the abdominal cavity through non-haematogenous routes make PM lesions different from other metastatic lesions. Survival of patients with PM is worse than for other metastatic sites despite systemic chemotherapy. Additional treatments for PM include surgery to remove visible tumor lesions in combination with local application of heated chemotherapy (HIPEC) or PIPAC, where chemotherapies are introduced in the abdominal cavity as aerosol. In pre-selected patients, these local treatments prolonged survival of PM patients compared to systemic chemotherapy alone. Our previously generated data suggest that the benefit of local treatment (HIPEC) is primarily mediated by immune activation within the tumor microenvironment (In revision, Nature communications). Nevertheless, more than 70% of patients relapse within two years affecting long-term survival. The reason for fast recurrence can be due to inefficient treatments or due to PM tumor biology. Therefore, in this study, we explored the therapeutic potential of existing drugs and drug combinations to induce tumor-specific immunity against PM lesions to improve long-term survival of PM patients. In addition, once we have identified these drugs, it may create a possibility to combine such drugs with immunotherapies to secure sustained tumor-specific immunity. Overall, as an outcome, we are hoping to offer a new PM-specific treatment modality that would be suitable to the majority of PM patients.

To do so, the following aims were pursued:

Aim 1: Investigate the cytotoxic effect of different drugs and drug combinations on CRC cell lines and patient-derived PM organoids *in vitro*

Aim 2: Examine drug-induced immunogenic changes on CRC cell lines and patient-derived PM organoids *in vitro*

Aim 3: Examine the efficacy of selected drugs on PM lesions in our PM mouse model and understand the underlying immunogenic mechanism *in vivo*

3. Material and Methods

Cell culture

For *in vitro* drug studies, the human CRC cell lines HT29, HCT8, Caco2, LS180, Colo205, Lovo, LS1034, SW1116 and SW480 were used. Lovo, LS1034, SW1116 and SW480 were purchased from ATCC. HT29 and HCT8 were kindly provided by Prof. M. Scharl (University Hospital Zurich). Caco2, LS180 and Colo205 were kindly provided by Prof. L. Borsig (University of Zurich). HT29 was cultured in Dulbecco's modified Eagles medium (DMEM, Cat. No. 31966047 from Thermo Fisher Scientific), HCT8, Lovo and LS1034 in RPMI 1640 medium (Cat. No. 61870044 from Thermo Fisher Scientific), SW1116 and SW480 in Leibovitz's L-15 Medium (Cat. No. 31415086 from Thermo Fisher Scientific) and Caco2 and LS180 in MEM Medium (Cat. No. 41090036 from Thermo Fisher Scientific). All Media were supplemented with 10% heat-inactivated fetal bovine serum (FBS, Cat. No. A5209501 from Thermo Fisher Scientific) and penicillin/streptomycin (P/S, 100U/ml, Cat. No. 15070063 from Thermo Fisher Scientific). Cells growing in MEM were additionally supplemented with 1% NEAA (Cat. No. 11140035 from Thermo Fisher Scientific).

For *in vivo* studies, the syngeneic murine CRC cell lines MC-38, MC-38-Ova and MC-38-PDL1KO were used. MC-38 cells were purchased from Kerablast. MC-38-Ova and MC-38-PDL1KO were received from Prof. M. van den Broek (University of Zurich). All three murine cell lines were cultured in complete DMEM medium.

All cell lines were kept at 37°C in a 5% CO₂ atmosphere, except SW1116 and SW480, which were kept at 0% CO₂.

Patient-derived tumor organoids

Tumor samples were collected during laparoscopy or CRS according to the cantonal ethic approval (Nr.: 2019-01031) at the University Hospital Zurich. Processing of samples and establishment of organoids were performed at the laboratory of Prof. C. Pauli at the Department of Pathology and Molecular Pathology at the University Hospital Zurich. Organoids were cultured in WRN Medium (details listed in Figure 9) using ultra low attachment plates (6-well, Cat. No. 3471; Corning).

Organoids were kept at 37°C in a 5% CO₂ atmosphere.

Reagent Name	Location	Amount Conc	Volume Solvent	Solvent	Stock Conc	Aliquot	Aliquot Storage	Final Conc in Media	Ordering
DMEM advanced	4°C					500ml			Invitrogen 12491-023
N-Acetylcysteine	4°C	5g	61.278mL	DW	500mM	1250uL	-20°C	1.25mM	Sigma-Aldrich A9165
Human Recombinant EGF	-20°C	500ug	25mL	PBS/BSA** (.1% BSA)	20ug/mL	1250uL	-20°C	50ng/mL	Sigma-Aldrich E9644
Human Recombinant FGF-10	-20°C	500ug	5mL	PBS/BSA** (.1% BSA)	100ug/mL	100uL	-20°C	20ng/mL	Peprotech 100-26
Recombinant Human FGF-basic	-20°C	50µg	10mL	PBS/BSA** (.1% BSA)	5ug/mL	100uL	-20°C	1ng/mL	Peprotech 100-18B
Y-27632 (Rocki)	-20°C	50mg	1.56mL	DMSO	100mM	50uL	-20°C	10uM	Selleckchem S1049
A-83-01	-20°C	5mg	2.37mL	DMSO	5mM	50uL	-20°C	500nM	Sigma-Aldrich SML0788
SB202190	-20°C	25mg	1.51mL	DMSO	50mM	100uL	-20°C	10uM	Selleckchem S1077
Nicotinamide	RT	6.11g	50mL	DW	1M	5mL	-20°C	10mM	Sigma-Aldrich N0636
PGE2	-20°C	10 mg	5.674 mL	DMSO	5mM	100uL	-20°C	1uM	R&D Systems 2296
Noggin (conditioned media)*	-20°C					50mL	-20°C	10ng/mL	
R-Spondin (conditioned media) *	-20°C					25mL	-20°C	10ng/mL	
B27 Supplement	-20°C	50x				10mL	-20°C	1x	Invitrogen 17504001
A/A	-20°C	100x				5mL	-20°C	1x	Invitrogen 15240062
Glutamax	4°C	100x				5ml		1x	Invitrogen 35050038
[Leu15]-Gastrin I Human	-20°C	500ug	0.474 mL	DW	500 uM	10 uL (dilute stocksol. 1:10 with DW)	-20°C	1nM	Sigma-Aldrich G9145

**PBS/BSA: 0.01 g in 10 mL PBS

*Instead of 50ml Noggin and 25ml R-Spondin, 50ml WRN (Noggin + R-Spondin) can be used

Figure 9: Composition of WRN Medium for patient-derived organoids

Cell Viability Assay

For viability assays, 6000-25000 cells/well for cell lines and 3000 cells/well for organoids were plated in triplicates in a 96-well plate. 24 hours after seeding, cells were treated with drugs shown in Table 3 as single drugs (range: 10^{-3} M – 10^4 M, as indicated) or in combination (range: $10^{-0.5}$ M to 10^2 M, as indicated). After 48 hours of treatment, cell viability was detected using CellTiter-Glo 2.0 (Cat. No. G9241 from Promega) according to the manufacturer's protocol.

Western Blotting

Protein extraction of cells was performed in RIPA Buffer containing protease inhibitor cocktail (Cat. No. 5892970001 from Roche Diagnostics) and 1mM of PMSF. Protein concentrations were determined using a DC Protein Assay Reagents Package (Cat. No.5000116 from BioRad). Samples were separated by SDS–PAGE electrophoresis on a 4%-20% Tris-Glycerin-Gel (Cat. No. M00655 from Genscript) together with a pre-stained protein ladder (PageRuler Plus, Cat. No. 26619 from Thermo Scientific). Proteins were then blotted on PVDF membranes (Cat. No.1704156 from Biorad) using a V3 Western Workflow system (BioRad) according to the manufacturer's instruction. Primary antibodies Table 4. were incubated overnight at 4°C in TBST or Milk containing 5% BSA. Following several washing steps with TBST-T, membranes were incubated with a horseradish peroxidase-

conjugated secondary antibody (1:2000, Cat. No.7074S from Cell Signaling) and visualized by chemoluminescence (Cat. No. 34577 from Thermo Fisher).

HMGB1 and extracellular ATP detection

20 000 HT-29 cells/well were seeded in triplicates in a Nunc Microwell 96-well plate (Nunclon Delta-Treated Cat. No. 136101 from Thermo Scientific). 24 hours after seeding cells were treated with 30µM Oxaliplatin (Zentiva, Kantonsapotheke) and 0.3µM ATR inhibitor (Elimusertib (BAY-1895344), Cat. No. S8666 from Selleckchem)). At 6 hours, 24 hours and 48 hours post treatment extracellular ATP was detected using the Real-Time-Glo Extracellular ATP Assay (Cat. No. GA5010 from Promega) and HMGB1 using the Lumit HMGB1 (Human/Mouse) Immunoassay (Cat. No. W6110 from Promega) according to the manufacturer's protocol.

Co-culture killing assay

10 000 MC-38-OVA cells/well were plated in triplicates in a 96-well plate. 24 hours after seeding cells were treated with 10µM Oxaliplatin (Zentiva, Kantonsapotheke) and 0.3µM ATR inhibitor (Elimusertib (BAY-1895344), Cat. No. S8666 from Selleckchem). The following day a spleen from an OT-1 transgenic mice on C57BL/6 background was harvested and to isolate CD8a+ T cells using MACS purification. In brief: Spleen was smashed through a 70µm filter and kept in MACS Buffer (PBS + 0.5% BSA + 2mM EDTA) for 10min until all clumps reached the bottom of the falcon tube. Supernatant was transferred into a fresh falcon tube, centrifuged at 1500rpm for 5min and the pellet was re-suspended in 500µl MACS Buffer. 40µl of CD8a (Ly-2) MicroBeads (Cat. No.130-117-044 from Milteny Biotech) were added to the suspension and incubated for 20min on a roller band at 4°C. After washing, cells were put on MACS MS columns plus (Cat. No.130-041-301 from Milteny Biotech) to purify labeled cells. Purity was confirmed using flow cytometry. Subsequently purified cells were counted and co-cultured for six hours at 1:1 ratio with pre-treated MC-38-OVA. After co-culture killing capacity of OT-1 cells was measured using CellTiter-Glo 2.0 (Cat. No. G9241 from Promega) according to the manufacturer's protocol.

Mice studies

Mice were kept under specific pathogen-free conditions in individually ventilated cages (IVC) at the LASC animal facility in Schlieren. Mice had access to food and water *ad libitum* and were maintained on a 12 hour light/dark cycle. Experiments were performed according to the Swiss Federal Animal regulations and approved by the cantonal veterinary office of Zurich (License Nr. 165/2017 and

022/2021). 8-10 weeks old C57BL/6 mice were purchased from Envigo and kept two weeks prior to experiment start to adapt them to new environment.

0.5×10^6 MC-38 Wildtype, MC-38-OVA or MC-38-PDL1KO murine CRC cells in 100 μ l PBS were injected intraperitoneally (i.p.). Six days after tumor cell injection, mice were treated with 2.5mg/kg Oxaliplatin (Zentiva, Kantonsapotheke) i.p. every third day for a total of three times together with a daily 15mg/kg ATR inhibitor (Elimusertib (BAY-1895344), Cat. No.S8666 from Selleckchem) i.p. injection until the end of the experiment.

15 days after tumor cells injection mice were sacrificed. Tumor load was assessed using the peritoneal cancer index(1) and tumor weight of the tumor lesion located next to the spleen was measured. Additional tumor lesions were collected for flow cytometry and immuno-histological analysis.

If indicated, for CD8+ T cell depletion mice were injected i.p. once per week starting one day prior of treatment start with 100 μ g anti-mouse CD8 antibody (clone YTS 169.4, Cat. No. BP0117 from bioXcell). For PD-1 blockade, mice were injected i.p. every third day starting at day six with 150 μ g anti-PD-1 antibody (clone 29F.1A12, Cat. No. BP0273 from bioXcell).

For *ex vivo* OVA tumor re-stimulation, mice were sacrifice at day 13. Treatment was stopped 96 hours prior to tumor harvest.

Flow Cytometry

Collected tumors from *in vivo studies* were enzymatically digested (DMEM + collagenase D (Cat. No.11088858001 from Roche) and DNase I (Cat. No. 04536282001 from Roche) for 40min at 37°C on a shaker. *In vitro* tumor samples were detached from culture plates and transferred to FACS tubes without digestion. After washing and filtering the samples through a 100 μ m filter, cells were surface stained in PBS for 30min at 4°C. After surface staining, the cells were either fixed in 4% formaldehyde or further stained intracellularly. Thereby, cells were fixed with FoxP3 Fixation/Permeabilization Buffer (Cat. No 00-5523-00 from Thermo Fisher), for 60min at room temperature. Afterwards, cells were washed with Permeabilization buffer (Cat. No. 421403 from Biolegend) and intracellularly stained over night at 4°C. After the last washing step, cells were kept in Permeabilization buffer for the acquisition at the BD LRS II Fortessa.

For *ex vivo* OVA tumor re-stimulation digested tumors were washed and re-suspended in RPMI complete + 100 μ M 2-Mercaptoethanol (Cat. No. M3148 from Sigma). 100 μ l cell suspension was distributed to a pre-prepared u-bottom 96-well plate (Cat. No. 92097 from TPP). The plate contained either 100 μ l Media + Brefeldin A (to avoid vesicle exocytosis, Cat. No. 420601 from Biolegend) as unstimulated control, additional SIINFEKL 257-264 peptide (final conc.:10 μ M, Cat. No. vac-sin from Invivogen) to induce re-stimulation of CD8+ T-cells or Ionomycin/Phorbol myristate acetate (PMA/I) (final conc. 500ng/ml and 5 μ g/ml respectively, Cat. No. inh-ion and tlr-pma from Invivogen) as positive control. Plate was incubated for 6h at 37°C. Afterwards, cells were washed with PBS + Brefeldin A (5 μ g/ml), surface stained for 30min at 4°C and fixed with 4% paraformaldehyde for 5 min at RT. Finally, cells were permeabilized with PB Buffer (PBS + 2mM EDTA + 0.5% BSA + 0.1%Saponin) for 10min at RT and intracellularly stained over night at 4°C. The next day, cells were washed and kept in PB Buffer until the acquisition at the BD LRS II Fortessa or Cytex Aurora Spectral Analyzer.

For quantitative analysis, Precision Counting Beads (100 μ l/sample, Cat. No. 424902 from Biolegend) were additionally used for *in vivo* samples. Data analysis was performed using FlowJo (V10.7.1, BD). Directly labelled primary antibodies for flow cytometry are found in Table 4.

Immunostaining and Multispectral imagine

Collected mouse tissues were fixed 24 hours in 4% paraformaldehyde followed by dehydration in an Excelsior AS Tissue Processor (Thermo Scientific). Afterwards, samples were embedded in paraffin, cut into 3 μ m thick sections and mounted on a superfrost plus slide (Cat. No. 10019419 from Thermo Scientific). Immunostaining was performed using the Opal 7-color Manual IHC Kit (Cat. No. NEL811001KT from Akoya Bioscience) according to the manufacturer's protocol. In brief, slides were pressure cooked for 17 minutes at high heat in AR Buffer pH6 (Cat. No. AR6001KT from Akoya Bioscience) for antigen retrieval. Afterwards, to avoid unspecific antibody binding, slides were blocked with 3% H₂O₂ for 15min at RT. After washing with TBS-T three times for two minutes, slides were incubated with a primary antibody (Table 4) either two hours at RT or overnight at 4°C. Subsequently, an Opal HRP polymer (Cat. No. ARH1001EA (Akoya Bioscience)) was added for 10min at RT. After washing, following Opal Fluorophores were used to bind the polymer (10min at RT): for CD8a Opal 620 or Opal 780 (FP1495001KT and FP1501001KT from Akoya Bioscience)), for PD-L1 Opal 520 (FP1487001KT from Akoya Bioscience), for GranzymeB Opal 480 (FP1500001KT from Akoya

Bioscience). Finally, for nuclear staining, slides were incubated with DAPI (two drops in 1ml TBS-T, Cat. No.FP1490 from Akoya Bioscience) for 10min at RT, washed again and mounted with Vectashield Vibrance Antifade medium (Cat. No. H-1800-10 from Vector Laboratories). Slides were scanned using the automated imaging system Vectra Polaris (Akoya Bioscience) in Schlieren. Afterwards images were processed using the software QuPath (V0.3.2) or HALO (v3.6.4134.263)

Statistics

GraphPad Prism version 9.5.1 was used to construct figures. Statistical analysis was performed using one-way ANOVA with Tukey's multiple-comparison test. Analyzed statistical differences were considered statistically significant if $P \leq 0.05$ and marked with an asterisk. Asterisks indicate: *: $P \leq 0.05$; **: $P \leq 0.01$, ***: $P \leq 0.001$.

Drug	Cat. No.	Company
Oxaliplatin	Kantonsapotheke	Zentiva
Cisplatin	Kantonsapotheke	Sandoz
Mitomycin C	Kantonsapotheke	Curatis
Doxorubicin	D1515	Sigma Aldrich
5-FU	F6627-1G	Sigma Aldrich
SN38 (Irinotecan)	H0165	Sigma Aldrich
ATR inhibitor Elimusertib (BAY-1895344)	S8666	Selleckchem
ATM inhibitor KU-55933	ab1203637	Abcam
CHK 1 inhibitor PF-477736	S2904	Selleckchem
PARP inhibitor Olaparib (AZD2281)	S1060	Selleckchem
ERK inhibitor Ulixertinib (BVD-523)	S7854	Selleckchem
BRAF inhibitor Dabrafenib (GSK2118436)	S2807	Selleckchem
MEK inhibitor Trametinib (GSK1120212)	S2673	Selleckchem
Sorafenib BAY 43-9006	S7397	Selleckchem
Pazopanib GW786034	S3012	Selleckchem

Table 3: List of Drugs used in this study

Antibody	Cat. No.	Company	Application	Dilution
γ -H2AX	9718	Cell Signaling	Western Blot	1:1000
CHK1	2360	Cell Signaling	Western Blot	1:1000
Phosphor-CHK1	2341	Cell Signaling	Western Blot	1:1000
α -Tubulin	2125	Cell Signaling	Western Blot	1:2000
Anti-PD-1 in FITC clone 29F.1A12 anti-mouse	135214	Biolegend	Flow cytometry	3:100
Anti-Ly6G in FITC clone 1A8 anti-mouse	127606	Biolegend	Flow cytometry	0.25:100
Anti-Perforin in FITC clone S16009a anti-mouse	154310	Biolegend	Flow cytometry	1:100
Anti-CD137 in APC clone 17B5 anti-mouse	106110	Biolegend	Flow cytometry	2:100
Anti-CD11b in APC clone M1/70 anti-mouse	101212	Biolegend	Flow cytometry	1:100
Anti-CD11c in APC clone N418 anti-mouse	117310	Biolegend	Flow cytometry	1:100
Anti- CD274 (B7-H1, PD-L1) in APC clone 10F.9G2 anti-mouse	124312	Biolegend	Flow cytometry	1:100
Ant-H-2Kb/H-2Db in APC clone 34-1-2S anti-mouse	114608	Biolegend	Flow cytometry	1:100
Anti-IFN γ in APC clone XMG1.2 anti-mouse	505810	Biolegend	Flow cytometry	1:100
Anti-FoxP3 in AF700 clone MF-14 anti-mouse	126422	Biolegend	Flow cytometry	1:100
Anti-CD39 in PE clone Duha59 anti-mouse	143804	Biolegend	Flow cytometry	3:100
Anti-CD11b in PE clone M1/70 anti-mouse	101208	Biolegend	Flow cytometry	0.5:100

Anti-CD8b in PE clone YTS156.7.7 anti-mouse	126608	Biolegend	Flow cytometry	1:100
Anti-CD45.2 in PB clone 104 anti-mouse	109820	Biolegend	Flow cytometry	1:100
Anti-CD8a in PE-Cy5 clone 53-6.7 anti-mouse	100709	Biolegend	Flow cytometry	0.2:100
Anti-CD4 in PE-Cy7 clone GK1.5 anti-mouse	100422	Biolegend	Flow cytometry	0.6:100
Anti-GranzymeB in Pe-Cy7 clone QA16A02 anti-mouse	372214	Biolegend	Flow cytometry	1:100
Anti-Ly6C in PE-Cy7 clone HK1.4 anti-mouse	128018	Biolegend	Flow cytometry	1:100
Anti-CD39in PE Dazzle 594 clone Duha59 anti-mouse	143811	Biolegend	Flow cytometry	1:100
Anti-LAG-3 in PE Dazzle 594 clone C9B7W anti-mouse	125224	Biolegend	Flow cytometry	2:100
Anti-OX40 in BV605 clone OX-86 anti-mouse	119419	Biolegend	Flow cytometry	2:100
Anti-CD44 in BV605 clone IM7 anti-mouse	103047	Biolegend	Flow cytometry	1:100
Anti-NK1.1 in BV605 clone PK136 anti-mouse	108739	Biolegend	Flow cytometry	2:100
Anti-LAG-3 in BV650 clone C9B7W anti-mouse	125227	Biolegend	Flow cytometry	1:100
Anti-CD3 in BV650 clone 17A2 anti-mouse	100229	Biolegend	Flow cytometry	1:100
Anti-Tim3 in BV711 clone B8.2c12 anti-mouse	134021	Biolegend	Flow cytometry	2:100
Anti-Ki67 in BV711 clone 11F6	151227	Biolegend	Flow cytometry	1:100

anti-mouse and anti-human				
Anti-CD19 in BV711 clone 6D5 anti-mouse	115555	Biolegend	Flow cytometry	1:100
Anti-CD25 in BV785 clone PC61 anti-mouse	102051	Biolegend	Flow cytometry	2:100
Anti-CD4 in BV785 clone GK1.5 anti-mouse	100453	Biolegend	Flow cytometry	1:100
Anti-IA/IE in PerCP clone M5/114.15.2 anti-mouse	107624	Biolegend	Flow cytometry	1:100
Zombie-NIR fixable viability dye anti-mouse and anti-human	423106	Biolegend	Flow cytometry	1:100
Anti- CD274 (B7-H1, PD-L1) in APC clone MIH2 anti-human	393610	Biolegend	Flow cytometry	1:100
Anti-CD80 in BV711 clone 2D10 anti-human	305236	Biolegend	Flow cytometry	1:100
Anti-CD86 in PE/Dazzle clone BU63 anti-human	374217	Biolegend	Flow cytometry	1:100
Anti-HLA-A,B,C in PE clone W6/32 anti-human	311406	Biolegend	Flow cytometry	1:100
Anti-Galectin9 in BV421 clone 9M1-3 anti-human	348920	Biolegend	Flow cytometry	1:100
CD8a	ab217344	Abcam	Multiplex staining	1:2000
GranzymeB	ab255598	Abcam	Multiplex staining	1:2000
PD-L1	64988	Cell Signaling	Multiplex staining	1:200

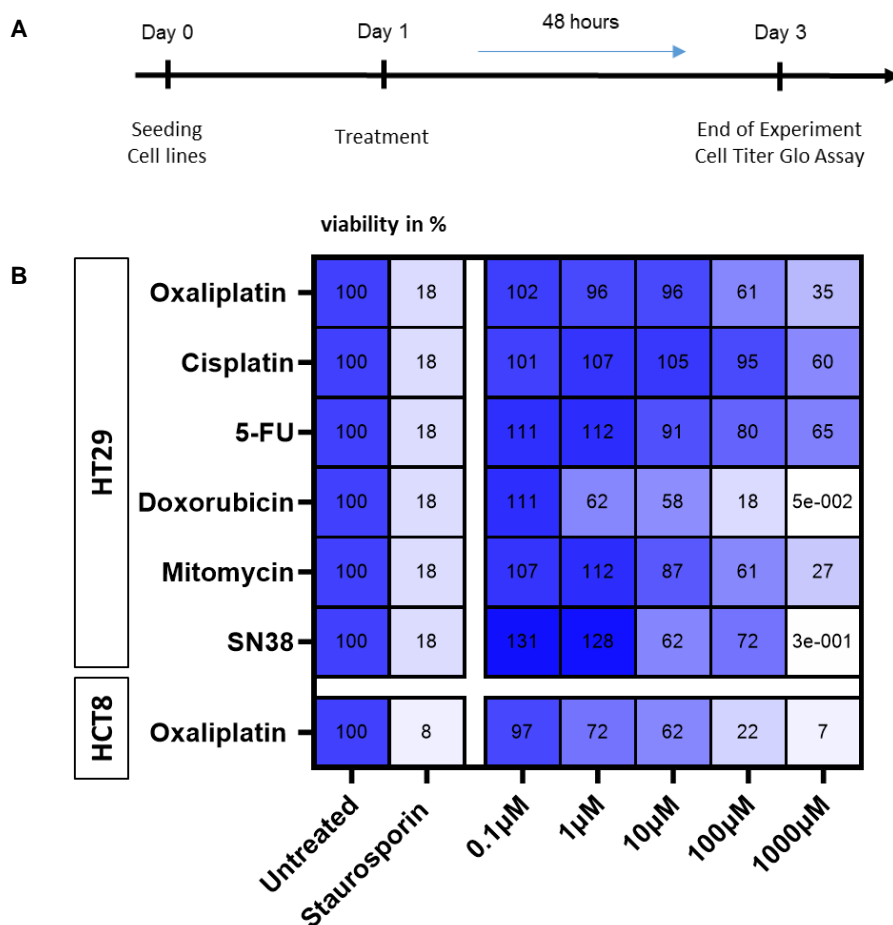
Table 4: List of Antibodies used in this study

4. Results

4.1 Cytotoxic drug screening on CRC cell lines

As a first step, we were interested in investigating the cytotoxic potential of various drugs on selected CRC cell lines (HT29 and HCT8). Therefore, we used chemotherapeutic agents (Oxaliplatin, Cisplatin, 5-FU, Doxorubicin, Mitomycin, SN38 (Irinotecan), inhibitors of the DNA repair pathway (ATR, ATM, PARP, CHK1), inhibitors of the growth and proliferation pathway (MEK, ERK, BRAF) and multikinase inhibitors (Sorafenib, Pazopanib). Drugs were applied in increasing concentrations and cell viability was assessed 48 hours post treatment (**Figure 10A**). We observed that higher drug concentrations resulted in lower cell viability (**Figure 10B & 10C**), whereas Doxorubicin (**Figure 10B**) and MEKi (**Figure 10C & 10D**) already affected cell viability at lower concentrations. On the contrary, ATMi, PARPi, BRAFi, Sorafenib and Pazopanib demonstrated little efficacy at low concentrations on both cell lines (**Figure 10C & 10D**).

Figure 10



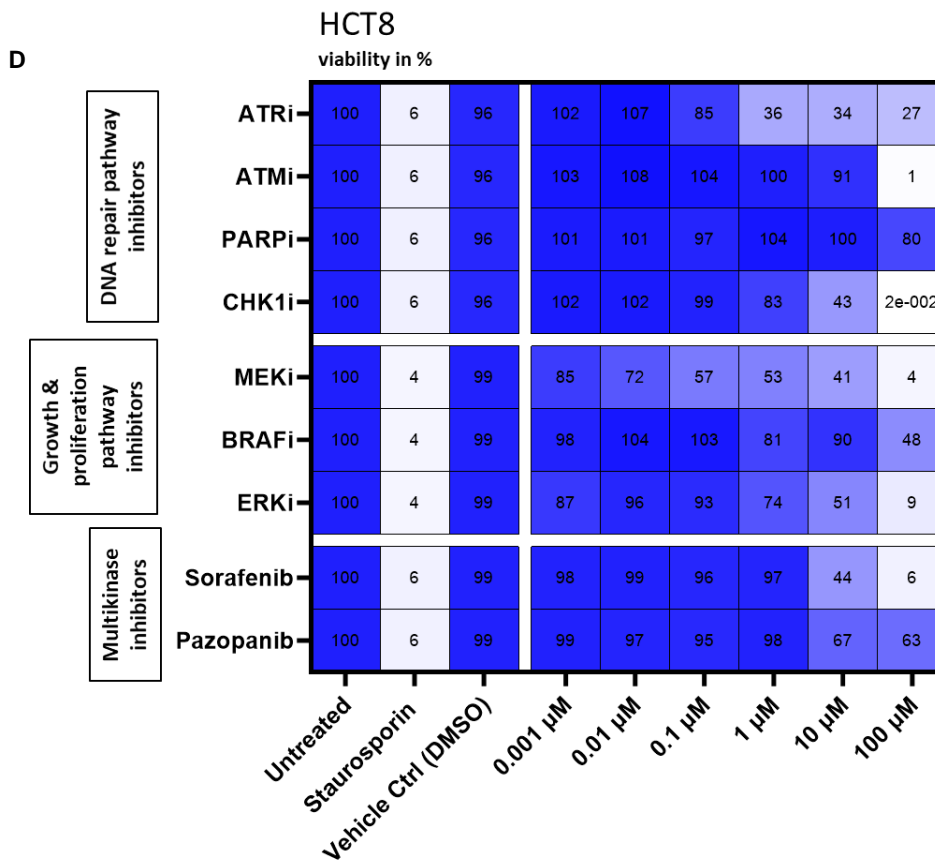
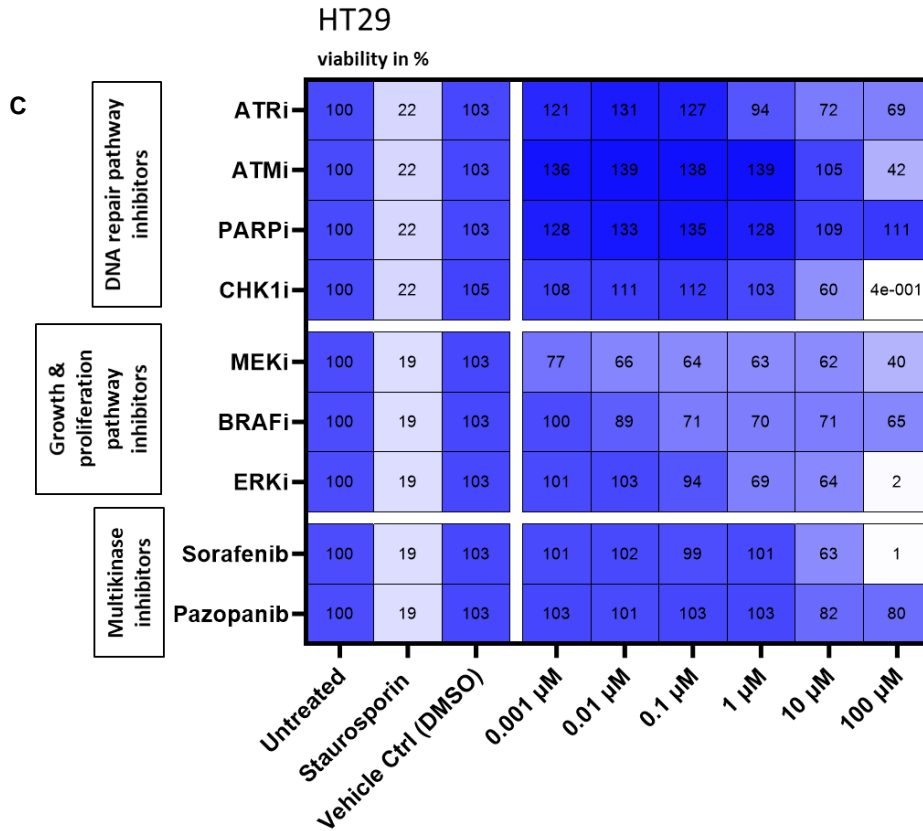


Figure 10: Drug screening on human CRC cell lines HT29 and HCT8

(A) Timeline for viability assessment. (B) Chemotherapy screening on HT29 and HCT8. (C) Small molecule inhibitor screening on HT29. (D) Small molecule inhibitor screening on HCT8.

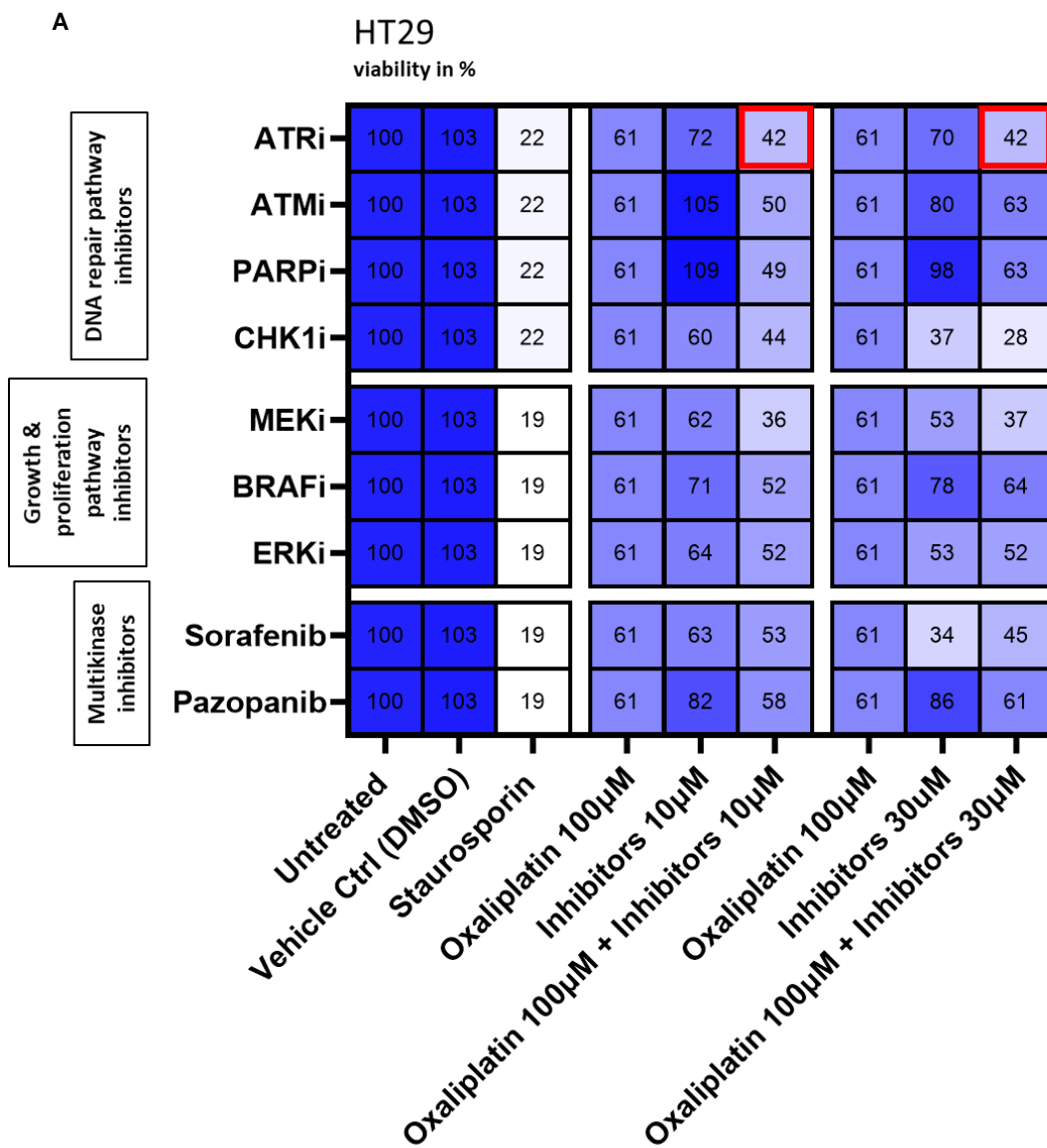
Numbers illustrate viability mean in % of one to three independent experiments in triplicates for chemotherapy screening and three independent experiments in triplicates for small molecule inhibitor screening.

4.2 Combination of Oxaliplatin and ATRi enhances cytotoxicity in human CRC cell lines

Furthermore, we explored the cytotoxic potential of drug combinations on CRC cell lines. Thereby, we used Oxaliplatin, a platinum-based agent commonly used for systemic chemotherapy and for HIPEC, together with the inhibitors tested above. Combination treatment resulted in increased cytotoxicity amongst all combinations but was less effective in the MSI cell line HCT8 (**Figure 11A & 11B**).

Compared to Oxaliplatin or inhibitor alone the greatest additive effect was observed with Oxaliplatin and ATRi (61% and 72% vs. 41%) or Oxaliplatin and MEKi (61% and 62% vs. 36%) in the MSS cell line HT29 (**Figure 11A**). Furthermore, increasing inhibitor concentrations did not provide additional benefit in the combination treatment.

Figure 11



B

HCT8
viability in %

	Untreated	Vehicle Ctrl (DMSO)	Staurosporin	Oxaliplatin 10µM	Inhibitors 10µM	Oxaliplatin 10µM + Inhibitors 10µM	Oxaliplatin 10µM	Inhibitors 30µM	Oxaliplatin 10µM + Inhibitors 30µM
ATRi	101	99	6	62	34	32	62	37	35
ATMi	101	99	6	62	91	57	62	56	44
PARPi	101	99	6	62	100	55	62	90	56
CHK1i	101	99	6	62	43	41	62	4	6
MEKi	101	99	5	62	41	35	62	31	24
BRAFi	101	99	5	62	90	52	62	89	49
ERKi	101	99	5	62	51	46	62	31	30
Sorafenib	101	99	5	62	44	45	62	9	14
Pazopanib	101	99	5	62	67	50	62	61	43

DNA repair pathway inhibitors

Growth & proliferation pathway inhibitors

Multikinase inhibitors

Figure 11: Exploration of combination drug screening Oxaliplatin + small molecule inhibitors
(A) Combination drug screen on MSS cell line HT29. **(B)** Combination drug screen on MSI cell line HCT8.
 Numbers illustrate viability mean in % of three independent experiments in triplicates.

At this point, we needed to decide which drug combination should be investigated in more detail. Based on literature search we learned that in other cancer settings, ATR is known to be involved in immunogenic changes, like PD-L1 upregulation (a molecule known to inhibit activated T-cell), whereas MEK varied depending on the experimental context. Since we seek to find a drug treatment which induces tumor-specific immunity, we decided to pursue Oxaliplatin in combination with ATRi. Prior to investigating the potential of Oxaliplatin with ATRi to induce immunogenic changes, we validated the enhanced cytotoxicity effect on different CRC cell lines. Therefore, we tested Oxaliplatin

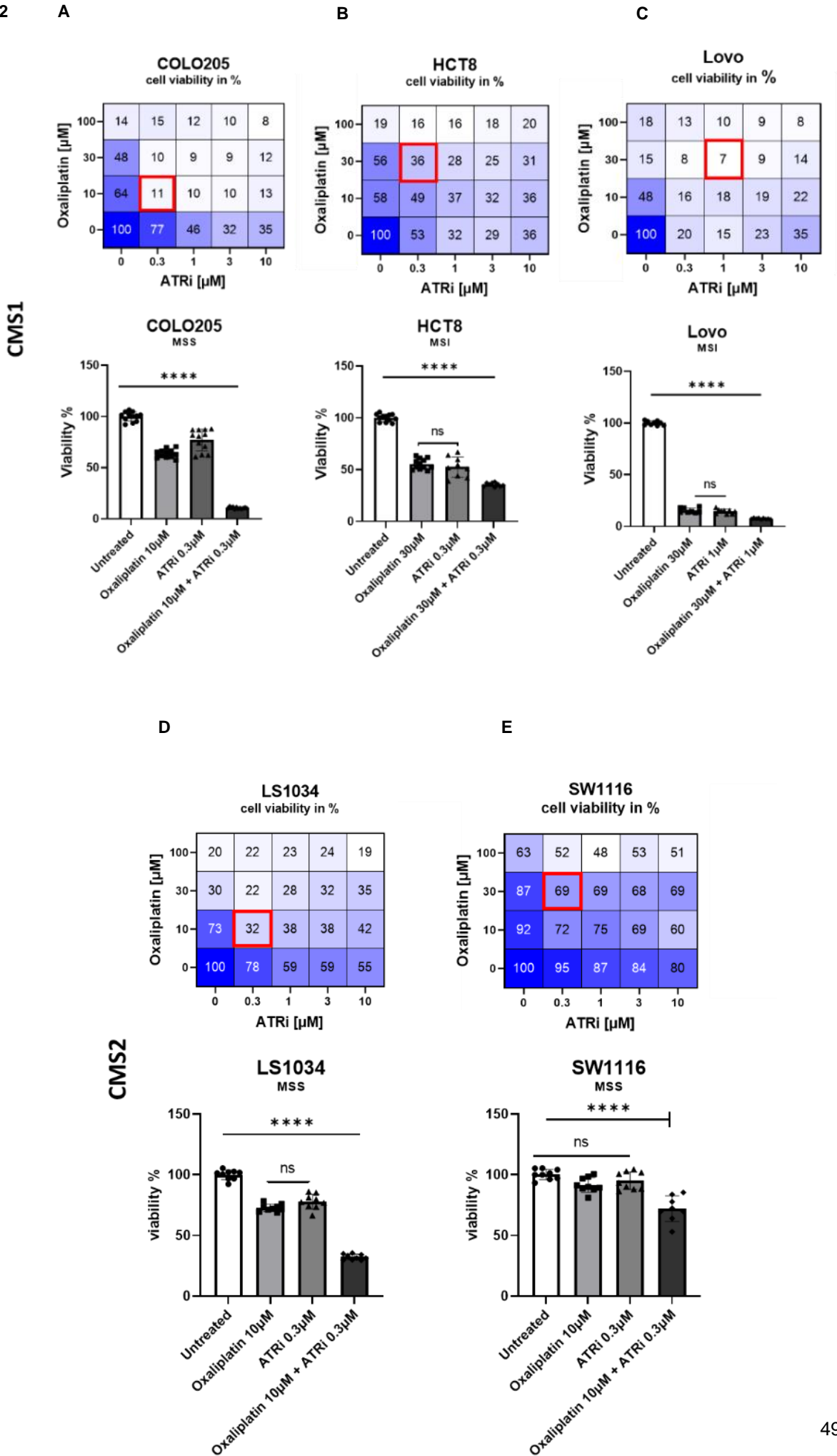
and ATRi in different concentrations on total nine human CRC cell lines. The chosen cell lines are shown in **Table 5** and represent all common driver mutations for CRC from all four CMS groups. Cell lines from CMS group 1, group 2 and group 3 demonstrated enhanced cytotoxicity after treatment with low ATRi concentrations (0.3-1 μ M) and low to moderate Oxaliplatin concentrations (10-30 μ M) (**Figure 12A-G**). Representative cell lines from CMS 4 revealed the greatest additive killing effect only with high Oxaliplatin doses (100 μ M) (**Figure 12H&I**). This is potentially explained due to the high sensitivity of CACO2 towards ATRi alone and the lack of responsiveness of SW480 towards Oxaliplatin. Furthermore, CACO2 appear to be already highly sensitive to ATRi alone like the MSI cell lines HCT8 (**Figure 12B**), LoVo (**Figure 12C**), and LS180 (**Figure 12G**). Taken together, this screening suggests that the combination of Oxaliplatin and ATRi results in enhanced cytotoxicity in a broad spectrum of MSS human CRC cell lines.

MUTANT GENE	CMS CLASSIFICATION								
	CMS 1			CMS 2		CMS 3		CMS4	
APC	COLO205	HCT8	LOVO	LS1034	SW1116	HT29	LS180	SW480	CACO2
TP53		HCT8		LS1034	SW1116	HT29		SW480	CACO2
ERBB2	COLO205						LS180	SW480	
KRAS		HCT8	LOVO	LS1034	SW1116		LS180	SW480	
PTEN							LS180		
BRAF	COLO205		LOVO			HT29	LS180		
MSS / MSI	MSS	MSI	MSI	MSS	MSS	MSS	MSI	MSS	MSS

Table 5: Overview of tested human CRC cell lines to validate enhanced cytotoxicity of Oxaliplatin + ATRi treatment

Table 1 contains 9 human CRC cell lines illustrated according to the CMS classification and labeled according to mutated genes and MSS / MSI status.

Figure 12



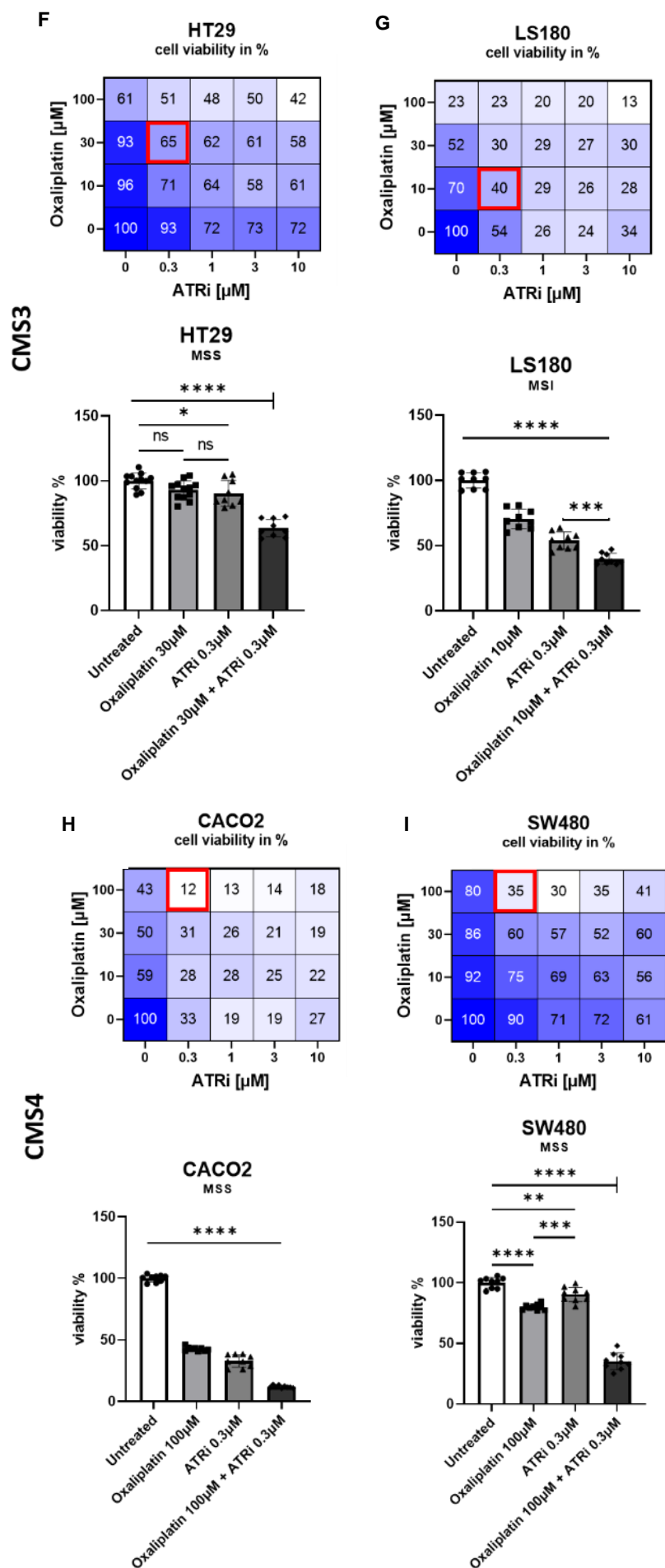


Figure 12: Enhanced cytotoxicity of Oxaliplatin in combination with ATRi on different human CRC cell lines

(A-I) Viability screening of different Oxaliplatin (10-100 μM) and ATRi (0.3-10 μM) concentrations on total nine different human CRC cell lines. The greatest additive cytotoxic effect is marked with a red square and additionally illustrated as bar graph. Numbers illustrate viability mean in % of three independent experiments in triplicates. Error bars show the mean \pm SD. **** = $p \leq 0.0001$, *** = $p \leq 0.001$, ** = $p \leq 0.01$, * = $p \leq 0.05$, ns = $p > 0.05$.

4.3 The combination of Oxaliplatin and ATRi shows enhanced cytotoxicity on Patient-derived PM organoids

After examining the cytotoxic effects of Oxaliplatin in combination with ATRi on CRC cell lines, we decided to examine this effect on patient material. Therefore, we used patient-derived PM organoids and treated them with similar Oxaliplatin and ATRi concentrations as the cell lines above (**Figure 13A**). Due to limited availability of organoids, we examined four different PM organoids (**Table 6**). Even though high Oxaliplatin doses (100 μ M) were needed, three of four PM organoids demonstrated additive cytotoxicity when treated with the combination treatment (**Figure 13B, 13D & 13E**). We assume that high doses of Oxaliplatin were needed, since the organoids were generated from patients that were heavily pre-treated with chemotherapies. Interestingly, one PM organoid harboring no relevant therapy mutations (KRAS, NRAS, BRAF and TP53 wildtype) showed significantly reduced viability when treated with ATRi alone (**Figure 13C**).

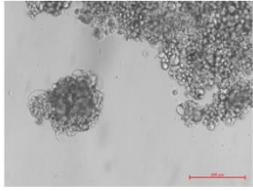
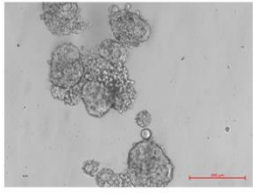
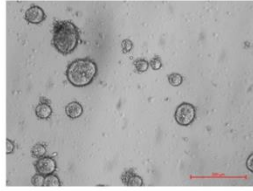
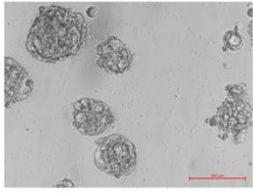
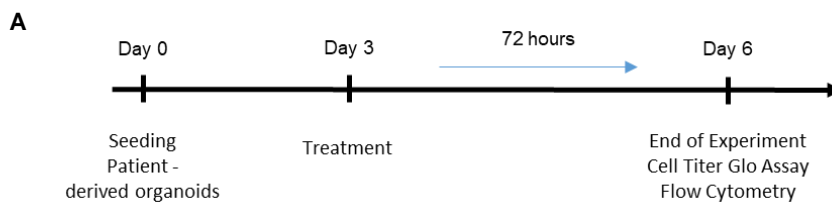
PATIENT-DERIVED PM ORGANOID INFORMATION				
USZ Name	Tumor Type	MSS / MSI *	Genetic alteration	Image
USZ.PM1	Metastatic Gastric cancer	MSS (Foundation assay)	TP53, ARID1A, CDH1	
USZ.PM2	Metastatic CRC	MS proficient (IHC)	No therapy relevant mutations (KRAS, NRAS, TP53, BRAF wt)	
USZ.PM3	Metastatic CRC	MS proficient (IHC)	No information available (external patient)	
USZ.PM4	Metastatic Small intestine cancer	MS proficient (IHC)	KRAS	

Table 6: Overview of patient-derived PM organoids

Table 2 contains information of four patient-derived PM organoids about their primary tumor type, MSS / MSI status, genetic alterations and representative images (bar scale 200µm).

*only with a Foundation assay (sequencing performed in Pathology Department) MSS or MSI status can be defined. If no sequencing was performed, MSS / MSI status is histologically checked.

Figure 13



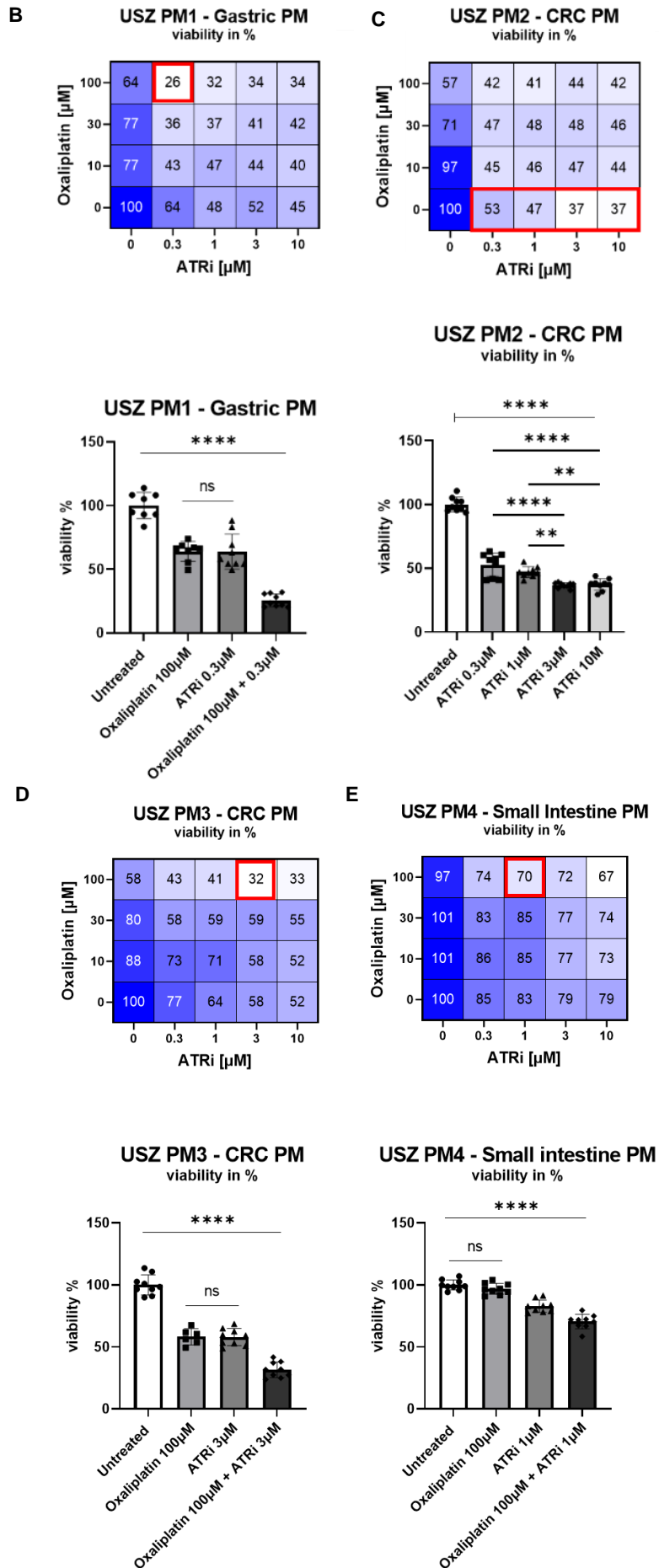


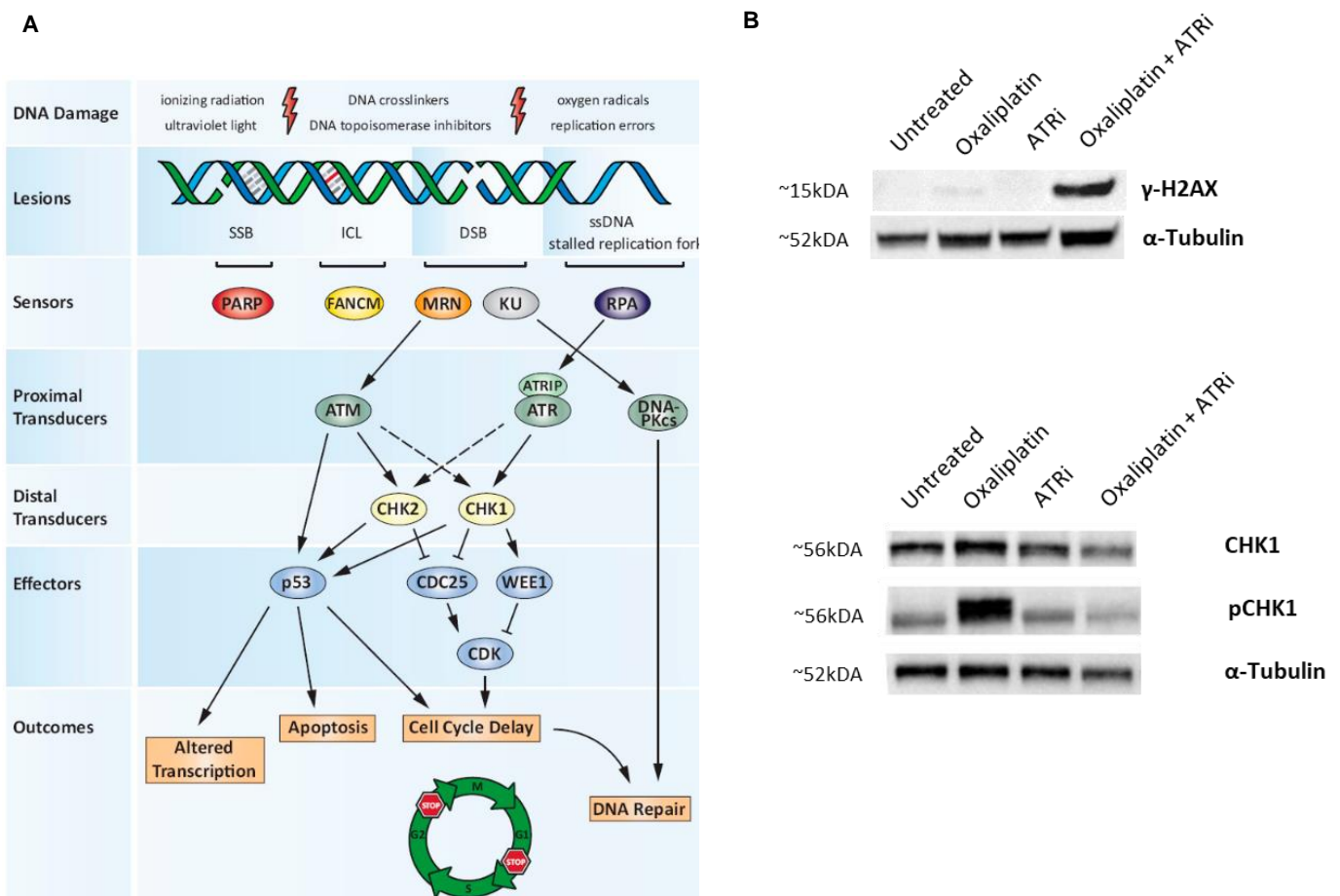
Figure 13: Enhanced cytotoxicity of Oxaliplatin in combination with ATRi on patient-derived PM organoids

(A) Timeline for viability assessment in PM organoids. (B-E) Viability screening of different Oxaliplatin (10-100 μM) and ATRi (0.3-10 μM) concentrations on four different patient-derived organoids. Greatest additive cytotoxic effect is marked with a red square and additionally illustrated as bar graph. Numbers illustrate viability mean in % of two to three independent experiments in triplicates. Error bars show the mean \pm SD. **** = $p \leq 0.0001$, *** = $p \leq 0.001$, ** = $p \leq 0.01$, * = $p \leq 0.05$, ns = $p > 0.05$.

4.4 Combination of Oxaliplatin and ATRi enhanced protein levels of DNA damage marker γ H2AX and lowered protein levels of pCHK1

To confirm that the combination of Oxaliplatin and ATRi block the DNA damage repair ATR-CHK1 pathway, we investigated the DNA damage marker γ H2AX and the activation of the ATR downstream target CHK1 at protein levels (**Figure 14A**). Western Blot analysis (**Figure 14B**) confirmed that Oxaliplatin induced pCHK1 activation is blocked when combined with ATRi, suggesting an inactivation of the ATR-CHK1 pathway upon combination treatment (**Figure 14D**). Furthermore, combination treatment leads to the highest expression of γ H2AX indicating that Oxaliplatin induces DNA damage, which cannot be repaired efficiently due to the addition of the inhibitor (**Figure 14C**). Moreover, both drugs do not have any significant impact on the inactivated non-phosphorylated form of CHK1 (**Figure 14E**). These results suggest that cells die due to accumulated DNA damage, which is not efficiently repaired.

Figure 14



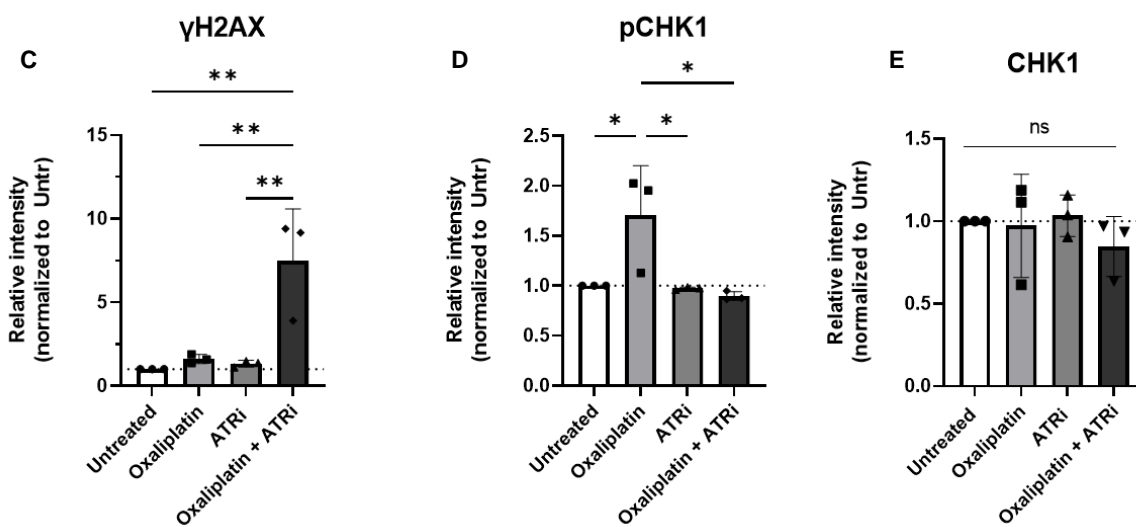


Figure 14: Analysis of DNA damage caused by Oxaliplatin and disrupted ATR-CHK1 Pathway by ATRi
(A) DNA damage repair pathway. Image source: (7) **(B)** Western Blot for DNA damage marker γ -H2AX and ATR downstream target CHK1 and phospho-CHK1. **(C-E)** Relative protein expression of γ -H2AX, pCHK1 and CHK1. Normalized to untreated condition. Cells were treated with $30\mu\text{M}$ Oxaliplatin and $10\mu\text{M}$ ATRi. One representative experiment out of two to three independent experiments. Error bars show the mean \pm SD. **** = $p \leq 0.0001$, *** = $p \leq 0.001$, ** = $p \leq 0.01$, * = $p \leq 0.05$, ns = $p > 0.05$.

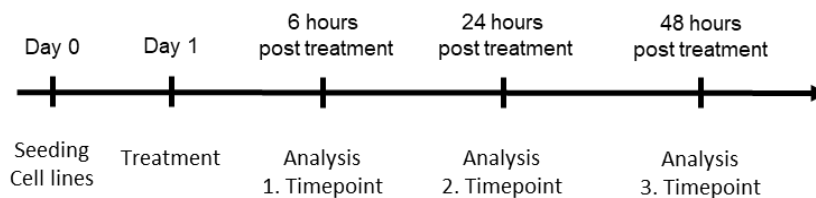
4.5 Combination of Oxaliplatin and ATRi leads to immunogenic changes on CRC cell lines

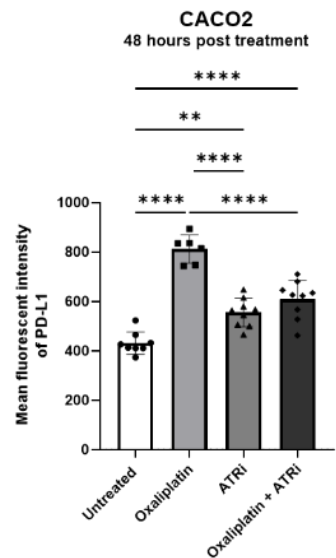
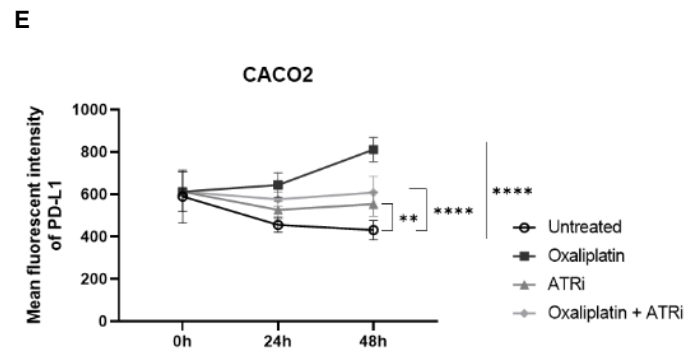
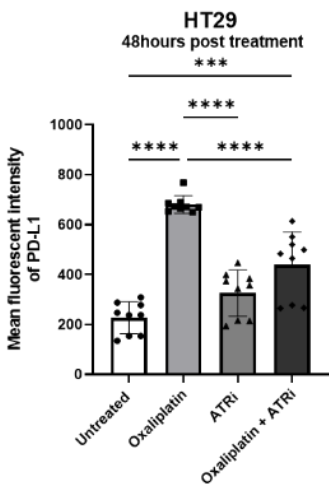
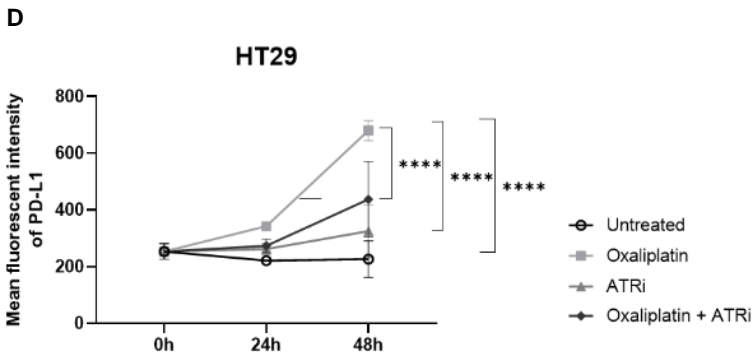
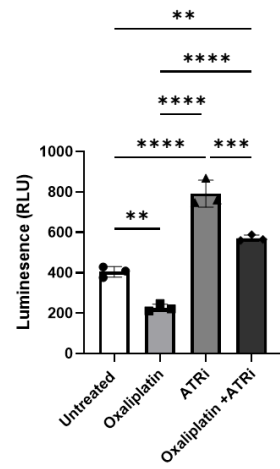
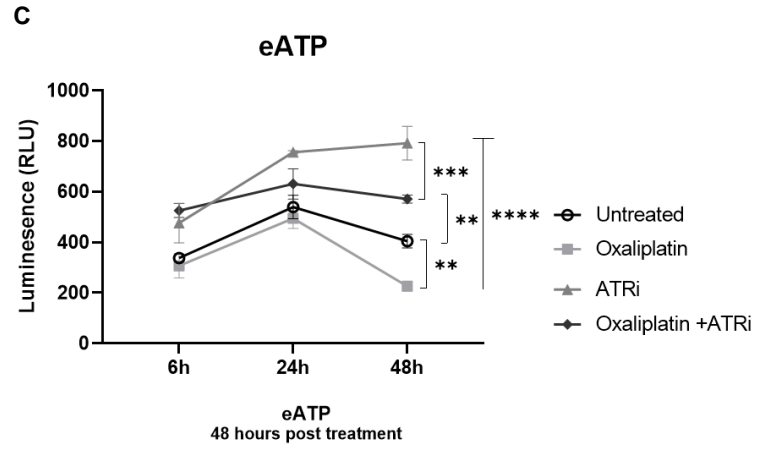
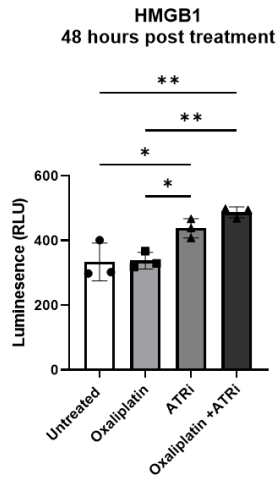
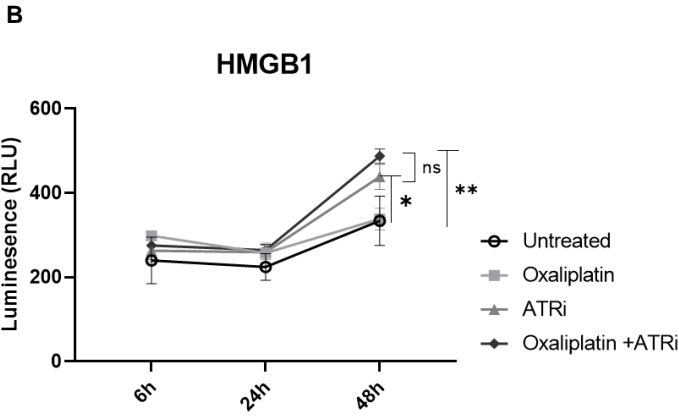
After confirming the ability of Oxaliplatin and ATRi to enhance cytotoxicity in a broad spectrum of CRC cell lines, we examined the potential of this combination to induce immunogenic changes. Therefore, we assessed the secretion of ICD molecules such as HMGB1 and eATP. Additionally, we investigated the expression of antigenicity marker MHC class I and checkpoint molecules like PD-L1, Galectin-9, CD80 and CD86 at 6, 24 and 48 hours post treatment (**Figure 15A**). Since mainly CRC from CMS4 and partially CMS3 are known to metastasize to the peritoneum, we decided to use CACO2, SW480 and HT29 cell lines for this set of experiments. Gating strategy for flow cytometry analysis is shown in **Figure 15L**.

Using HT29 cells, we noticed that HMGB1 and eATP were elevated 48 hours after ATRi or combination treatment (**Figure 15B & 15C**). In addition, Oxaliplatin induced PD-L1 upregulation, which was blocked when ATRi was added (**Figure 15D**). The latter was also observed on CACO2 cells (**Figure 15E**). On the contrary, the expression of other checkpoint molecules like Galectin-9, CD80 and CD86 were increased in the combination treatment compared to other treatment groups (**Figure 15F-H**). Furthermore, Oxaliplatin induced MHC class I upregulation in HT29, CACO2 and SW480 was significantly reduced in combination with ATRi (**Figure 15I-K**). This data suggests that the combination treatment of Oxaliplatin and ATRi leads to expression of pro-immunogenic and anti-immunogenic molecules suggesting a complex and dynamic interplay of these molecules skewing immune responses.

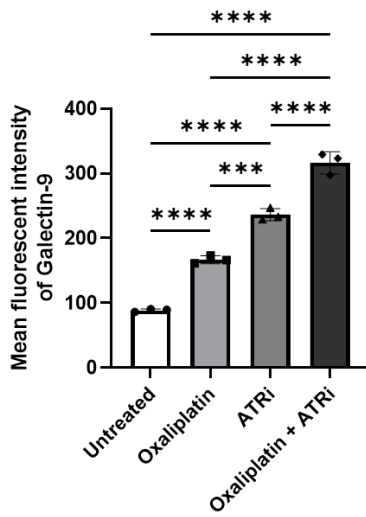
Figure 15

A

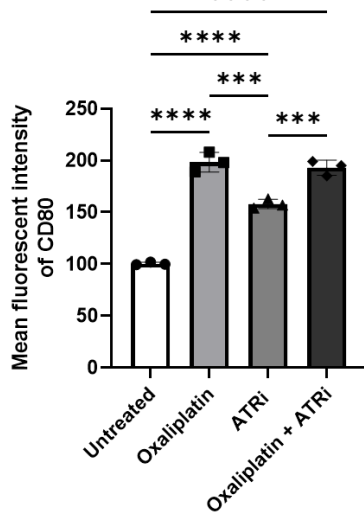




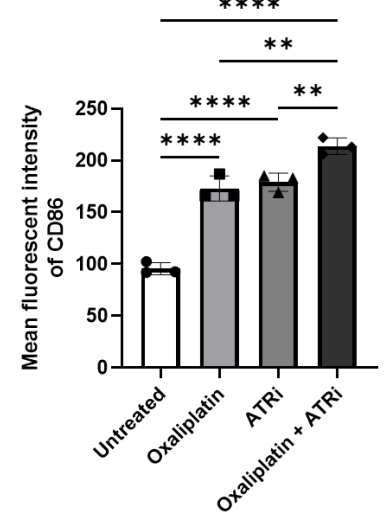
F Galectin-9
48 hours post treatment



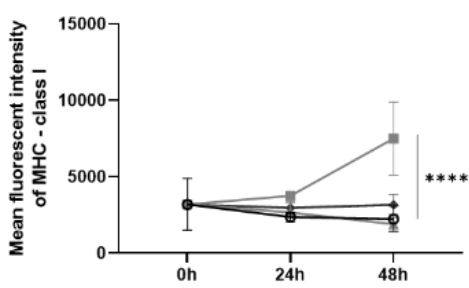
G CD80
48 hours post treatment



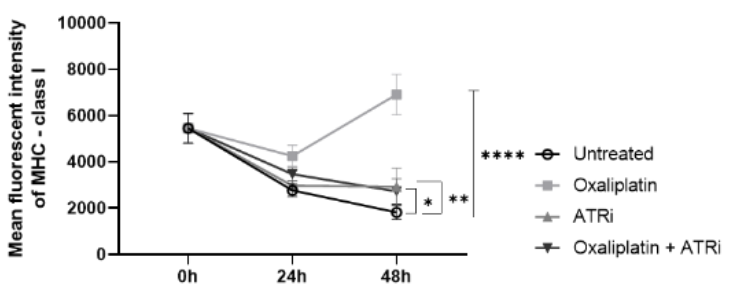
H CD86
48 hours post treatment



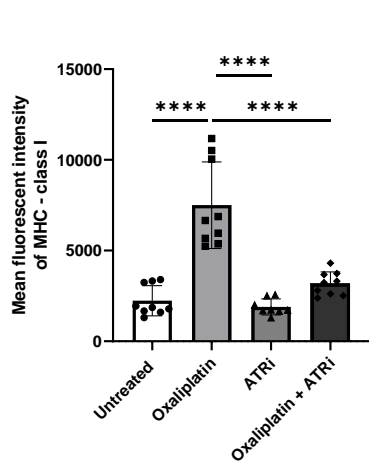
I HT29



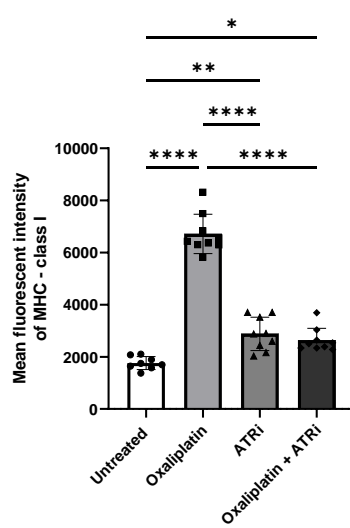
J CACO2



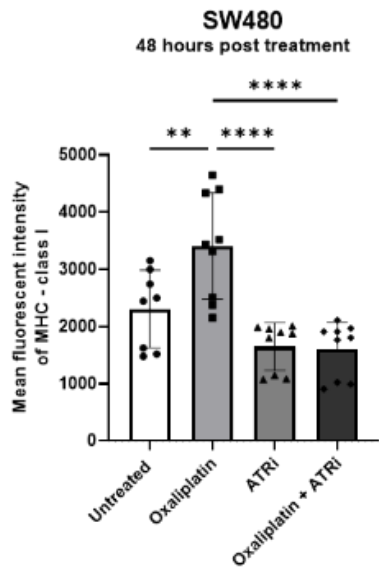
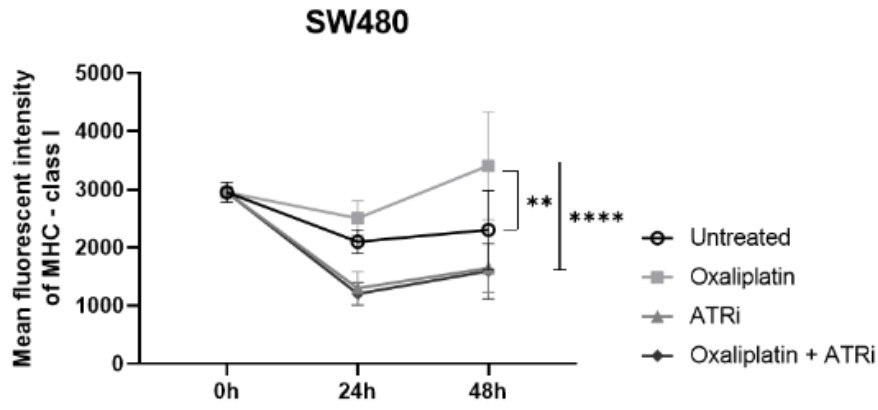
HT29
48 hours post treatment



CACO2
48 hours post treatment



K



L

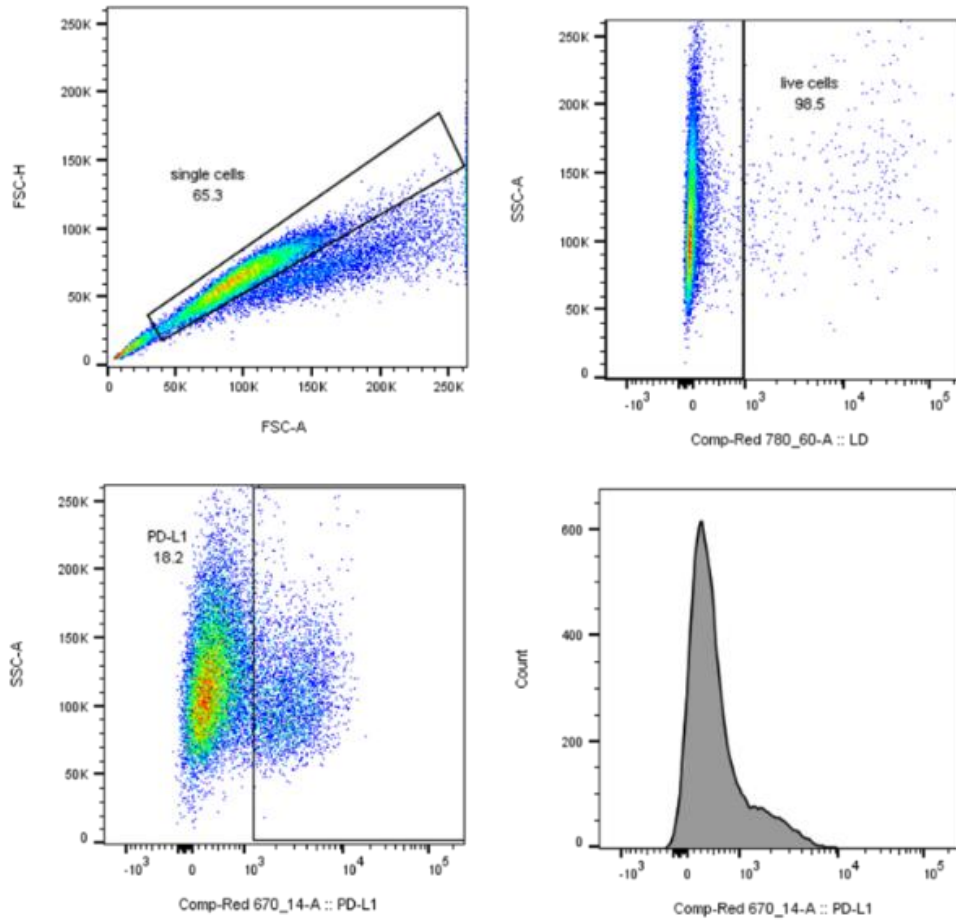


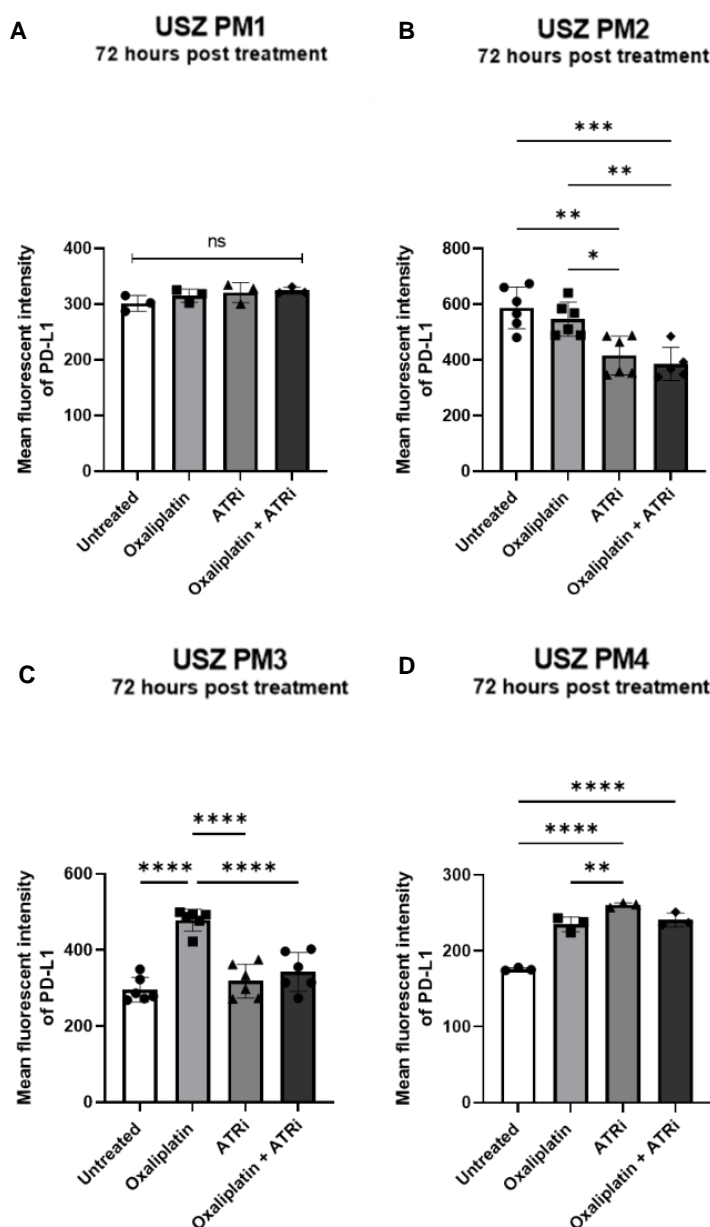
Figure 15: Immunogenic changes on CRC cell lines after treatments

(A) Timeline for experiment with possible analysis time points. **(B)** HMGB1 analysis of Oxaliplatin 30 μ M and ATRi 0.3 μ M treated HT29 cells after 6, 24 and 48 hours with Lumit Immunoassay. 48 hours post treatment additionally illustrated as bar graph. **(C)** eATP analysis of Oxaliplatin 30 μ M and ATRi 0.3 μ M treated HT29 cells after 6, 24 and 48 hours with Real-Time-Glo Assay. 48 hours post treatment additionally illustrated as bar graph. **(D-E)** Flow cytometry data of PD-L1 expression after 24 and 48 hours on HT29 and CACO2 cells. Cells were treated with 30 μ M Oxaliplatin / 10 μ M ATRi and 10 μ M Oxaliplatin / 0.3 μ M ATRi, respectively. 48 hours post treatment additionally illustrated as bar graph. **(F-H)** Flow cytometry data of Galectin-9, CD80 and CD86 analysis 48 hours post treatment with 30 μ M Oxaliplatin and 10 μ M ATRi. **(I-K)** Flow cytometry data of MHC-1 expression after 24 and 48 hours on HT29, CACO2 and SW480 cells. Cells were treated with 30 μ M Oxaliplatin / 10 μ M ATRi (HT29 & SW480) and 10 μ M Oxaliplatin / 0.3 μ M ATRi (CACO2). 48 hours post treatment additionally illustrated as bar graph. **(L)** Gating strategy, representative example for PD-L1 gating on HT29 cells (Exclusion of debris, only considered living cells). Same gating strategy was used for other cell lines (CACO2, SW480), patient-derived organoids and for other markers (MHC class-I, Galectin-9, CD80 and CD86). One to three independent experiments with triplicates were performed. Error bars show the mean \pm SD. **** = $p \leq 0.0001$, *** = $p \leq 0.001$, ** = $p \leq 0.01$, * = $p \leq 0.05$, ns = $p > 0.05$.

4.6 The combination treatment prevents Oxaliplatin-mediated upregulation of MHC class I and PD-L1 in patient-derived PM organoids and in murine CRC cell lines

To understand if the complex interplay between pro- and anti-immunogenic signals is also found in patient material, we investigated the expression of MHC class I and PD-L1 on our patient-derived PM organoids. Interestingly, USZ PM2 and USZ PM3 originating from a primary CRC showed a similar expression pattern as human CRC cell lines. Oxaliplatin induced also an upregulation of MHC class I and PD-L1 that was significantly reduced in combination with ATRi in USZ PM3 (**Figure 16C & 16G**). USZ PM2 significantly decreased the expression when treated with ATRi or the combination treatment (**Figure 16B & 16F**). Whereas the expression pattern of USZ PM1 (Gastric cancer as primary) was not affected by the treatment (**Figure 16A & 16E**) and USZ PM4 (Small intestine as primary) showed even an increase of MHC class-I and PD-L1 expression when treated with the combination treatment. (**Figure 16D & 16H**).

Figure 16



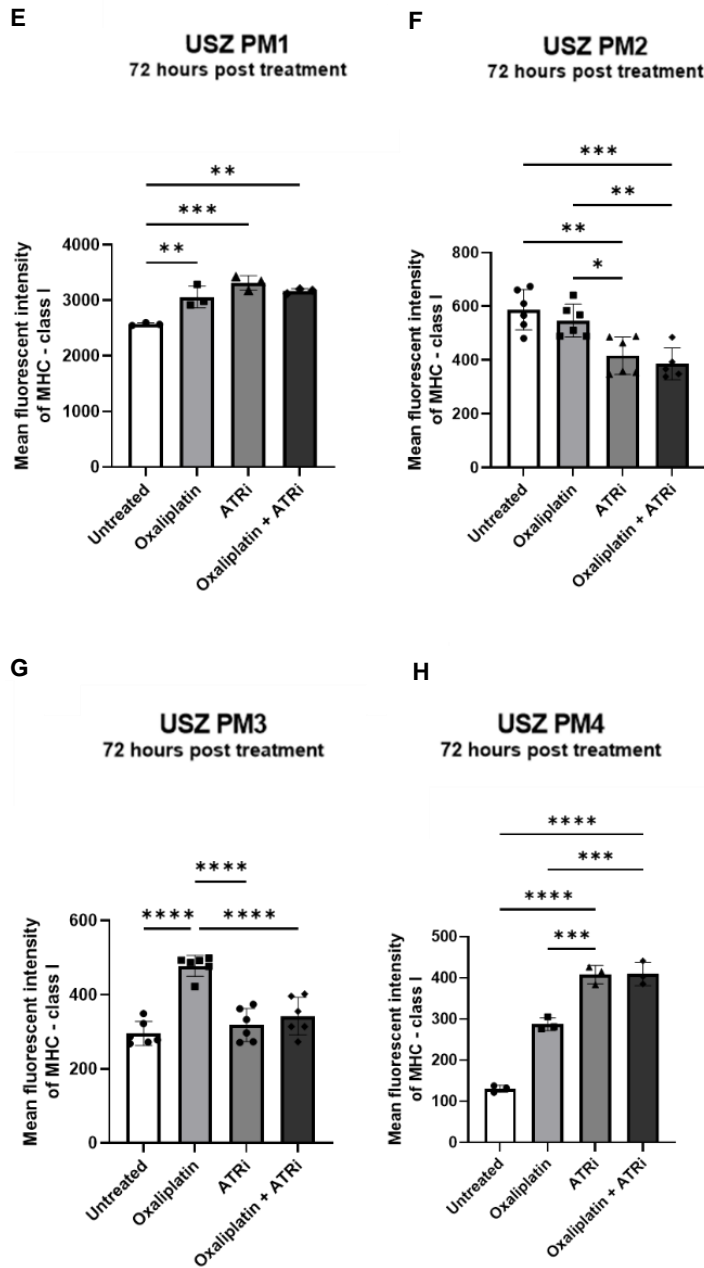


Figure 16: Immunogenic alterations in patient-derived organoids

(A-D) Flow cytometry data of PD-L1 expression 72 hours post treatment on patient-derived organoids. (E-H) Flow cytometry data of MHC class-I expression 72 hours post treatment on patient-derived organoids. Organoids were treated with 30 μ M Oxaliplatin and 10 μ M ATRi. Gating strategy according to Figure 6L. One to two independent experiments with triplicates were performed. Error bars show the mean +/-SD. **** = $p \leq 0.0001$, *** = $p \leq 0.001$, ** = $p \leq 0.01$, * = $p \leq 0.05$, ns = $p > 0.05$.

Prior performing *in vivo* experiments, we also examined MHC class I (H-2Kb/H-2Db for murine cells) and PD-L1 expression on murine CRC cell line MC-38. Therefore, we treated the murine cell line *in vitro* and confirmed that Oxaliplatin promotes the upregulation of MHC class I and PD-L1, which is blocked in combination with ATRi (**Figure 17A-D**). These experiments suggest that human CRC cell lines, patient-derived CRC PM organoids and murine CRC cell lines have similar expression pattern of pro- and anti-immunogenic molecules.

Figure 17

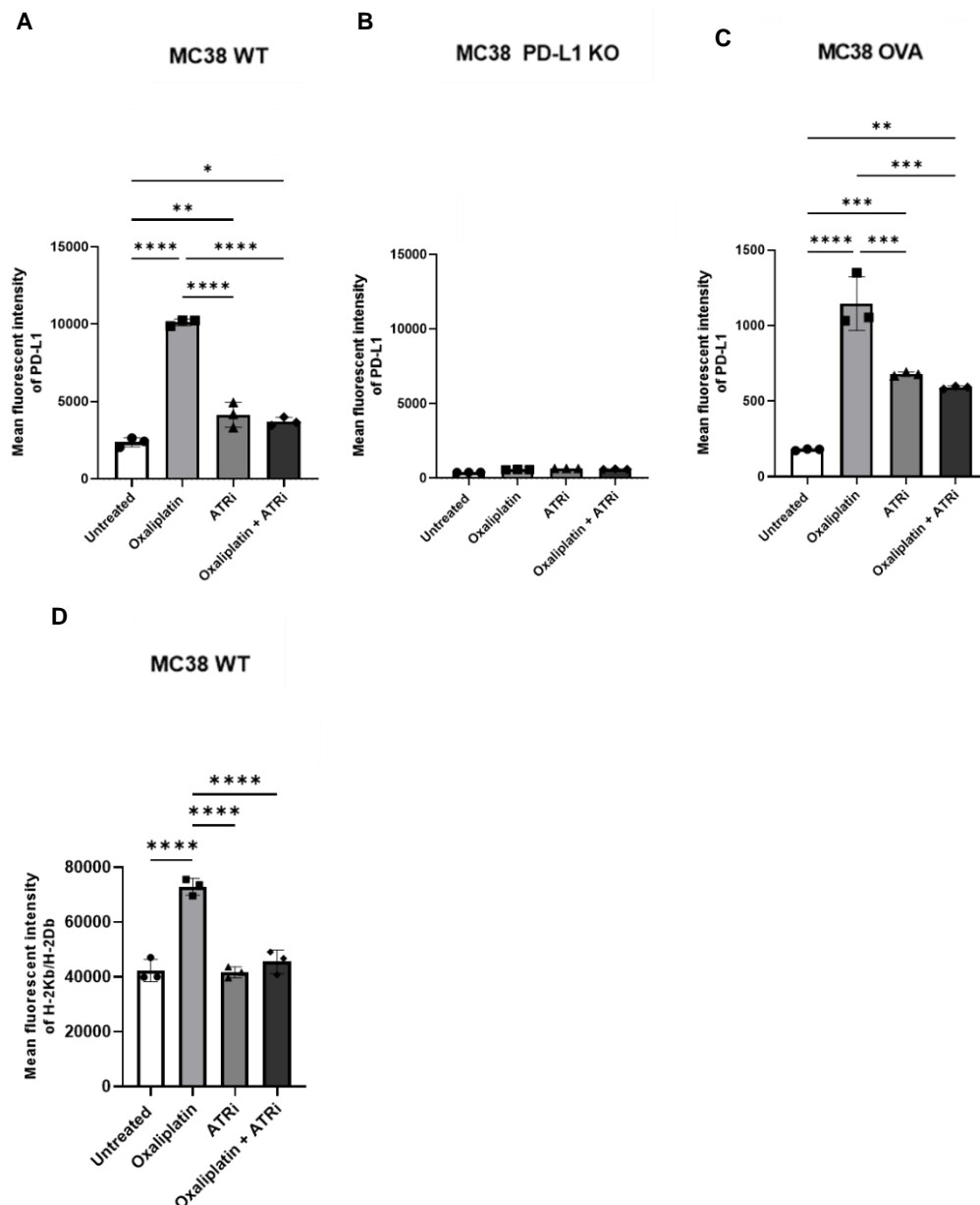


Figure 17: Modulation of PD-L1 expression on murine CRC cell line MC38

(A-C) Flow cytometry data of PD-L1 expression after 48 hours on MC38 wildtype, PD-L1 KO and OVA cell line. Cells were treated with 30 μ M Oxaliplatin and 10 μ M ATRi. **(D)** Flow cytometry data of H-2Kb/H2Db expression after 48 hours on MC38 wildtype cell line. Cells were treated with 30 μ M Oxaliplatin and 3 μ M ATRi. Gating strategy according Figure 6L. One experiment with triplicates was performed. Error bars show the mean \pm SD. **** = $p \leq 0.0001$, *** = $p \leq 0.001$, ** = $p \leq 0.01$, * = $p \leq 0.05$, ns = $p > 0.05$.

4.7 Oxaliplatin in combination with ATRi facilitates enhanced recognition of tumor cells by antigen-specific CD8+T cells *in vitro*

Having observed that Oxaliplatin in combination with ATRi is able to induce both, pro- and anti-immunogenic changes, we were interested to understand the subsequent functional consequences, for example whether such changes enhance killing of tumor cells by CD8+T cells or prevent it. To do so, we co-cultured treated MC38-OVA cells (expressing ovalbumin as a target antigen) with MACS-purified OT-I CD8+ T-cells (transgenic CD8+T cells that are specifically able to recognize OVA) for 6 hours (**Figure 18A**). As shown in **Figure 18B**, we noticed increased cell death in all treated groups when OT-1 CD8+ T-cells were added. Whereas cells treated with the combination of Oxaliplatin and ATRi showed the greatest killing capacity compared to single drug treated cells. This indicates that even though pro- and anti- immunogenic changes occur after treatment, Oxaliplatin in combination

with ATRi promotes recognition of cancer cells by antigen-specific CD8+T cells.

Figure 18

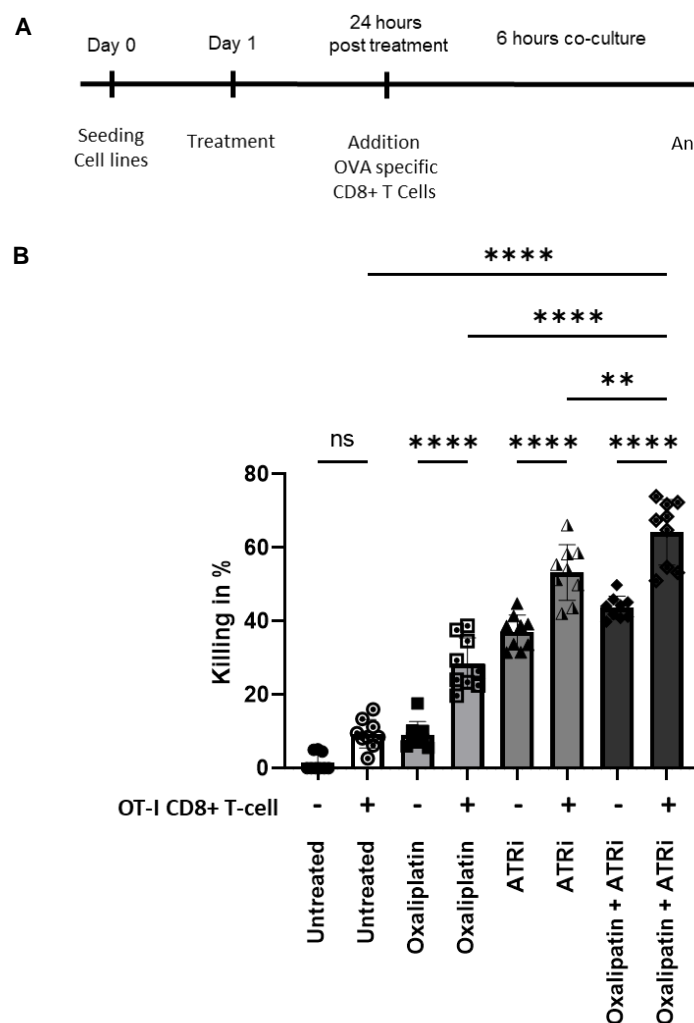


Figure 18: CD8+ T-cell specific killing after treatments

(A) Timeline of co-culture experiment. (B) Analysis of dead cancer cells after six hours of co-culture with MACS purified CD8+ T cells. Cancer cells were pre-treated with 10µM Oxaliplatin and 0.3µM ATRi. Three independent experiments with triplicates were performed. Error bars show the mean +/-SD. **** = p ≤ 0.0001, *** = p ≤ 0.001, ** = p ≤ 0.01, * = p ≤ 0.05, ns = p > 0.05.

4.8 Development of PM mouse model

In order to validate our findings *in vivo*, we established a PM mouse model (**Figure 19A**). To develop PM, we inject tumor cells directly intraperitoneally. Using different cell numbers, mouse strains and timepoints for harvest, we managed to develop a reliable model to test our treatments. Tumor lesions grew at various locations in the abdominal cavity of our mouse model, but were pre-dominantly found below the spleen at the omentum, between the small intestine at the mesentery and below the liver. The initial idea to assess tumor development was using an *in vivo* imaging system (IVIS) approach. However, this turned out to be inaccurate due to potential signal covering by other organs. Therefore, we started to use the peritoneal cancer index (PCI) (**Figure 19B**). PCI is normally used in clinical practice to assess tumor load within the peritoneal cavity. Thereby, the abdomen is divided into different sections that can be scored from 0-3 depending on the size and number of lesions. The sum of all scores represents the PCI score. However, evaluating the PCI score is subjective, thus can differ between researchers and affect reproducibility and accuracy. Therefore, we additionally measure the tumor weight of the peri-splenic site in order to improve tumor load assessment.

Figure 19

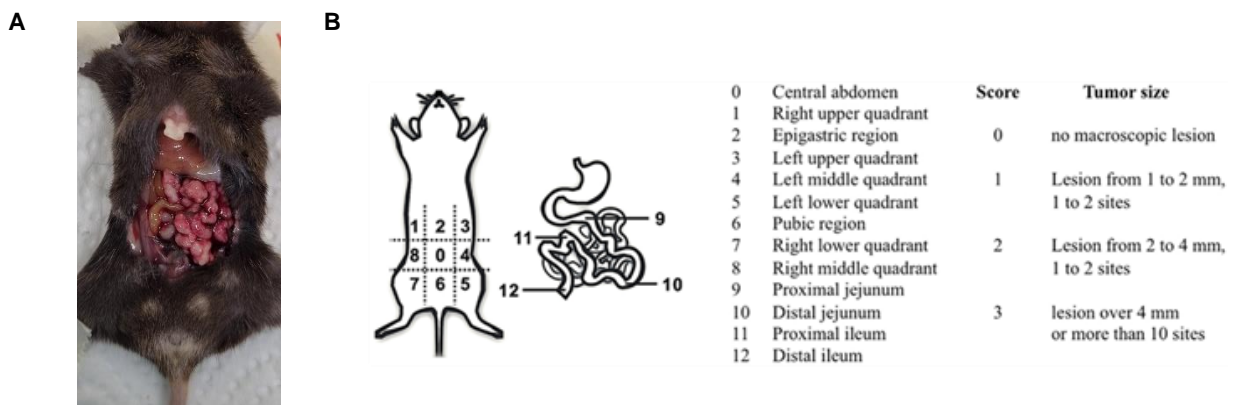


Figure 19: PM mouse model

(A) Representative picture of PM mouse model 15 days after tumor cell injection. **(B)** PCI legend (1) and PCI scoring system.

4.9 Enhanced control of PM lesions in PM mouse model upon combination treatment

Our *in vitro* data revealed that Oxaliplatin in combination with ATRi results in enhanced cytotoxicity and promoted immunogenic cell death. To examine the efficacy of this drug combination on tumor growth, we tested this drug combination in our PM mouse model. To do so, six days after i.p. tumor cell injection, mice received three times 5mg/kg Oxaliplatin every third day and daily 15mg/kg ATRi until the end of the experiment on day 15 as shown in **Figure 20A**. To quantify tumor load, the murine PCI score was assessed during harvest. As shown in **Figure 20B**, PCI score already decreased when mice were treated with either Oxaliplatin or ATRi alone, but the greatest treatment effect was observed in the combination (Oxaliplatin + ATRi) treatment. As mentioned above, the assessment of the PCI is subjective, therefore we additionally measure the tumor weight of the lesions growing in the peri-splenic region. Measuring the tumor weight, we observed that mice receiving the combination treatment had the smallest tumors (**Figure 20C**). This data suggests that the combination of Oxaliplatin and ATRi can significantly reduce tumor growth *in vivo*.

Figure 20

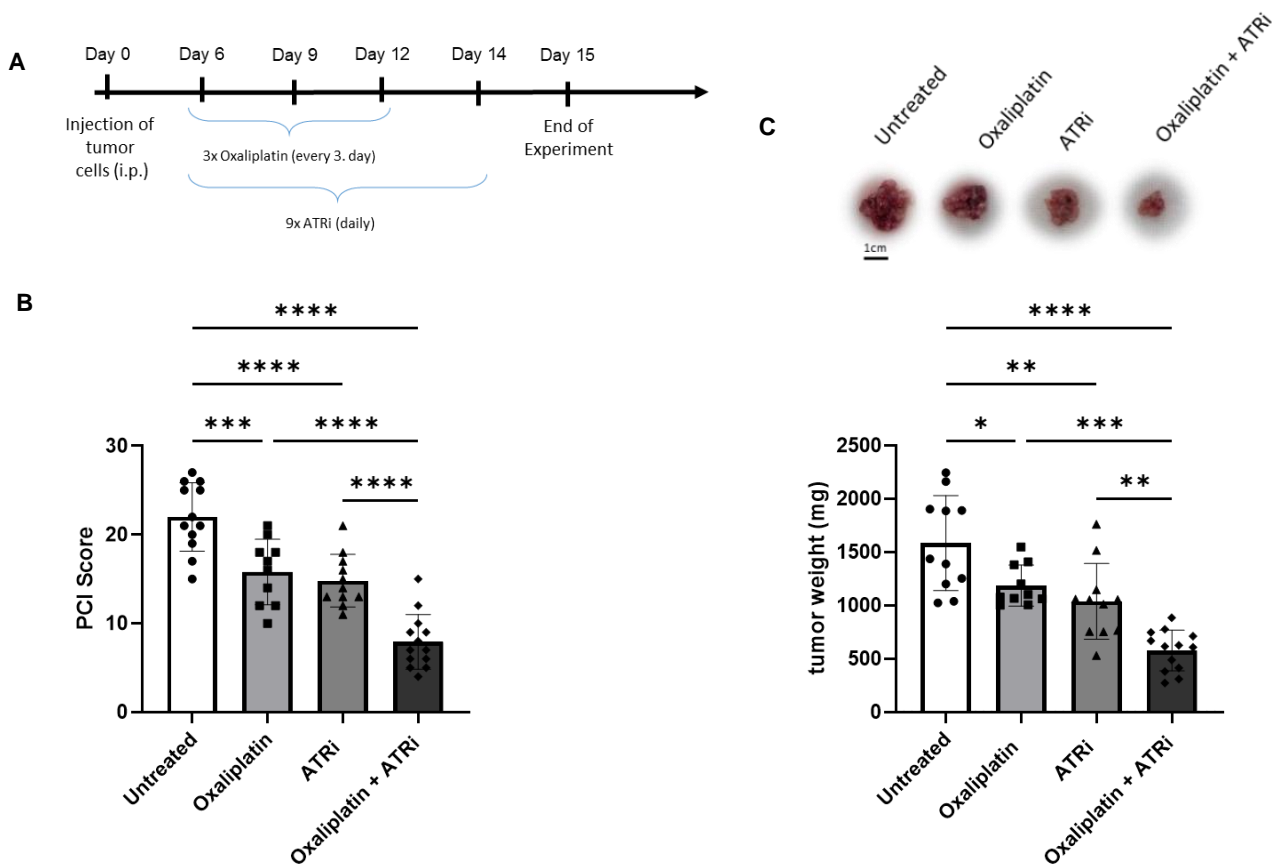


Figure 20: Treatment of PM lesions in a mouse model

(A) Timeline of experiment. (B) PCI score of treated mice. (C) Representative pictures of PM lesions from peri-splenic region (scale bar 1cm) and weight of peri-splenic tumors. Each dot represents one mouse. All groups n = 10. Error bars show the mean +/-SD. **** = p<0.0001, *** = p<0.001, ** = p<0.01, * = p<0.05, ns = p>0.05.

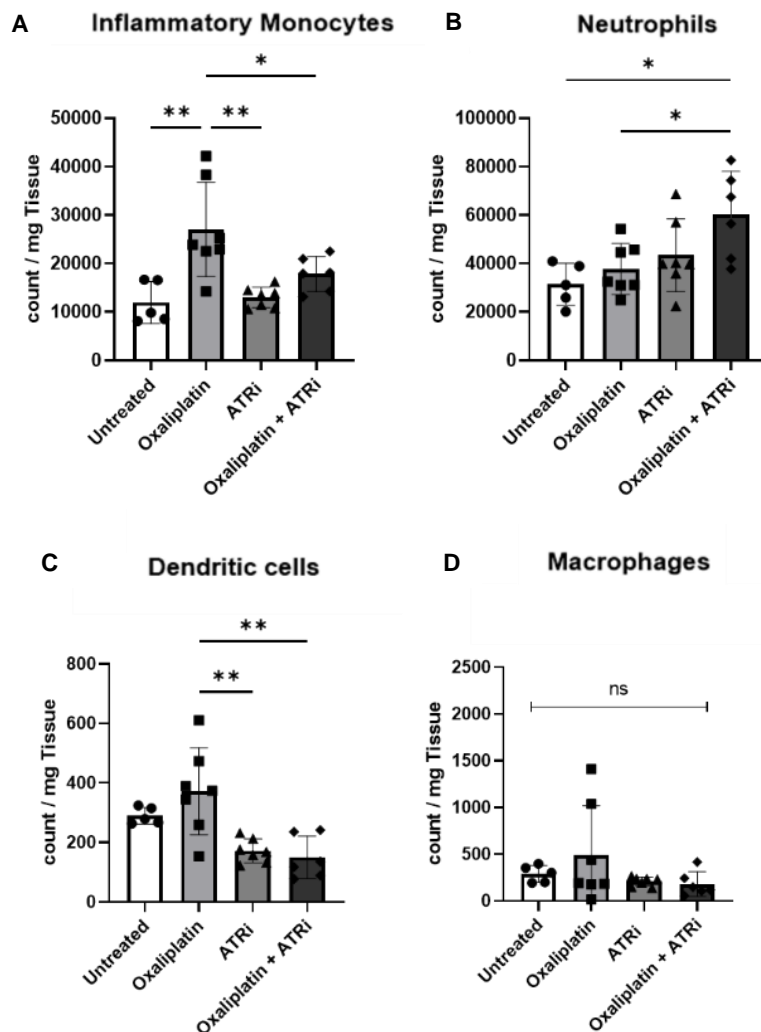
4.10 Characterization of mouse PM tumor microenvironment (TME)

To understand how the combination treatment is superior to single treatment, we were interested in immunological changes within the TME after treatments at day 15. To characterize immune cell composition, tumor lesions were collected and prepared for flow cytometry analysis. Gating strategy is shown in **Figure 21L**. The number of total immune cells (CD45+), macrophages (CD11b+, Ly6C-, CD11c-, I-A,I-E+), NK cells (NK1.1+), B-cells (CD19+), cytotoxic T-cells (CD8+) and T-regulatory cells (CD4+ FoxP3+) did not change significantly across all treatment groups (**Figure 21D, 21E, 21G, 21H, 21J**). However, Neutrophils (CD11b+, Ly6G+) and NK-T-cells (NK1.1+, CD3+) increased (**Figure 21B & 21F**) and T-helper cells decreased (CD4+) (**Figure 21I**) in the combination treatment compared to untreated mice. Furthermore, inflammatory Monocytes (CD11b+, Ly6Chi) and Dendritic cells (I-A,I-E+, CD11c+) were enriched in Oxaliplatin treated mice (**Figure 21A & 21C**). Interestingly, the CD8+/T-regulatory cell ratio

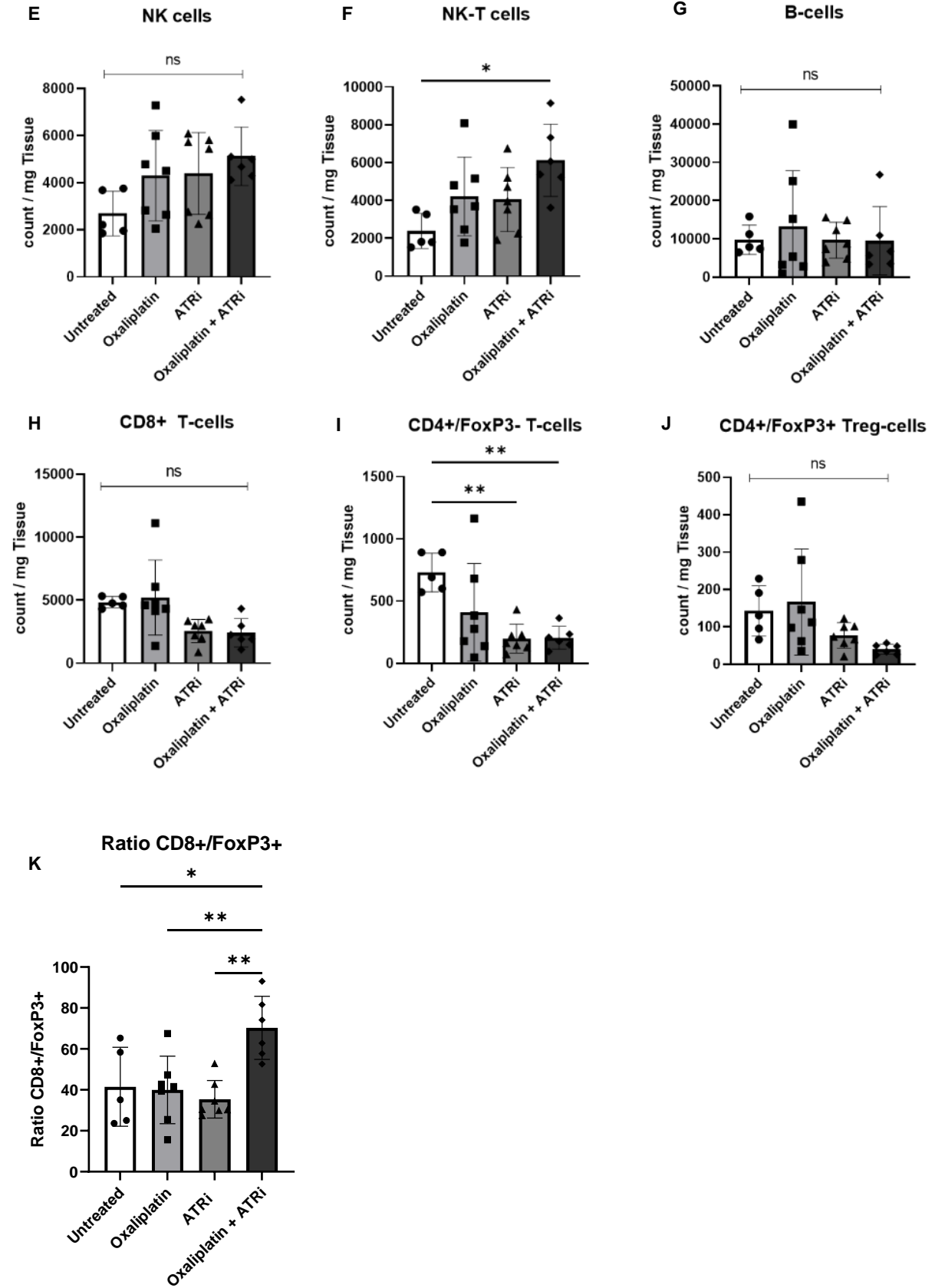
significantly increased in mice treated with Oxaliplatin and ATRi combination (**Figure 21K**), leading to the hypothesis that CD8+ T cells might be less inhibited by T-regulatory cells and are therefore able to control tumor growth better.

Figure 21

Myeloid Cells



Lymphoid Cells



L

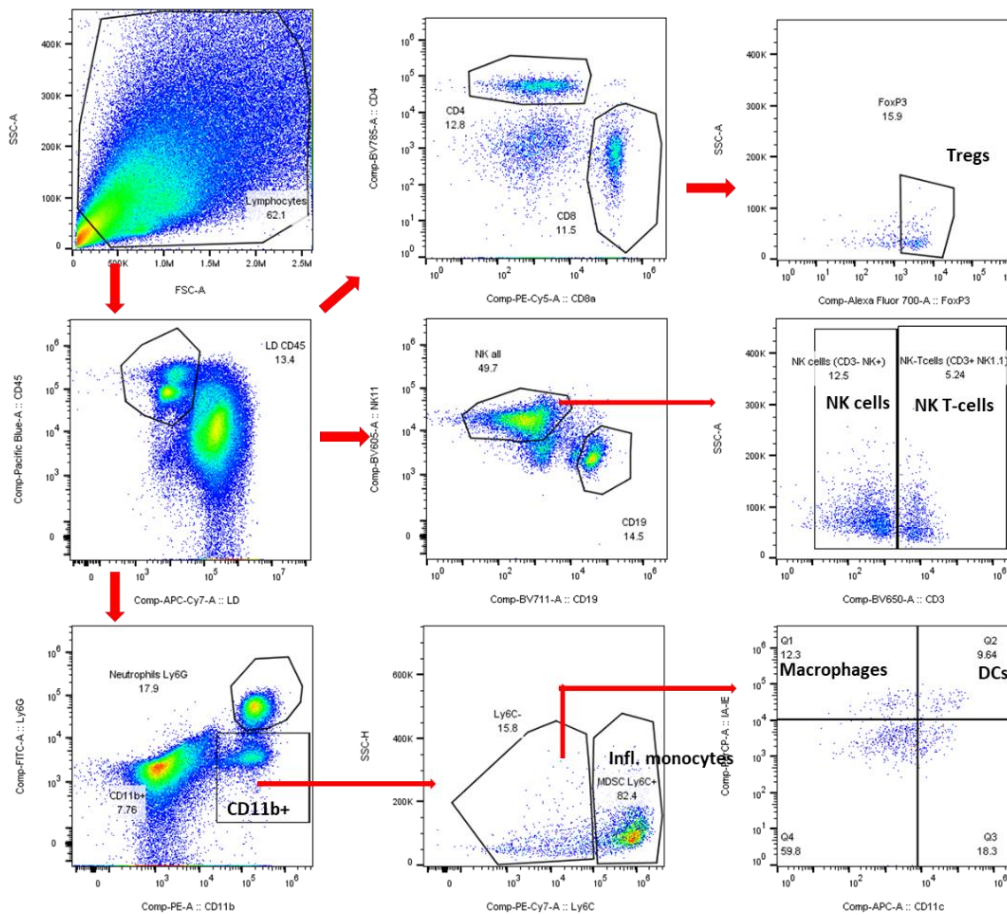
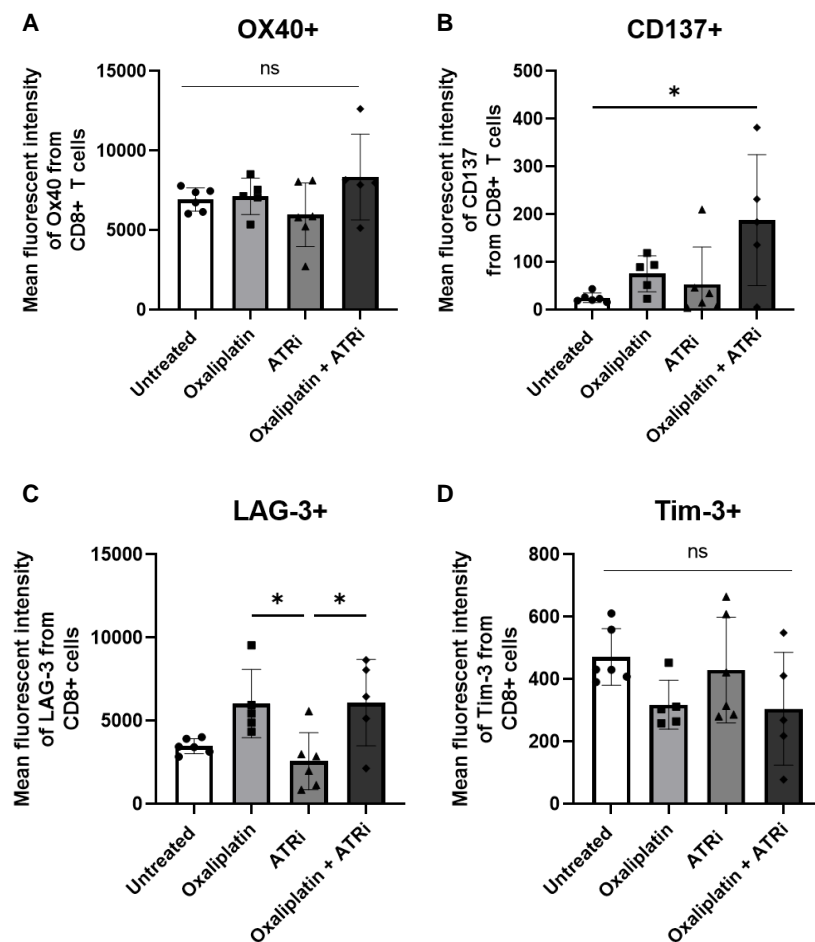


Figure 21: Immune cell composition of PM lesions after treatment

(A-D) Flow cytometry data (count) of myeloid cells within PM lesions. **(E-J)** Flow cytometry data (count) of lymphoid cells within PM lesions. **(K)** CD8+ T-cell / FoxP3+ T-regulatory cell ratio. **(L)** Gating strategy to characterize PM lesions (Exclusion of debris, only considered living immune cells). Each dot represents one mouse ($n = 5-7$). Error bars show the mean \pm SD. **** = $p \leq 0.0001$, *** = $p \leq 0.001$, ** = $p \leq 0.01$, * = $p \leq 0.05$, ns = $p > 0.05$.

Since functional and activation status of immune cells are relevant to control tumor growth, we assessed CD8+ T-cells for activation and exhaustion markers at day 15. Gating strategy is shown in **Figure 22H**. As illustrated in **Figure 22**, T-cell activation marker CD137 in combination treated mice is enriched compared to untreated mice (**Figure 22B**). However, OX40, another T-cell activation marker, did not significantly differ within the treatment groups (**Figure 22A**). Furthermore, exhaustion marker PD-1 was elevated within tumors of those mice that were treated with the combination treatment compared to untreated and ATRi treated mice, but not Oxaliplatin treated mice (**Figure 22E**). Other exhaustion markers such as CD39, Tim-3 and LAG-3 did not differ to untreated and Oxaliplatin treated mice (**Figure 22C, 22D & 22F**).

Figure 22



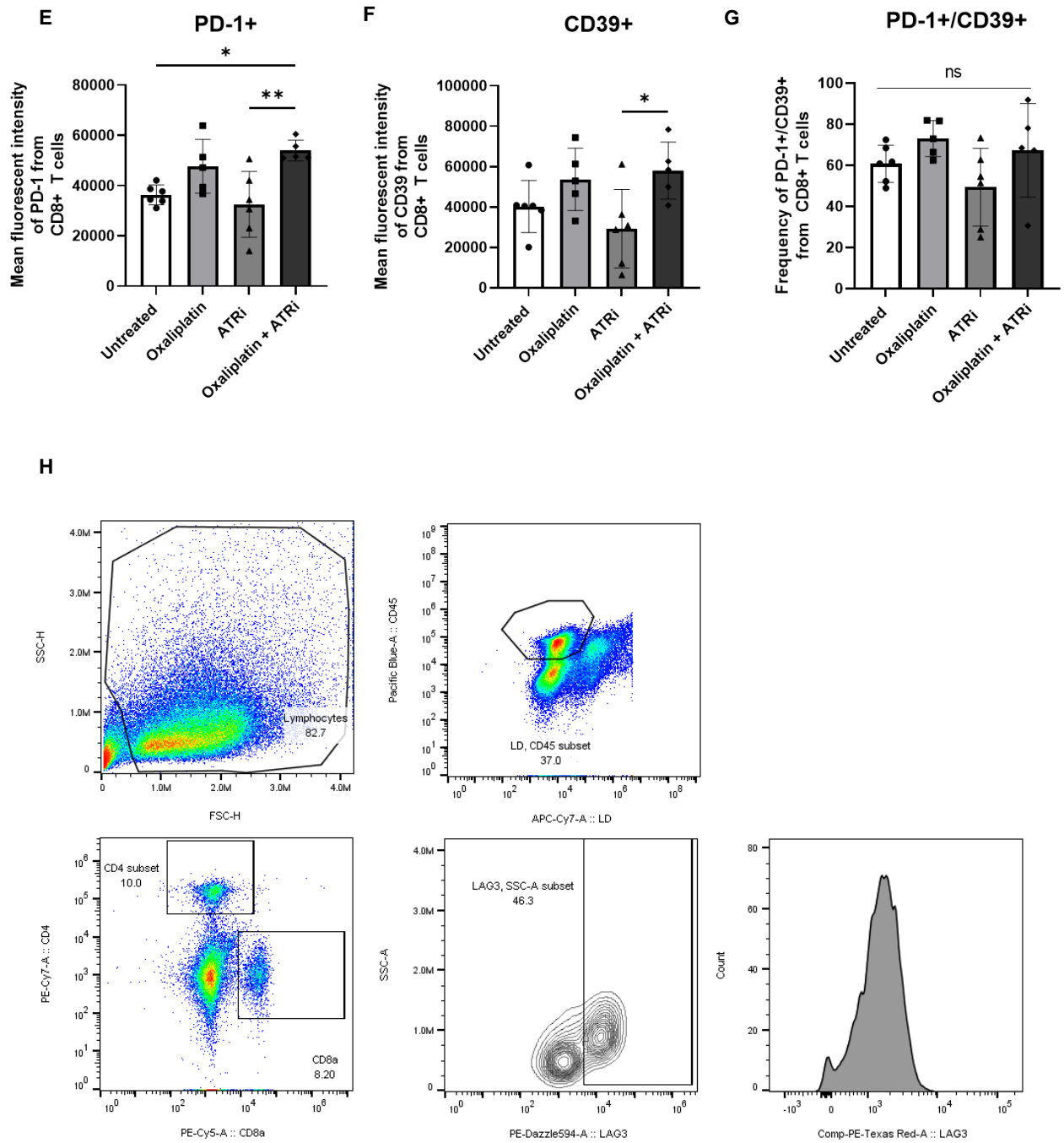


Figure 22: CD8+ T-cell characterization after treatment

(A-B) Flow cytometry data of T-cell activation marker. (C-G) Flow cytometry data of T-cell exhaustion marker. Each dot represents one mouse (n = 5-6). (H) Representative example for LAG-3 gating on CD8+ T-cells of PM lesions (Exclusion of debris, only considered living immune cells). Same gating strategy was used also for other markers (PD-1, Tim-3, OX40, CD137, CD39). Error bars show the mean +/-SD. **** = $p \leq 0.0001$, *** = $p \leq 0.001$, ** = $p \leq 0.01$, * = $p \leq 0.05$, ns = $p > 0.05$.

4.11 PM lesion in PM mouse model are controlled in a CD8+ T-cell-dependent manner after combination treatment

Our flow cytometry data revealed a higher CD8/Tregs ratio, in the combination treatment. Therefore, to understand if CD8+ T-cells are crucial for enhanced control of tumor growth, we used anti-CD8+ depletion antibody and compared tumor growth to non-depleted mice according to timeline shown in **Figure 23A**. Depletion of CD8+ T-cells resulted in bigger tumors in all treatment groups (**Figure 23B & 23C**). Moreover, depletion in combination treated mice abrogated protective treatment effects causing similar tumor load and tumor weight as in Oxaliplatin or ATRi alone treated mice (**Figure 23B & 23C**). This indicates that CD8+ T-cells are crucial to control PM lesion growth after combination treatment.

Figure 23

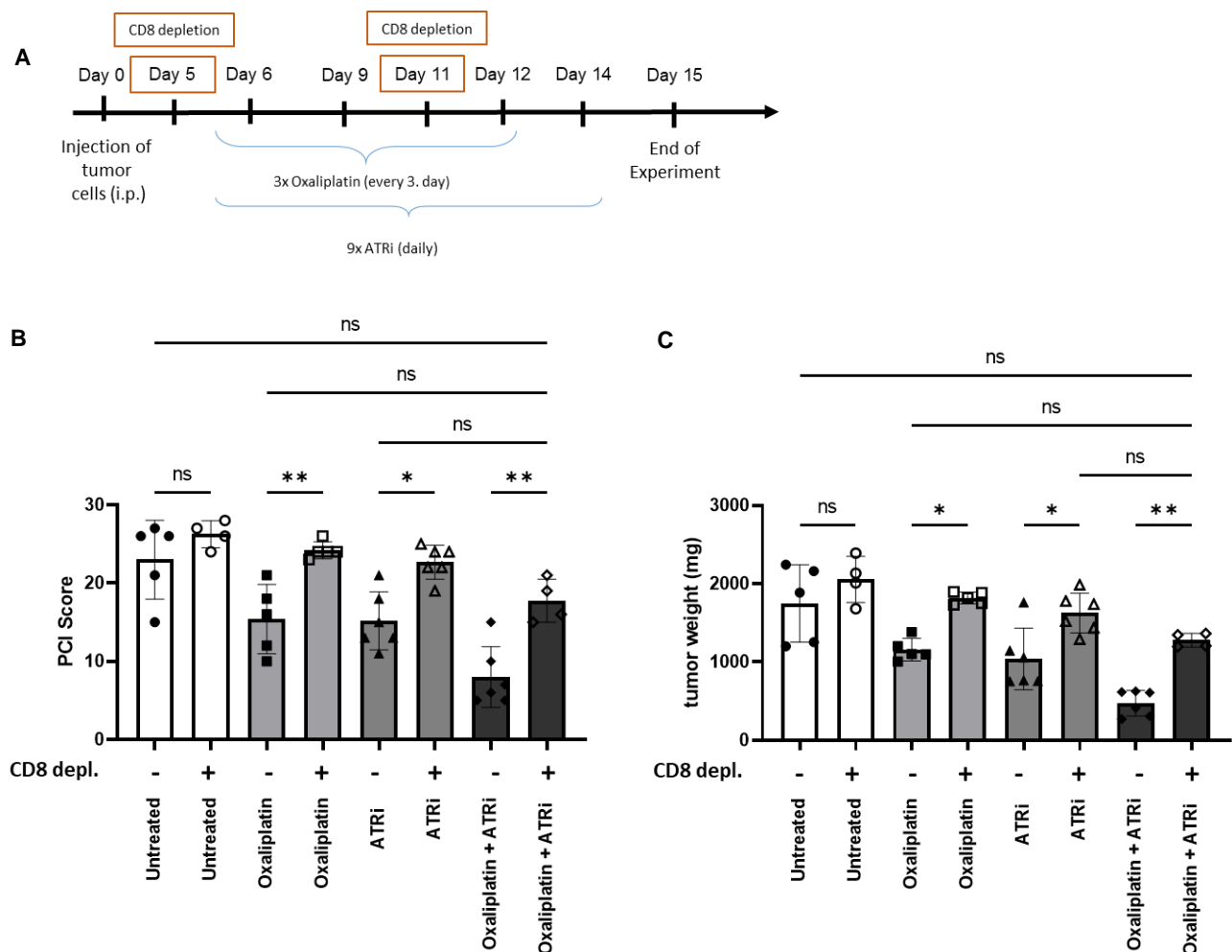


Figure 23: CD8+ T-cells are crucial to control PM tumor

(A) Timeline of experiment. (B) PCI score of CD8 depleted and non-depleted mice. (C) Tumor weight of lesion from peri-splenic region of CD8 depleted mice and non-depleted mice. Each dot represents one mouse (n = 5-6). Error bars show the mean +/-SD. **** = p<0.0001, *** = p<0.001, ** = p<0.01, * = p<0.05, ns = p>0.05.

4.12 Combination treatment promotes antigen-specific CD8+ T-cell effector function

Having confirmed that CD8+ T-cells play an important role in PM lesion control, we were interested in subsequent effector functions. Therefore, we treated mice harboring MC38-OVA tumors according to the scheme mentioned above in **Figure 20A**. At day 15, tumors were collected, digested and *ex vivo* re-stimulation was performed for 6 hours with OVA peptide (SIINFEKL 257-264 peptide) to assess cytokine production by CD8+ T-cells. Gating strategy for flow cytometry analysis is shown in **Figure 24Q**. Except for Oxaliplatin treated mice, IFN- γ production was not significantly increased after stimulation (**Figure 24A**). However, a good amount of IFN- γ was noted within all tumor samples without addition of the OVA-peptide suggesting a significant presence of the Ova antigen within samples. Furthermore, Perforin and Granzyme B production did not increase (**Figure 24B & 24C**). This surprising result led us to think that maybe this timepoint is not ideal to assess effector functions of CD8+T cells, as effector functions would have been on the peak earlier than 15 days after tumor injection leading to enhanced control of tumors in those mice that received the combination treatment. To test our hypothesis, we stopped the treatment earlier (**Figure 25A**) and performed immune cell characterization and cytokine assessment as described above. The total number of total immune cells (CD45+), T-helper cells (CD4+, FoxP3-), T-regulatory cells (FoxP3+, CD25+) and the ratio of CD8+/T-regulatory cells did not differ within treatment groups (**Figure 25B-D, 25G**). However, cytotoxic T-cells (CD8+) and myeloid cells (CD11b+) were increased in mice treated with Oxaliplatin + ATRi and Oxaliplatin alone (**Figure 25E & 25F**). Furthermore, characterizing CD8+ T-cells in more detail we observed no significant changes in exhaustion markers like PD-1, LAG-3 and CD39 as well as proliferation marker Ki67 and effector memory marker CD44 (**Figure 25H-L**). Nevertheless, assessing cytokine production, we detected increased IFN- γ in all treatment groups when OVA stimulated, but Oxaliplatin in combination with ATRi resulted in the greatest IFN- γ production compared to untreated and ATRi alone treated mice, but not Oxaliplatin treated mice (**Figure 25N**). Analyzing Multiplex stainings we further detected the highest frequency of Granzyme B + CD8+ T-cells within the combination treatment (**Figure 25O**).

Furthermore, using a MHC-class I pentamer, we assessed the highest antigen specificity in the combination treatment (**Figure 25M**). This data indicates that the combination treatment promotes increased and antigen-specific CD8+ T-cell function after short treatment exposure.

Figure 24

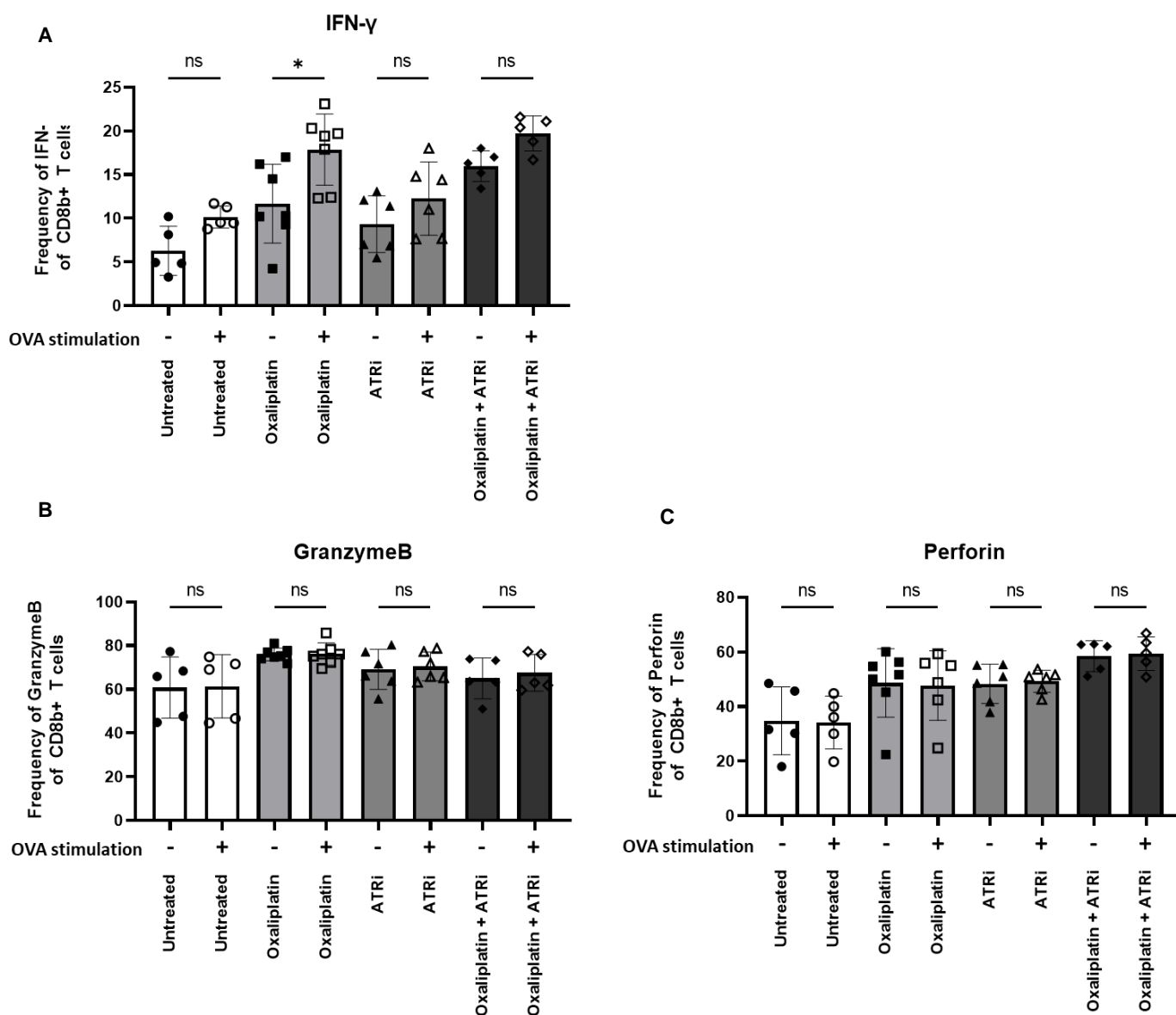
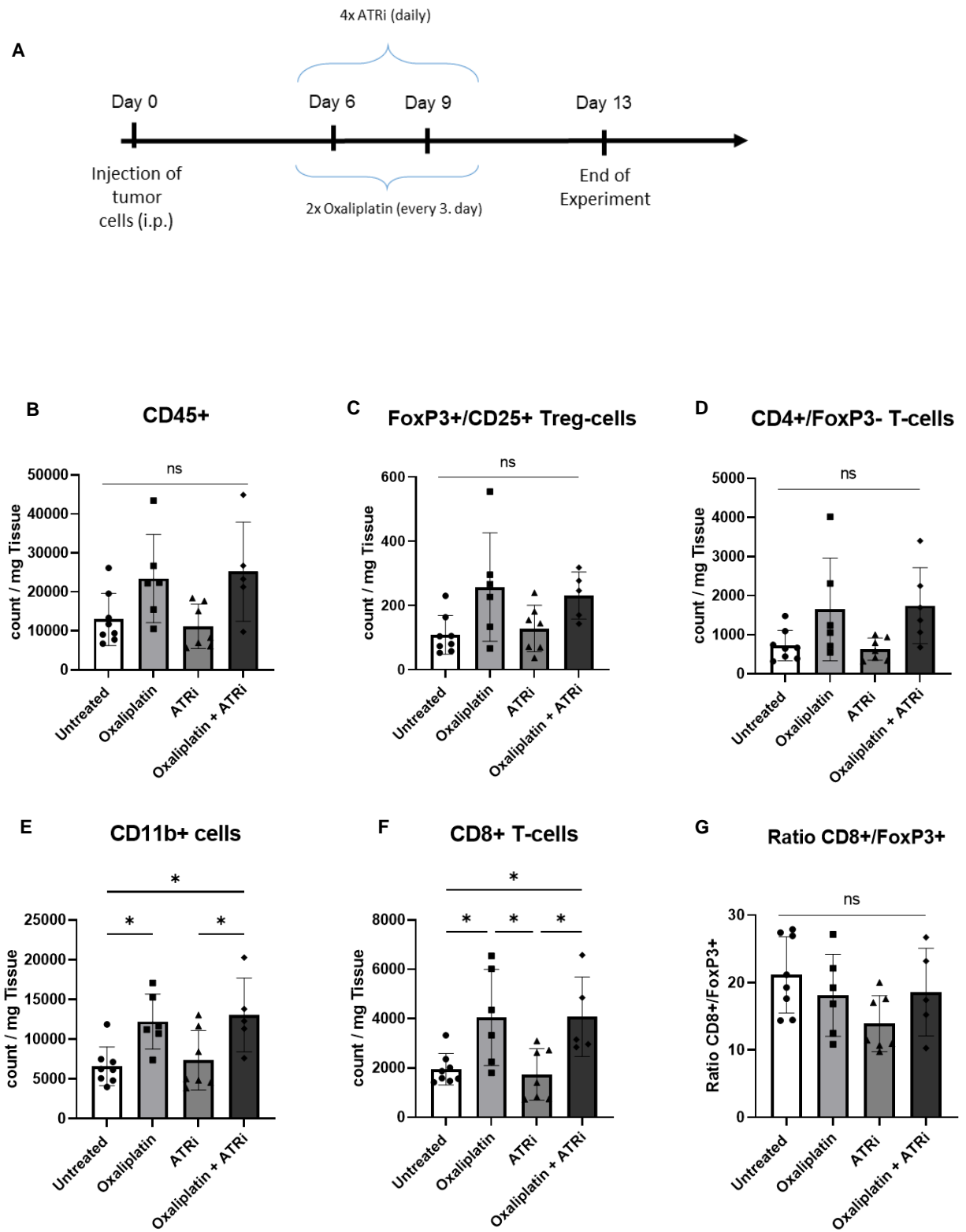
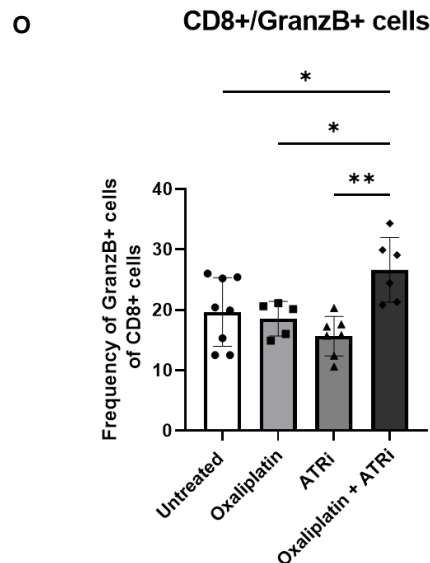
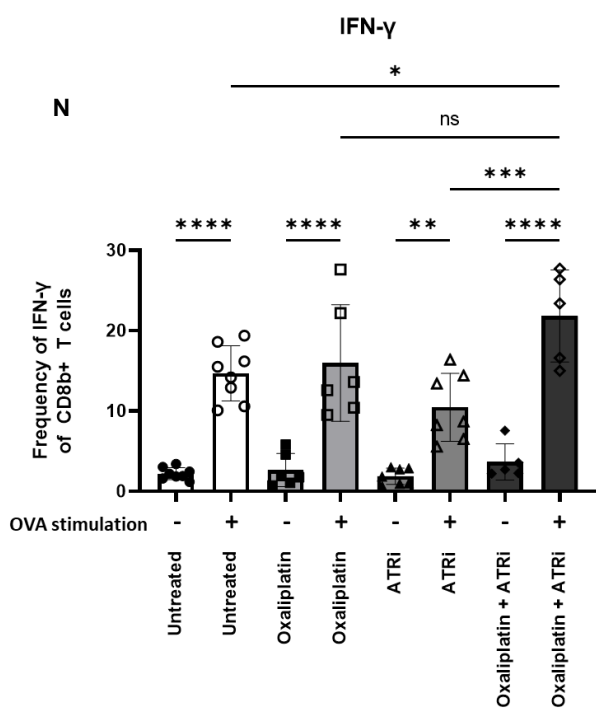
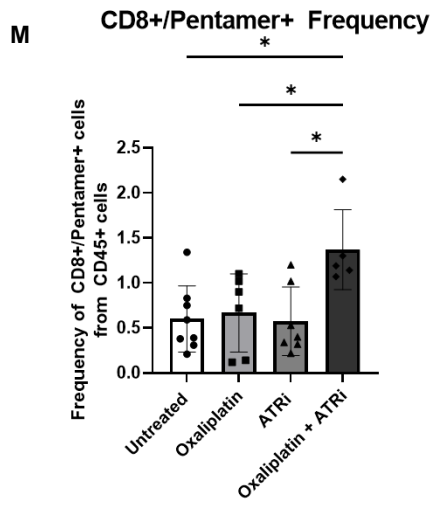
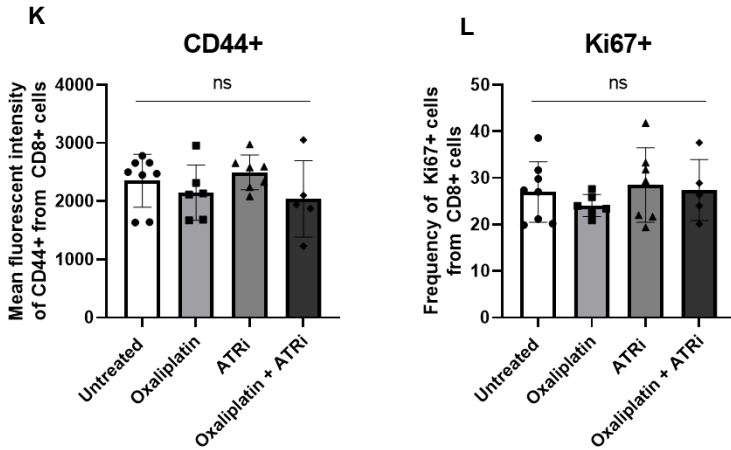
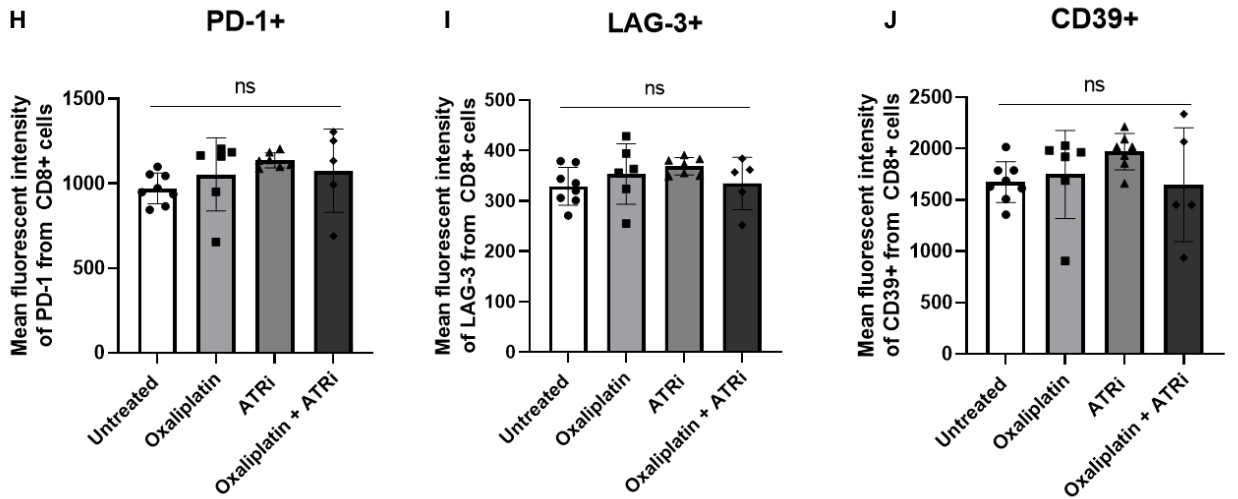


Figure 24: CD8+ T-cell effector function after long treatment exposure

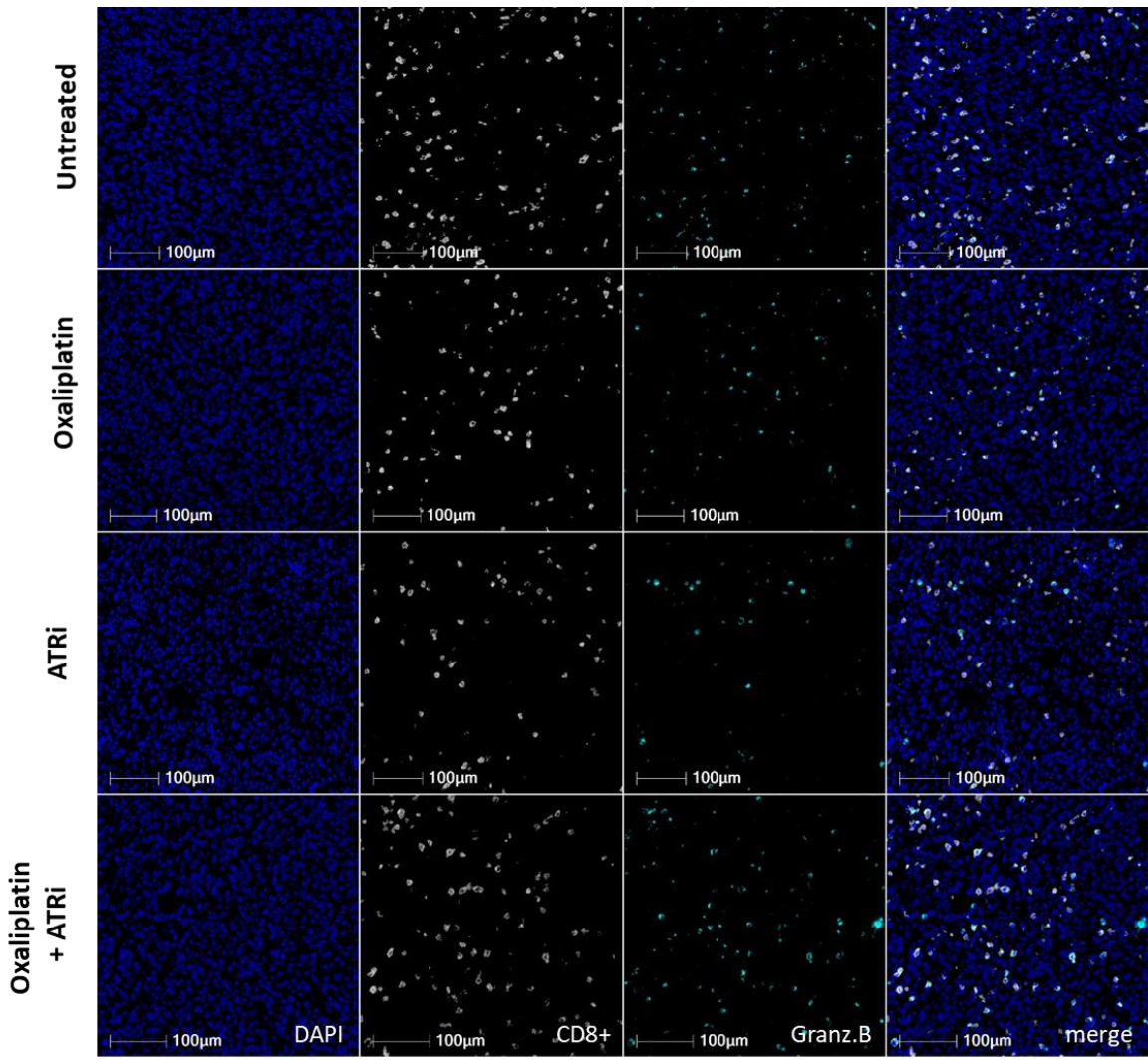
(A) IFN- γ production of CD8b+ T-cells after ex vivo re-stimulation with OVA peptide. **(B)** Granzyme B production of CD8+ T-cells after ex vivo re-stimulation with OVA peptide. **(C)** Perforin production of CD8+ T-cells after ex vivo re-stimulation with OVA peptide. Each dot represents one mouse (n = 5-7). Error bars show the mean +/-SD. **** = $p \leq 0.0001$, *** = $p \leq 0.001$, ** = $p \leq 0.01$, * = $p \leq 0.05$, ns = $p > 0.05$.

Figure 25

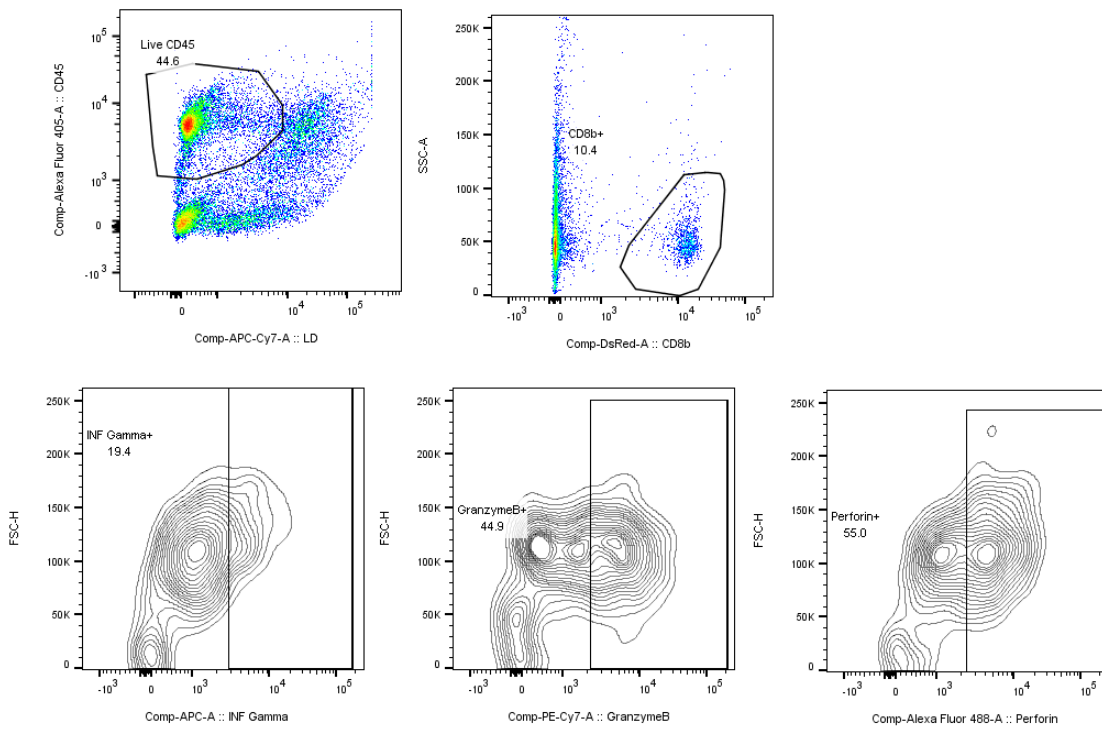




P



Q



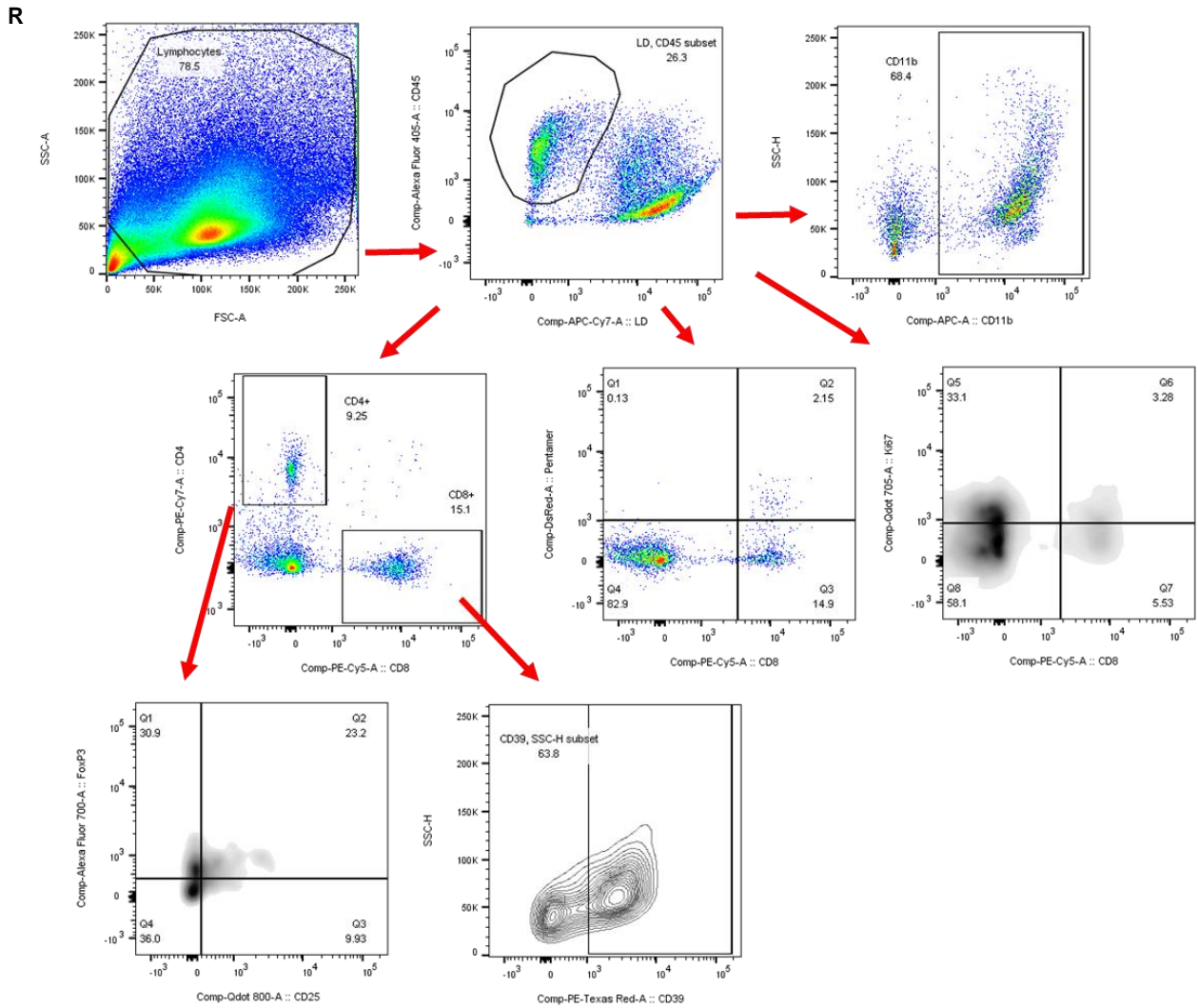


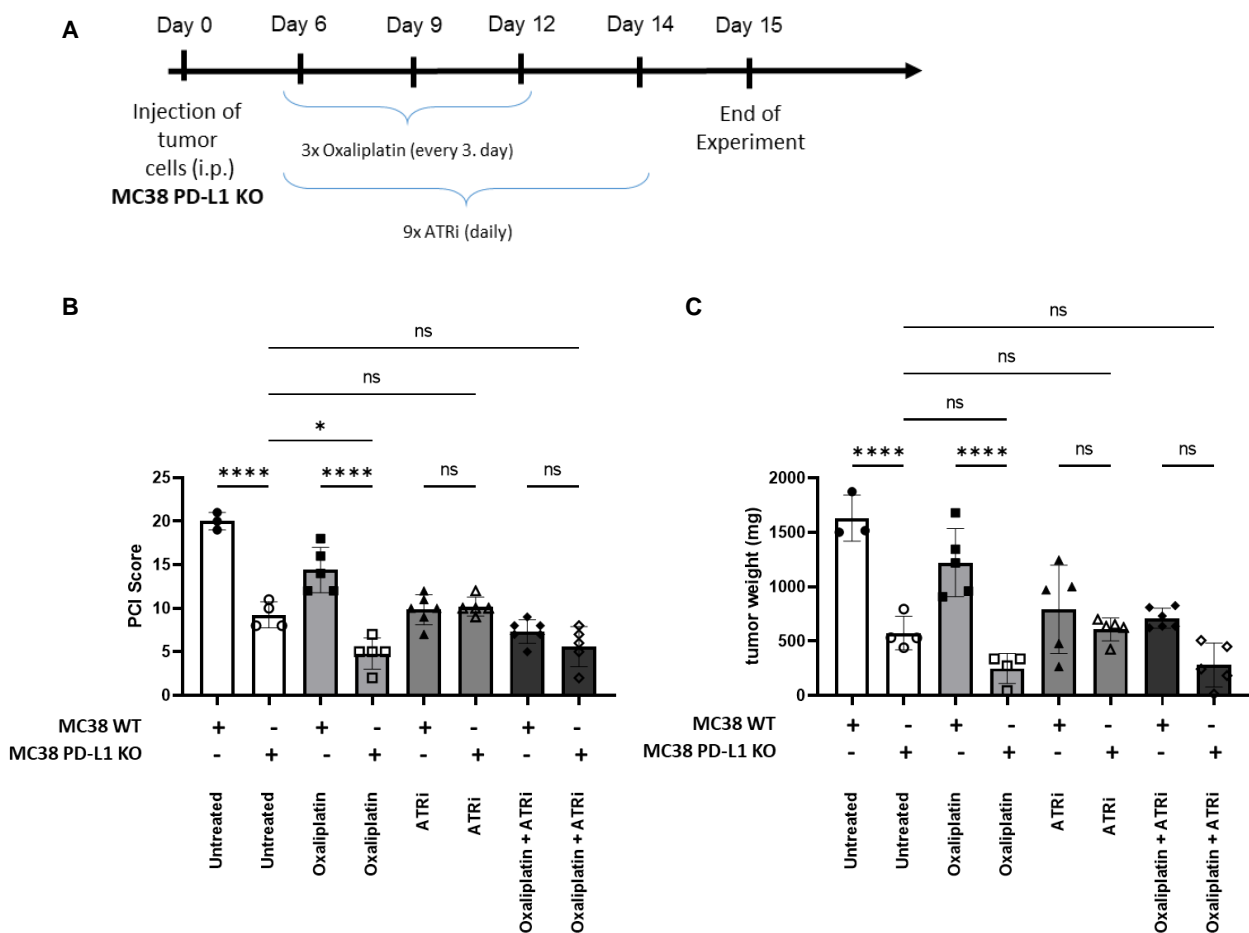
Figure 25: Immune cell composition and characterization after short treatment exposure

(A) Timeline of experiment. **(B-F)** Flow cytometry data (count) of different immune cells within PM lesions. **(G)** CD8+ T-cell / FoxP3+ T-regulatory cell ratio. **(H-J)** Flow cytometry data of T-cell exhaustion marker. **(K)** Mean fluorescence intensity of effector memory marker CD44. **(L)** Frequency of proliferation marker Ki67. **(M)** Frequency of antigen specific Pentamer+ CD8+ cells. **(N)** IFN- γ production of CD8b+ T-cells after ex vivo re-stimulation with OVA peptide. **(O)** Quantification of GranzymeB+ CD8+ T-cells from multiplex staining. **(P)** Representative pictures of multiplex staining (scale bar 100 μ m). **(Q)** Gating strategy to assess effector function (only considered living immune cells). **(R)** Gating strategy to characterize PM lesions with representative example for CD39 gated on CD8+ T-cells. Same gating strategy was used for other markers (PD-1 and LAG-3, Exclusion of debris, only considered living immune cells). Each dot represents one mouse (n = 5-7). Error bars show the mean \pm SD. **** = p \leq 0.0001, *** = p \leq 0.001, ** = p \leq 0.01, * = p \leq 0.05, ns = p>0.05.

4.13 The therapeutic effect of ATRi is mediated by reduced PD-L1 expression

Since we observed that ATRi downregulated Oxaliplatin-induced PD-L1 expression *in vitro* on human and murine CRC cell lines, we were interested whether gain in CD8+T cell functions *in vivo* might be due to reduced PD-L1 expression within tumors via ATRi. To assess this, we injected mice with MC-38 PD-L1 KO cell lines and MC-38 cells and compared tumor load after treatments. The timeline of this experiment is shown in **Figure 26A**. Mice injected with MC38 PD-L1 KO cells showed skewed tumor growth in untreated and Oxaliplatin treated mice and had significantly smaller tumors. Treatment with ATRi alone or in combination with Oxaliplatin did not further reduce tumor size of mice that harbored PD-L1 deficient tumors suggesting that tumor reductions in mice after treatment with ATRi ± Oxaliplatin is due to loss of PD-L1 within tumors (**Figure 26B&26C**). This suggests, as observed *in vitro*, that *in vivo* ATRi is responsible for PD-L1 downregulation. Analysis of Multiplex stainings also confirmed PD-L1 downregulation in ATRi treated mice (**Figure 26D &26E**).

Figure 26



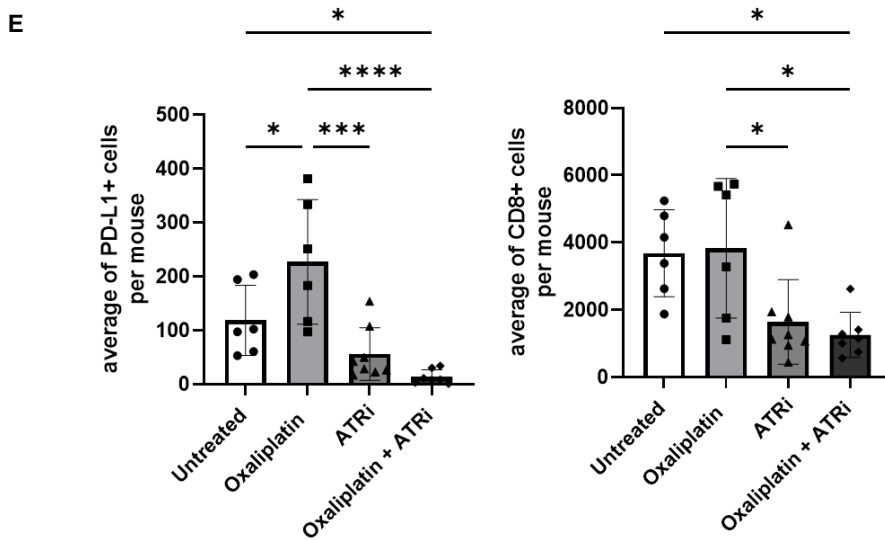
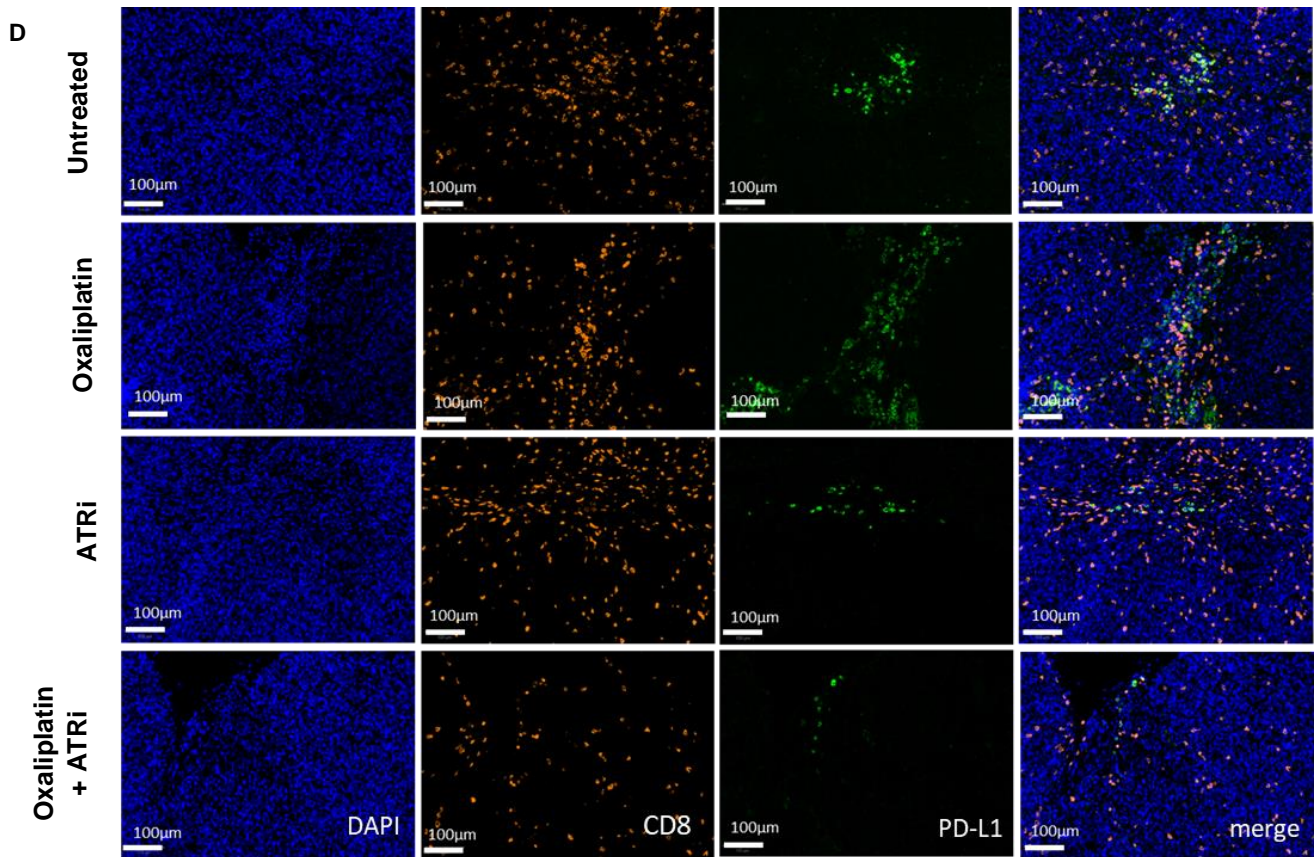


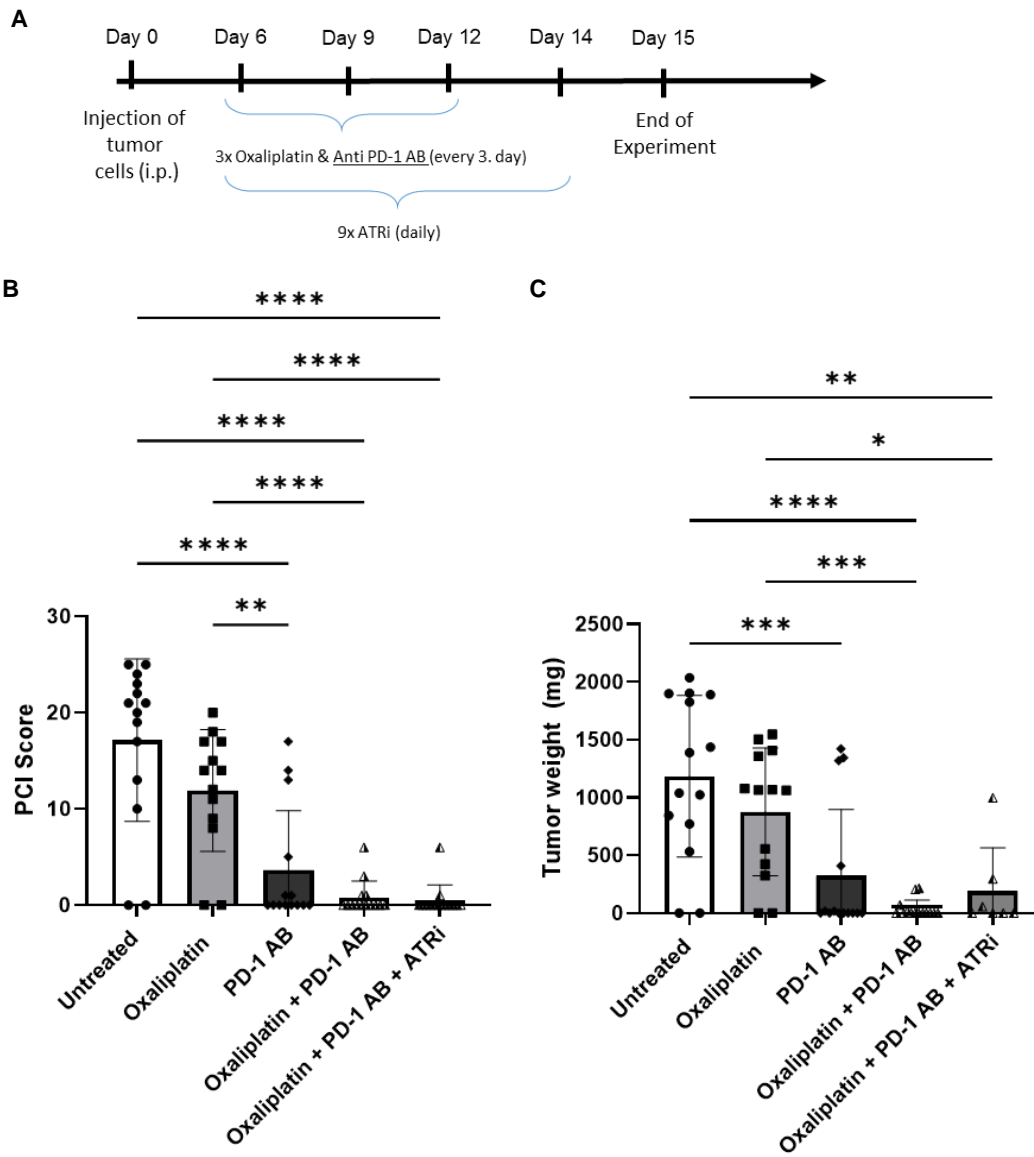
Figure 26: ATRi downregulates PD-L1 expression *in vivo*

(A) Timeline of experiment. (B) PCI score of mice injected with MC38 PD-L1 KO and MC38 wildtype cell lines. (C) Tumor weight of lesion from peri-splenic region of mice injected with MC38 PD-L1 KO and MC38 wildtype cell lines. (D) Representative pictures of multiplex staining (scale bar 100µm). (E) Quantification of CD8+ and PD-L1+ cells from multiplex staining. Each dot represents one mouse (n = 3-6). Error bars show the mean +/-SD. **** = p ≤ 0.0001, *** = p ≤ 0.001, ** = p ≤ 0.01, * = p ≤ 0.05, ns = p > 0.05.

4.14 Blockade of PD-1 provides greater control of PM lesions

Having observed that tumor of mice that were treated with the combination treatment are enriched in PD-1+ CD8+ T-cells, we were curious if adding PD-1 blocking antibody to our treatment would lead to enhanced tumor control. Therefore, we injected PD-1 blocking antibody alone or in combination with chosen treatment drugs and assessed the tumor load (**Figure 27A**). Interestingly, 50% of mice treated with PD-1 blocking antibody alone were tumor free. Furthermore, PD-1 blocking antibody combined with either Oxaliplatin, ATRi or both resulted in approx. 75% tumor free mice. In addition, the remaining mice had significantly less tumor load compared to Oxaliplatin or ATRi alone (**Figure 27B-27E**). This indicates that the addition of PD-1 depletion provides enhanced control of PM lesions.

Figure 27



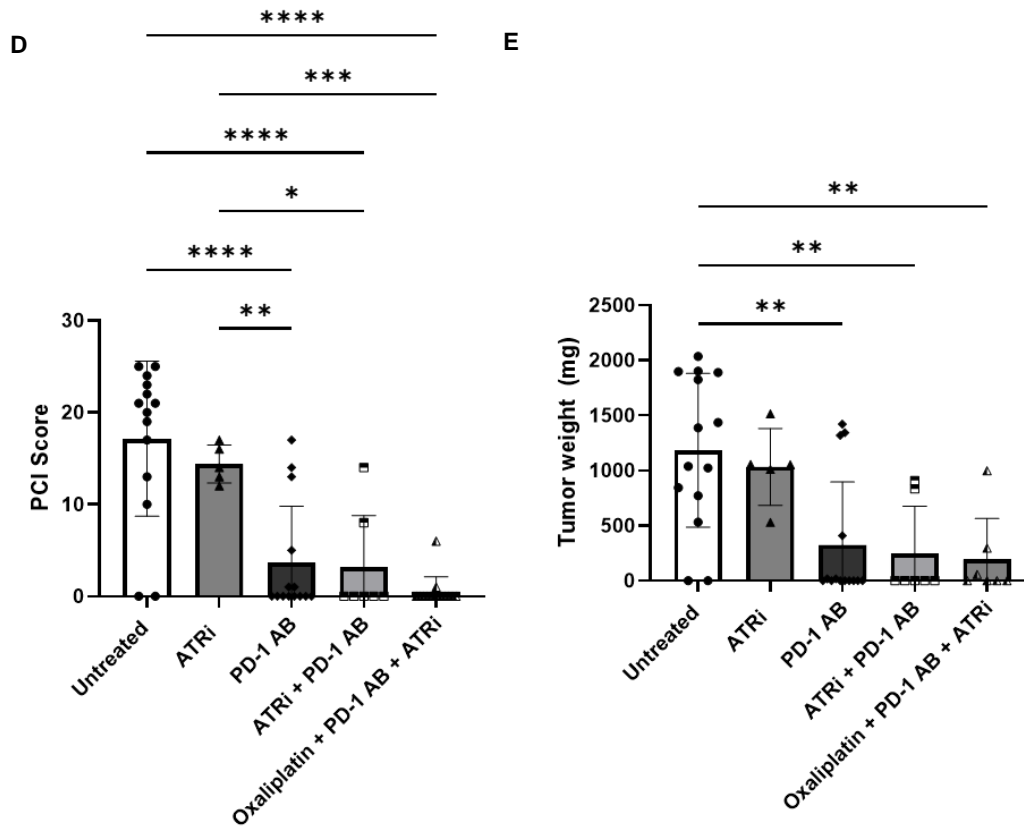


Figure 27: PD-1 blocking antibody strongly reduces PM tumor load

(A) Timeline of experiment. (B) PCI score of mice treated with Oxaliplatin, PD-1 depletion AB and Triple-combination. (C) Tumor weight of lesion from peri-splenic region of mice treated with Oxaliplatin, PD-1 depletion AB and Triple-combination. (D) PCI score of mice treated with ATRi, PD-1 depletion AB and Triple-combination. (E) Tumor weight of lesion from peri-splenic region of mice treated with ATRi, PD-1 depletion AB and Triple-combination. Each dot represents one mouse (n = 6-10).

Tumor free mice per treatment group: Untreated ~13%, Oxaliplatin ~25%, ATRi ~25%, PD-1 depleted ~50%, Oxaliplatin + PD-1 depleted ~75%, ATRi + PD-1 depleted ~75%, Oxaliplatin + ATRi + PD-1 depleted ~75%. Error bars show the mean +/-SD. **** = p<0.0001, *** = p<0.001, ** = p<0.01, * = p<0.05, ns = p>0.05.

5. Discussion

The spread of malignant cells from primary cancers within the body, forming metastatic lesions at various sites, is often categorized as an advanced disease stage. Normally, at this stage, not many treatment options are available for those patients. Furthermore, resistance to treatments and a lack of proper molecular and cellular understanding of metastatic lesions makes it difficult to have metastasis-specific treatments. The work presented in the thesis focused on developing treatments for those patients who are suffering from advanced metastatic disease. Thus, an attempt was made to reassess the therapeutic potential of existing drugs alone or in combination with the hope for faster clinical translation. Among others, we focused on the metastatic spread of colorectal cancer (CRC) cells to the peritoneal cavity, forming multiple malignant lesions at different locations known as peritoneal metastasis (PM). Patients harboring PM show dismal survival and without treatment, most of them die within 5 months (73). During PM development, cancer cells tend to disseminate from different primary tumors such as CRC, gastric cancer, ovarian cancer or pancreatic cancer (32). The development of PM in CRC patients demonstrates significant differences in terms of clinical behavior, prognosis, and overall-survival (OS) compared to metastasis occurring through hematogenous routes to the liver or lungs (30, 33). At present, most of the patients with PM are primarily treated with systemic chemotherapy using those agents that are used against their respective primary tumors. In the case of PM originating from CRC, patients receive varied combinations of chemotherapies: 5-FU, Folinic acid, Oxaliplatin, and Irinotecan. In addition to systemic chemotherapy, depending upon their molecular signatures, PM patients may also receive monoclonal antibodies against VEGF or EGFR (41).

While systemic therapy is often used, a subset of patients might receive additional local treatments such as CRS/HIPEC or PIPAC as described in the introduction. Rational to use CRS/HIPEC treatment is to reduce tumor load by the surgery and then eradicate microscopic lesions with local application of heated chemotherapies, mostly Oxaliplatin or the combination of Mitomycin C and Doxorubicin (33). This approach is very risky and includes high rates of postoperative infection-related complications requiring prolonged stay in the hospital (46). However, once recovered, patients seem to survive much longer than systemic chemotherapy alone (43). Whether the prolonged survival is due to surgery alone or due to combined effects of CRS/HIPEC is controversial, with clinical data offering both benefits and doubts on HIPEC procedure. Furthermore, the lack of scientific studies also

makes it difficult to clarify HIPEC-associated benefits after CRS. Recent investigations have attempted to examine the immunological benefits of HIPEC treatment. By mimicking HIPEC-like conditions in vitro and performing HIPEC on microscopic tumors in a PM mouse model, it was concluded that HIPEC can induce CD8+ T-cell dependent tumor-specific immunity. Such findings are of great importance as it can be speculated that sustained effector functions of CD8+ T cells, especially by using immunotherapies, might provide long-term control of PM lesions. These experimental findings are very interesting and strengthen ongoing clinical trials that are exploring the potential of immunotherapy approaches like CAR-T cells, checkpoint inhibitors, and cancer vaccines, as well as multifunctional monoclonal antibodies (MOC31PE) for metastatic CRC but not specific for PM lesions (58, 59). Success of these trials can be useful for applying these treatments either directly or indirectly on PM lesions through systemic routes, locally through minimally invasive laparoscopic surgery, or even after a local approach if required. While there seem to be benefits from the CRS/HIPEC approach, a recent study from our group showed that recurrence occurs frequently and compared to liver metastasis patients with PM have showed a shorter OS after recurrence. The study also identified risk factors promoting early recurrence of PM, such as mutated RAS, high PCI, and nodal status (33). The underlying reasons for this high recurrence rate are still not fully understood and may be attributed to treatment inefficiency, variability in treatment response, or characteristics of the tumor microenvironment of PM lesions.

Therefore, to prevent fast recurrence, effective treatments are needed. This urgent need led us to explore drugs or drug combinations that are currently being tested on metastatic CRC to examine their potential to have immunogenic effects on cancer cells. Thus, targeting the immunosuppressive TME to convert it into an immune-active phenotype supporting immune cell-mediated control of PM lesions.

Hence, in this thesis, many targeted drugs were tested first for their capacity to eradicate CRC cell lines and patient-derived organoids either alone or in combination with Oxaliplatin and later to examine the immunogenic potential of selected drug candidates. As a last assessment, the best drug combination was given to our PM mouse model to examine its efficacy and its impact on the tumor microenvironment. So far, such approaches have been little explored, as not many laboratories have experimental models (PM model) to elucidate the most efficient drug. There are quite a few clinical studies that have tried to gain knowledge about the pathophysiology and the TME of PM. (22, 30, 74).

For example, Seebauer et. al. compared the tumor microenvironment of primary CRC vs. PM, where they found that primary CRC harbored increased amounts of CD4+ T-cells, CD8+ cytotoxic T-cells and PRG2+ eosinophilic granulocytes. Whereas in PM, they found prevalent presence of IL-15 activated NK-cells that possibly release cytokines such as IFN- γ and TNF- α . Furthermore, they also observed reduced tumor cell proliferation and increased senescence markers in PM lesions (75). However, the limitation of this observational study was the absence of paired patient samples and the lacking correlation with survival of patients. Moreover, a recent Dutch study performed an extensive molecular characterization of PM that originated from CRC. This study classified PM lesions predominantly to CMS4 subtype that is further divided into three additional subgroups. These subgroups differ in terms of RAS mutation (CMS4A), mucinous phenotype (CMS4B) and high immune infiltration (CMS4C) (21, 38). Furthermore, our first in kind but simple study demonstrated in 42-paired samples (primary CRC vs. PM) that high CD8+ T-cell infiltration in vital tumor areas correlated with prolonged overall and disease-free survival (under revision, ***Nature communications***). What remains to be explored is the differences between PM lesions arising from various primary tumors, since it is not exactly known how the composition of PM lesions are shaped by various primary tumors. Furthermore, it is unknown if the location of PM lesions within the peritoneal cavity is crucial for treatment response. Such information will be important to develop PM-specific treatments. The huge amount of valuable information about PM lesions has come from patient samples. These studies have provided insights into molecular and cellular composition of PM lesions and partially revealed that a less immunosuppressive TME tends to be associated with better survival of the patients. However, none of the study has directly shown treatment-mediated impact on TME of PM lesions due to the unavailability of patients' samples immediately or few days later after the treatments. Such studies are more feasible in experimental models. For that reason, our laboratory is involved in translational research, characterizing PM lesions from patients and mouse models, examining effects of drugs on patient-derived tumor organoids and treatment-mediated changes within TME of mouse PM tumors. Our aim is to have immune-stimulating treatments that could be offered to each PM patient with a hope to prolong their survival. To make faster translational into clinical use, this study has tested existing drugs that are in clinical trials for metastatic CRC or other types of cancer. Given the fact that not many laboratories are working with experimental models of PM, this approach is also ideal to bring PM-specific drugs to the clinics.

As it is a prerequisite for a drug to induce cancer cell-death, we began testing multiple drugs at different concentrations alone or in combination with Oxaliplatin. Considering that the genetic makeup of tumors shapes the outcome in response to the treatments, we chose both human CRC MSS cell line HT29 and MSI cell line HCT8 for our screening. Following literature, we focused on drug agents interfering with the DNA repair pathway, growth and proliferation pathways, and multikinase inhibitors. All small molecule inhibitors are currently investigated in clinical studies or are FDA approved for metastatic CRC or other cancer types. Of all tested drug combinations, the combination of Oxaliplatin and ATRi or Oxaliplatin with MEKi showed additive cytotoxicity. Furthermore, we observed that especially the MSI cell line HCT8 was more sensitive towards small molecule treatments alone than the MSS cell line HT29. It is to note that about 80% of CRC patients and their associated PM lesions are classified as MSS (76). Patients with MSI tumors are rarely treated with local therapy but rather receive immunotherapy together with systemic chemotherapy (77). The patients harboring MSI tumors respond well to immunotherapies due to high tumor mutational burden and high numbers of tumor infiltrating lymphocytes. On the other hand, MSS tumors fail to respond to immunotherapy alone, since they have been characterized with low T-cell infiltration, high myeloid-derived suppressor cells (MDSCs) and downregulated checkpoint inhibitors and HLA class-I and II (73, 74). However, currently many strategies are investigated to overcome the resistance to immunotherapy in MSS tumors. Thereby, aiming to modulate the tumor microenvironment, different clinical trials are ongoing where immunotherapy is combined with chemotherapy, irradiation, small molecule inhibitors and different immunotherapy strategies itself. In future, this may lead to improved treatment strategies for MSS tumors and to a better understanding of MSS biology (78, 79).

These data and observations from the clinics led us to think that among all drugs combinations tested it would be ideal to make MSS tumors sensitive to immunotherapies, if possible. Thus, immunotherapies may help in achieving such a goal as the vast majority of literature available from clinical and preclinical data show that immunotherapies can block immune inhibitory interactions between tumor cells and T-cells in order to control tumor growth. In this regard, anti-PD-1 and/or anti-PD-L1 has shown meaningful clinical responses in multiple tumor types. These antibodies block interactions of PD-L1 with PD-1 on activated T-cells providing sustained effector functions of CD8+T cells. So far, these antibodies has not shown benefits in clinics against MSS-CRC. We therefore stumbled upon a recent study that has shown that ATRi is able to down regulate radiation-mediated

up regulation of PD-L1. More specifically, this study demonstrated that double strand breaks induced by irradiation result in PD-L1 upregulation in osteosarcoma, lung carcinoma and prostate carcinoma cell lines which is dependent on ATM/ATR/CHK1 kinases. Subsequent ATR inhibition results in reduced PD-L1 expression (72). Furthermore, several clinical phase I and II studies using ATR inhibitors in combination with immunotherapy are ongoing due to promising pre-clinical data (80-82). While we also noticed enhanced cytotoxicity, when we combined MEKi+ Oxaliplatin in MSS cells, we did not pursue it further as MEK inhibitor combined with immunotherapy resulted in mixed outcome and failed to demonstrate a clear advantage (83).

To rule out cell line specific effects, cytotoxicity of Oxaliplatin, ATRi, and Oxaliplatin in combination with ATRi were examined on nine different CRC cell lines. Furthermore, since we are interested in a PM-specific treatment, we generated patient-derived PM organoids and tested cytotoxic effects among these treatments, where the combination treatment showed maximal cytotoxicity. As our aim was to sensitize tumor cells in a way that they become recognizable to the immune cells, we examined whether these treatments induced immunogenic cell death (ICD). To define if the treatments induced cell death that is associated with immunogenic changes, we assessed release of HMGB-1, secretion of extracellular ATP, expression of MHC class I, and effects of PD-L1 expression with different concentration of drug doses at different time points. Compared to single treatment, the combination treatment increased HMGB1 release, increased extracellular ATP secretion, and downregulated Oxaliplatin-induced PD-L1 expression. The latter was also noticed in patient-derived PM-organoids and in murine CRC cell lines. Interestingly, we also observed that the combination treatment increased the expression of Galectin-9, CD80, and CD86 that are known to inhibit DC and CD8+ T-cell activation. Through the interplay of immune-stimulatory and inhibitory molecules, it is always challenging to realize whether T cells, especially CD8+T cells, will show effector functions and furthermore how and when these molecules are important in promoting or inhibiting T-cells functions. This could be dependent on treatment type, doses of treatments, and duration of the treatments. Nevertheless, to clarify whether our tested drugs are pro-immunogenic and can prime CD8+T cells to recognize cancer cells, we designed in-vitro killing assays, where we added transgenic OT-1 CD8+ T cells to pre-treated murine MC38-OVA cells. Using this in vitro system, we could show that Oxaliplatin in combination with ATRi enhanced killing capacity of CD8+ T cells. In addition, it also indicated that treatment promotes antigen-specific CD8+ T-cells that are able to recognize antigens on cancer cells.

Having confirmed that Oxaliplatin together with ATRi increases cytotoxicity and induce pro-immunogenic alterations on cancer cells in vitro, we decided to evaluate the efficacy of these drugs in vivo in our established PM mouse model. To quantify tumor load in our PM mouse model we applied the murine PCI as described above and in addition we also measured weight of the tumors from the perisplenic site, as this site always hold PM lesions. This PM model provides a unique opportunity to study treatment efficacy, mechanism behind treatment success and the tumor microenvironment for PM lesions. When we treated PM lesions bearing mice with single treatment of Oxaliplatin or ATRi we noticed significant reduction in tumor growth. However, when mice were treated with the combination treatment we noticed additive effects and the greatest control of PM lesions in both PCI and in tumor weight. Upon TME examination of PM lesions from these treated mice, among many immune cells we noticed a higher CD8+/Tregs ratio in combination treatment suggesting that CD8+ T-cells might be involved in control of PM lesions. For this reason, we depleted CD8+ T-cells in all treatment groups. This resulted in bigger PM, as treatments became less effective suggesting that control of PM lesions following these treatments are CD8+ T-cells dependent. Furthermore, by analyzing effectors functions of CD8+ T-cells we could confirm enhanced effector functions (IFN- γ , GranzymeB production) within tumors of those mice that received the combination treatment explaining the greatest control of PM lesions in this group. We next examined, why these CD8+ T-cells were more effective in the combination treatment. Since we noticed that in vitro addition of ATRi led to a significant decrease in PD-L1 expression within tumors, we expected that in vivo this will lead to enhanced CD8+ T-cells functions and thus support PM lesions control. To confirm this, we injected mice with MC38 cells and cells lacking PD-L1 expression (MC38-PD-L1KO). When mice were injected with PD-L1 deficient MC38 cells, tumors were smaller in untreated and Oxaliplatin treated groups, but not in ATRi and combination treated mice. This suggests that treatment including ATRi did not further control PD-L1KO tumors, suggesting that tumor reductions in mice after treatment with ATRi with or without Oxaliplatin is due to the loss of PD-L1 within tumors. These encouraging results prompted us to try to combine these treatments with anti-PD-1 antibody immunotherapy. Fitting to our hypothesis, we saw a significant improvement in PM lesions control in all treatment groups by adding PD-1 blocking antibody, making up to 75% mice tumor free when giving Oxaliplatin or ATRi in combination with anti-PD-1 blocking antibody as well as when given as triple combination. The results of this study are in line with findings from Combès et al. that showed that Oxaliplatin in combination with ATRi enhanced

cytotoxicity and even overcomes Oxaliplatin resistance. Moreover, they demonstrated reduced growth of subcutaneous tumors in combination treated mice and that co-culturing spleens of treated animals with pre-treated MC38 cells in vitro resulted in enhanced INF- γ production (71). Nevertheless, it has to be noted that the outcome of our experimental PM model could be argued since MC38 cell are considered as MSI. However, a previous study examined the effect of Oxaliplatin combined with checkpoint inhibitors PD-1 and CTLA-4 on subcutaneous (sc) CRC animal models. They used the murine CRC cell line MC38 and murine CRC cell line CT26 that is considered as MSS. Interestingly, in their sc MC38 tumors checkpoint inhibitors alone failed to control tumor growth and thus resulted in similar survival as the control group. Whereas sc CT26 tumors were significantly controlled by checkpoint inhibitors alone, in terms of tumor growth and survival (84). This study led us to assume two important points. First, the location where tumors grow indeed matters in terms of treatment response as in our study, MC38 tumors located in the peritoneal cavity responded to PD-1 blocking antibody treatment alone, which was not the case with the previous study on sc tumors. Second, growth of sc CT26 tumors was reduced with immune checkpoint inhibitors alone, even though CT26 is characterized as MSS. This indicates that the distinction between MSS and MSI tumors that is crucial for treatment in human patients, seems to be irrelevant for experimental mouse models. This study clearly demonstrates that the combination of Oxaliplatin and ATRi results in enhanced cytotoxicity in various CRC cell lines with different genetic backgrounds regardless of whether the cell lines are considered as MSS or MSI. Even though cell lines are easy to use, cost-effective, and have a long lifespan, they do not compare to a tumor growing inside the body. Use of patient-derived organoids gave us the possibility to perform research on actual PM tissue that contains the genetic and phenotypic heterogeneity as well as features of the original tumor. For this study, we only managed to include four patient-derived organoids originating from PM lesions. Two of them had CRC as the primary tumor, whereas the others had gastric and small intestine primary tumors. Tissues for organoids generation were collected prior to HIPEC treatment at the University Hospital Zurich. Since these patients were heavily pretreated, generation of these organoids turned out to be quite challenging. Even though we only ended up with four patient-derived organoids, we could make conclusive observations. Irrespective of the primary tumor, we had three patient-derived organoids showing enhanced cytotoxicity with the combination treatment. Interestingly, all three organoids needed high Oxaliplatin doses to achieve this effect. We do not know if this is due to resistance

towards Oxaliplatin or because higher drug doses are needed to induce a cytotoxic effect in a 3D cell construct. Furthermore, only one organoid was highly sensitive towards ATRi alone. Nevertheless, we do not know specific reasons why ATRi was so effective for this organoid. Furthermore, PD-L1 and MHC class-I expression after combination treatment were lower in PM organoids with CRC as the primary tumor, which is in line with results obtained for CRC cell lines. This was not observed with PM organoids with gastric or small intestine as the primary tumor. Since we did not examine multiple markers for immunogenic changes on organoids, we cannot assume that this effect is specific to CRC-associated PM organoids.

When it comes to saving a cancer patient, clinicians optimize existing treatments, mix and match treatments to help them, as recurrence of the disease is quite common. An example of such an approach in PM treatment is the local use of heated chemotherapies, where the addition of heat was never mechanistically investigated. Regardless of cancer type, until three decades ago, most patients were treated either with surgery, chemotherapy, irradiation, or combinations of these traditional treatments without fully understanding the disease biology. Among these treatments, only surgery can cure cancers at an early stage and if the disease is local. For almost a century, chemotherapy has become a major player in the treatment of cancer. Until recently, systemic application of chemotherapies was the only choice for patients with metastatic disease.

The sophisticated technical development in the last four decades has allowed improved characterization of cellular and molecular components of the TME. This progress has led to the development of targeted therapies such as monoclonal antibodies against VEGF or EGFR. These drugs are in routine use and, when necessary, are often combined with chemotherapies. The most exciting development happened almost three decades ago when the role of the immune system in controlling cancer growth emerged. Since then, the era of modern cancer medicines has taken a huge leap, with more and more biosimilar drugs in development, such as engineered antigen-specific immune cells or antibodies that can block inhibitory interactions between cancer cells and the immune cells. The latest molecular studies focusing on treatment-mediated changes within TME have also examined the potential of chemotherapies and radiotherapy to induce immunogenic changes within TME. (59, 71, 72, 78). These studies were important to fine-tune doses and timing to open avenues to combine traditional treatments with modern immunotherapies, achieving objective treatment responses against cancer and providing longer survival to patients with fewer side effects. These

encouraging results have put immunotherapies in the limelight, leading to the initiation of thousands of clinical trials for different types of primary cancer and their associated cancers. In this study, we have taken a similar approach to develop PM-specific treatment as shown above. Furthermore, we are hoping that in the near future, each PM patient can be treated systemically by our proposed drug combinations with and without the addition of immunotherapies, translating to longer survival of PM patients.

6. Figures and Tables

Figure #	Name and Source
Figure 1	Pie chart of incidence and death for top ten most common cancer in males and females Source: (2)
Figure 2	Most recent version of Hallmarks of Cancer Source: (8)
Figure 3	The adenoma-carcinoma sequence of sporadic or serrated CRC Source: (6)
Figure 4	Illustration of cancer immunoediting hypothesis of the “three E’s” Source: (9)
Figure 5	Immunogenic cell death overview Source: (4)
Figure 6	Sugarbaker’s peritoneal cancer index Source: (3)
Figure 7	Comparison local application of chemotherapy. HIPEC vs. PIPAC Source: (10)
Figure 8	DNA damage response pathways Source: (7)
Figure 9	Composition WRN Medium received from C.Pauli, Department of Pathology and molecular Pathology USZ
Figure 10	Drug screening on human CRC cell lines HT29 and HCT8 Generated with GraphPad Prism
Figure 11	Exploration of combination drug screening Oxaliplatin + small molecule inhibitors Generated with GraphPad Prism
Figure 12	Enhanced cytotoxicity of Oxaliplatin in combination with ATRi on different human CRC cell lines Generated with GraphPad Prism
Figure 13	Enhanced cytotoxicity of Oxaliplatin in combination with ATRi on patient-derived PM organoids Generated with GraphPad Prism
Figure 14	Analysis of DNA damage caused by Oxaliplatin and disrupted ATR-CHK1 Pathway by ATRi Generated with GraphPad Prism
Figure 15	Immunogenic changes on CRC cell lines after treatments Generated with GraphPad Prism and FlowJo
Figure 16	Immunogenic alterations in patient-derived organoids Generated with GraphPad Prism
Figure 17	Modulation of PD-L1 expression on murine CRC cell line MC38 Generated with GraphPad Prism
Figure 18	CD8+ T-cell specific killing after treatments Generated with GraphPad Prism
Figure 19	PM mouse model Own picture and PCI calculation from Literature(1)
Figure 20	Treatment of PM lesions in a mouse model
Figure 21	Immune cell composition of PM lesions after treatment Generated with GraphPad Prism and FlowJo
Figure 22	CD8+ T-cell characterization after treatment Generated with GraphPad Prism and FlowJo
Figure 23	CD8+ T-cells are crucial to control PM tumor Generated with GraphPad Prism
Figure 24	CD8+ T-cell effector function after long treatment exposure Generated with GraphPad Prism
Figure 25	Immune cell composition and characterization after short treatment exposure Generated with GraphPad Prism, FlowJo and HALO
Figure 26	ATRi downregulates PD-L1 expression in vivo Generated with GraphPad Prism, FlowJo and QuPath
Figure 27	PD-1 blocking antibody strongly reduces PM tumor load Generated with GraphPad Prism

Table #	Name and Source
Table 1	Examples of Cancer Subtypes Adapted from The Biology of Cancer Source:(5)
Table 2	List of small molecule Inhibitors used in this study
Table 3	List of all drugs used in this study
Table 4	List of Antibody used in this study (for Flow cytometry, Western Blot and Immunostaining)
Table 5	Overview of tested human CRC cell lines to validate enhanced cytotoxicity of Oxaliplatin + ATRi treatment Sources; (22, 85-87)
Table 6	Overview of patient-derived PM organoids Information received from C.Pauli, Department of Pathology and molecular Pathology USZ. Own microscope imaging.

7. References

1. Derrien A, Gouard S, Maurel C, Gaugler MH, Bruchertseifer F, Morgenstern A, et al. Therapeutic Efficacy of Alpha-RIT Using a (213)Bi-Anti-hCD138 Antibody in a Mouse Model of Ovarian Peritoneal Carcinomatosis. *Front Med (Lausanne)*. 2015;2:88.
2. Sung H, Ferlay J, Siegel RL, Laversanne M, Soerjomataram I, Jemal A, Bray F. Global Cancer Statistics 2020: GLOBOCAN Estimates of Incidence and Mortality Worldwide for 36 Cancers in 185 Countries. *CA Cancer J Clin*. 2021;71(3):209-49.
3. Leimkuhler M, de Haas RJ, Pol VEH, Hemmer PHJ, Been LB, van Ginkel RJ, et al. Adding diagnostic laparoscopy to computed tomography for the evaluation of peritoneal metastases in patients with colorectal cancer: A retrospective cohort study. *Surg Oncol*. 2020;33:135-40.
4. Galluzzi L, Buque A, Kepp O, Zitvogel L, Kroemer G. Immunogenic cell death in cancer and infectious disease. *Nat Rev Immunol*. 2017;17(2):97-111.
5. Weinberg RA. *The biology of Cancer*. second edition ed. New York: W.W. Norton & Company; 2014.
6. Unnati Bhalerao AB, Suryabhan Bhalerao, Manjita Srivastava, Meenakshi Singh, Sai Tejaswi Lavuri, Muneesh Kumar Barman, Ananth Prasad Burada, Subash C. Sonkar & Prudhvi Lal Bhukya Diagnosis of Colorectal Cancer Using Molecular Techniques. *Colon Cancer Diagnosis and Therapy: Springer Link*; 2021. p. 143-70.
7. Huhn D, Bolck HA, Sartori AA. Targeting DNA double-strand break signalling and repair: recent advances in cancer therapy. *Swiss Med Wkly*. 2013;143:w13837.
8. Hanahan D. Hallmarks of Cancer: New Dimensions. *Cancer Discov*. 2022;12(1):31-46.
9. Lasek W. Cancer immunoediting hypothesis: history, clinical implications and controversies. *Cent Eur J Immunol*. 2022;47(2):168-74.
10. de Jong LAW, van Erp NP, Bijelic L. Pressurized Intraperitoneal Aerosol Chemotherapy: The Road from Promise to Proof. *Clin Cancer Res*. 2021;27(7):1830-2.
11. Mattiuzzi C, Lippi G. Current Cancer Epidemiology. *J Epidemiol Glob Health*. 2019;9(4):217-22.
12. Hanahan D, Weinberg RA. Hallmarks of cancer: the next generation. *Cell*. 2011;144(5):646-74.
13. Bruce Albert AJ, Julian Lewis, David Morgan, Martin Raff, Keith Roberts, Peter Walter. *Molecular Biology of the Cell*. 6th ed: W.W. Norton & Company; 2015.
14. Dekker E, Tanis PJ, Vleugels JLA, Kasi PM, Wallace MB. Colorectal cancer. *Lancet*. 2019;394(10207):1467-80.
15. Li J, Ma X, Chakravarti D, Shalapour S, DePinho RA. Genetic and biological hallmarks of colorectal cancer. *Genes Dev*. 2021;35(11-12):787-820.
16. Siegel RL, Miller KD, Fedewa SA, Ahnen DJ, Meester RGS, Barzi A, Jemal A. Colorectal cancer statistics, 2017. *CA Cancer J Clin*. 2017;67(3):177-93.
17. Fearon ER, Vogelstein B. A genetic model for colorectal tumorigenesis. *Cell*. 1990;61(5):759-67.
18. La Vecchia S, Sebastian C. Metabolic pathways regulating colorectal cancer initiation and progression. *Semin Cell Dev Biol*. 2020;98:63-70.
19. Currais P, Rosa I, Claro I. Colorectal cancer carcinogenesis: From bench to bedside. *World J Gastrointest Oncol*. 2022;14(3):654-63.
20. Hampel H, Kalady MF, Pearlman R, Stanich PP. Hereditary Colorectal Cancer. *Hematol Oncol Clin North Am*. 2022;36(3):429-47.
21. Guinney J, Dienstmann R, Wang X, de Reynies A, Schlicker A, Soneson C, et al. The consensus molecular subtypes of colorectal cancer. *Nat Med*. 2015;21(11):1350-6.
22. Lenos KJ, Bach S, Ferreira Moreno L, Ten Hoorn S, Sluiter NR, Bootsma S, et al. Molecular characterization of colorectal cancer related peritoneal metastatic disease. *Nat Commun*. 2022;13(1):4443.
23. Kenneth Murphy CW. *Janeway's Immuno Biology*. 9th ed: Garland Science; 2017.
24. Dunn GP, Old LJ, Schreiber RD. The three Es of cancer immunoediting. *Annu Rev Immunol*. 2004;22:329-60.
25. Kroemer G, Galluzzi L, Kepp O, Zitvogel L. Immunogenic cell death in cancer therapy. *Annu Rev Immunol*. 2013;31:51-72.
26. Kroemer G, Galassi C, Zitvogel L, Galluzzi L. Immunogenic cell stress and death. *Nat Immunol*. 2022;23(4):487-500.
27. Blank CU, Haining WN, Held W, Hogan PG, Kallies A, Lugli E, et al. Defining 'T cell exhaustion'. *Nat Rev Immunol*. 2019;19(11):665-74.

28. Dolina JS, Van Braeckel-Budimir N, Thomas GD, Salek-Ardakani S. CD8(+) T Cell Exhaustion in Cancer. *Front Immunol.* 2021;12:715234.
29. Jiang Y, Li Y, Zhu B. T-cell exhaustion in the tumor microenvironment. *Cell Death Dis.* 2015;6(6):e1792.
30. Pretzsch E, Bosch F, Neumann J, Ganschow P, Bazhin A, Guba M, et al. Mechanisms of Metastasis in Colorectal Cancer and Metastatic Organotropism: Hematogenous versus Peritoneal Spread. *J Oncol.* 2019;2019:7407190.
31. Tracey A, Martin LY, Andrew J, Sanders, Jane Lane, and Wen G. Jiang. *Cancer Invasion and Metastasis: Molecular and Cellular Perspective.* NBK164700 BI, editor: Landes Bioscience 2013.
32. Vassos N, Piso P. Metastatic Colorectal Cancer to the Peritoneum: Current Treatment Options. *Curr Treat Options Oncol.* 2018;19(10):49.
33. Breuer E, Hebeisen M, Schneider MA, Roth L, Pauli C, Frischer-Ordu K, et al. Site of Recurrence and Survival After Surgery for Colorectal Peritoneal Metastasis. *J Natl Cancer Inst.* 2021;113(8):1027-35.
34. Mikula-Pietrasik J, Uruski P, Tykarski A, Ksiazek K. The peritoneal "soil" for a cancerous "seed": a comprehensive review of the pathogenesis of intraperitoneal cancer metastases. *Cell Mol Life Sci.* 2018;75(3):509-25.
35. Zajac O, Raingeaud J, Libanje F, Lefebvre C, Sabino D, Martins I, et al. Tumour spheres with inverted polarity drive the formation of peritoneal metastases in patients with hypermethylated colorectal carcinomas. *Nat Cell Biol.* 2018;20(3):296-306.
36. Ceelen W, Ramsay RG, Narasimhan V, Heriot AG, De Wever O. Targeting the Tumor Microenvironment in Colorectal Peritoneal Metastases. *Trends Cancer.* 2020;6(3):236-46.
37. Roth L, Russo L, Ulugoel S, Freire Dos Santos R, Breuer E, Gupta A, Lehmann K. Peritoneal Metastasis: Current Status and Treatment Options. *Cancers (Basel).* 2021;14(1).
38. Laoukili J, Constantinides A, Wassenaar ECE, Elias SG, Raats DAE, van Schelven SJ, et al. Peritoneal metastases from colorectal cancer belong to Consensus Molecular Subtype 4 and are sensitised to oxaliplatin by inhibiting reducing capacity. *Br J Cancer.* 2022;126(12):1824-33.
39. Bhat AA, Nisar S, Singh M, Ashraf B, Masoodi T, Prasad CP, et al. Cytokine- and chemokine-induced inflammatory colorectal tumor microenvironment: Emerging avenue for targeted therapy. *Cancer Commun (Lond).* 2022;42(8):689-715.
40. Janssen E, Subtil B, de la Jara Ortiz F, Verheul HMW, Tauriello DVF. Combinatorial Immunotherapies for Metastatic Colorectal Cancer. *Cancers (Basel).* 2020;12(7).
41. Foster JM, Zhang C, Rehman S, Sharma P, Alexander HR. The contemporary management of peritoneal metastasis: A journey from the cold past of treatment futility to a warm present and a bright future. *CA Cancer J Clin.* 2023;73(1):49-71.
42. Sugarbaker PH. Peritonectomy procedures. *Surg Oncol Clin N Am.* 2003;12(3):703-27, xiii.
43. Franko J, Ibrahim Z, Gusani NJ, Holtzman MP, Bartlett DL, Zeh HJ, 3rd. Cytoreductive surgery and hyperthermic intraperitoneal chemoperfusion versus systemic chemotherapy alone for colorectal peritoneal carcinomatosis. *Cancer.* 2010;116(16):3756-62.
44. Glehen O, Mohamed F, Gilly FN. Peritoneal carcinomatosis from digestive tract cancer: new management by cytoreductive surgery and intraperitoneal chemohyperthermia. *Lancet Oncol.* 2004;5(4):219-28.
45. Steffen T, Putora PM, Hubner M, Gloor B, Lehmann K, Kettelhack C, et al. Diagnostic Nodes of Patient Selection for Cytoreductive Surgery and Hyperthermic Intraperitoneal Chemotherapy Among Colorectal Cancer Patients: A Swiss National Multicenter Survey. *Clin Colorectal Cancer.* 2019;18(4):e335-e42.
46. Schneider MA, Eshmuminov D, Lehmann K. Major Postoperative Complications Are a Risk Factor for Impaired Survival after CRS/HIPEC. *Ann Surg Oncol.* 2017;24(8):2224-32.
47. Seetharam R, Sood A, Goel S. Oxaliplatin: pre-clinical perspectives on the mechanisms of action, response and resistance. *Ecancermedicallscience.* 2009;3:153.
48. Lin Q, Luo L, Wang H. A New Oxaliplatin Resistance-Related Gene Signature With Strong Predicting Ability in Colon Cancer Identified by Comprehensive Profiling. *Front Oncol.* 2021;11:644956.
49. Chen G, Gong T, Wang Z, Wang Z, Lin X, Chen S, et al. Colorectal cancer organoid models uncover oxaliplatin-resistant mechanisms at single cell resolution. *Cell Oncol (Dordr).* 2022;45(6):1155-67.
50. Van der Speeten K, Lemoine L, Sugarbaker P. Overview of the optimal perioperative intraperitoneal chemotherapy regimens used in current clinical practice. *Pleura Peritoneum.* 2017;2(2):63-72.

51. Shimizu T, Murata S, Sonoda H, Mekata E, Ohta H, Takebayashi K, et al. Hyperthermic intraperitoneal chemotherapy with mitomycin C and 5-fluorouracil in patients at high risk of peritoneal metastasis from colorectal cancer: A preliminary clinical study. *Mol Clin Oncol.* 2014;2(3):399-404.
52. Thorn CF, Oshiro C, Marsh S, Hernandez-Boussard T, McLeod H, Klein TE, Altman RB. Doxorubicin pathways: pharmacodynamics and adverse effects. *Pharmacogenet Genomics.* 2011;21(7):440-6.
53. Quenet F, Elias D, Roca L, Goere D, Ghouti L, Pocard M, et al. Cytoreductive surgery plus hyperthermic intraperitoneal chemotherapy versus cytoreductive surgery alone for colorectal peritoneal metastases (PRODIGE 7): a multicentre, randomised, open-label, phase 3 trial. *Lancet Oncol.* 2021;22(2):256-66.
54. Verwaal VJ, van Ruth S, de Bree E, van Sloothen GW, van Tinteren H, Boot H, Zoetmulder FA. Randomized trial of cytoreduction and hyperthermic intraperitoneal chemotherapy versus systemic chemotherapy and palliative surgery in patients with peritoneal carcinomatosis of colorectal cancer. *J Clin Oncol.* 2003;21(20):3737-43.
55. Verwaal VJ, Bruin S, Boot H, van Slooten G, van Tinteren H. 8-year follow-up of randomized trial: cytoreduction and hyperthermic intraperitoneal chemotherapy versus systemic chemotherapy in patients with peritoneal carcinomatosis of colorectal cancer. *Ann Surg Oncol.* 2008;15(9):2426-32.
56. Demtroder C, Solass W, Zieren J, Strumberg D, Giger-Pabst U, Reymond MA. Pressurized intraperitoneal aerosol chemotherapy with oxaliplatin in colorectal peritoneal metastasis. *Colorectal Dis.* 2016;18(4):364-71.
57. Alyami M, Mercier F, Siebert M, Bonnot PE, Laplace N, Villeneuve L, et al. Unresectable peritoneal metastasis treated by pressurized intraperitoneal aerosol chemotherapy (PIPAC) leading to cytoreductive surgery and hyperthermic intraperitoneal chemotherapy. *Eur J Surg Oncol.* 2021;47(1):128-33.
58. Vierra MA, Morgan RB, Eng OS. Advances in therapeutics for peritoneal metastases from colorectal cancer: a narrative review. *Digestive Medicine Research.* 2022;5.
59. Ornella MSC, Badrinath N, Kim KA, Kim JH, Cho E, Hwang TH, Kim JJ. Immunotherapy for Peritoneal Carcinomatosis: Challenges and Prospective Outcomes. *Cancers (Basel).* 2023;15(8).
60. Yap TA, Tan DSP, Terbuch A, Caldwell R, Guo C, Goh BC, et al. First-in-Human Trial of the Oral Ataxia Telangiectasia and RAD3-Related (ATR) Inhibitor BAY 1895344 in Patients with Advanced Solid Tumors. *Cancer Discov.* 2021;11(1):80-91.
61. Waqar SN, Robinson C, Olszanski AJ, Spira A, Hackmaster M, Lucas L, et al. Phase I trial of ATM inhibitor M3541 in combination with palliative radiotherapy in patients with solid tumors. *Invest New Drugs.* 2022;40(3):596-605.
62. Kristeleit R, Plummer R, Jones R, Carter L, Blagden S, Sarker D, et al. A Phase 1/2 trial of SRA737 (a Chk1 inhibitor) administered orally in patients with advanced cancer. *Br J Cancer.* 2023;129(1):38-45.
63. Poveda A, Floquet A, Ledermann JA, Asher R, Penson RT, Oza AM, et al. Olaparib tablets as maintenance therapy in patients with platinum-sensitive relapsed ovarian cancer and a BRCA1/2 mutation (SOLO2/ENGOT-Ov21): a final analysis of a double-blind, randomised, placebo-controlled, phase 3 trial. *Lancet Oncol.* 2021;22(5):620-31.
64. Kirouac DC, Schaefer G, Chan J, Merchant M, Orr C, Huang SA, et al. Clinical responses to ERK inhibition in BRAF(V600E)-mutant colorectal cancer predicted using a computational model. *NPJ Syst Biol Appl.* 2017;3:14.
65. Tian J, Chen JH, Chao SX, Pelka K, Giannakis M, Hess J, et al. Combined PD-1, BRAF and MEK inhibition in BRAF(V600E) colorectal cancer: a phase 2 trial. *Nat Med.* 2023;29(2):458-66.
66. Tan L, Tran B, Tie J, Markman B, Ananda S, Tebbutt NC, et al. A Phase Ib/II Trial of Combined BRAF and EGFR Inhibition in BRAF V600E Positive Metastatic Colorectal Cancer and Other Cancers: The EVICT (Erlotinib and Vemurafenib In Combination Trial) Study. *Clin Cancer Res.* 2023;29(6):1017-30.
67. Samalin E, Fouchardiere C, Thezenas S, Boige V, Senellart H, Guimbaud R, et al. Sorafenib Plus Irinotecan Combination in Patients With RAS-mutated Metastatic Colorectal Cancer Refractory To Standard Combined Chemotherapies: A Multicenter, Randomized Phase 2 Trial (NEXIRI-2/PRODIGE 27). *Clin Colorectal Cancer.* 2020;19(4):301-10 e1.
68. Brady J, Corrie P, Chau I, Digumarti R, Adams LM, Botbyl J, et al. An open-label study of the safety and tolerability of pazopanib in combination with FOLFOX6 or CapeOx in patients with colorectal cancer. *Invest New Drugs.* 2013;31(5):1228-35.
69. Yano K, Shiotani B. Emerging strategies for cancer therapy by ATR inhibitors. *Cancer Sci.* 2023;114(7):2709-21.

70. Karnitz LM, Zou L. Molecular Pathways: Targeting ATR in Cancer Therapy. *Clin Cancer Res.* 2015;21(21):4780-5.
71. Combes E, Andrade AF, Tosi D, Michaud HA, Coquel F, Garambois V, et al. Inhibition of Ataxia-Telangiectasia Mutated and RAD3-Related (ATR) Overcomes Oxaliplatin Resistance and Promotes Antitumor Immunity in Colorectal Cancer. *Cancer Res.* 2019;79(11):2933-46.
72. Sato H, Niimi A, Yasuhara T, Permata TBM, Hagiwara Y, Isono M, et al. DNA double-strand break repair pathway regulates PD-L1 expression in cancer cells. *Nat Commun.* 2017;8(1):1751.
73. Kranenburg O, van der Speeten K, de Hingh I. Peritoneal Metastases From Colorectal Cancer: Defining and Addressing the Challenges. *Front Oncol.* 2021;11:650098.
74. Lemoine L, Sugarbaker P, Van der Speeten K. Pathophysiology of colorectal peritoneal carcinomatosis: Role of the peritoneum. *World J Gastroenterol.* 2016;22(34):7692-707.
75. Seebauer CT, Brunner S, Glockzin G, Piso P, Ruesmeyer P, Schlitt HJ, et al. Peritoneal carcinomatosis of colorectal cancer is characterized by structural and functional reorganization of the tumor microenvironment inducing senescence and proliferation arrest in cancer cells. *Oncoimmunology.* 2016;5(12):e1242543.
76. Gandini A, Puglisi S, Pirrone C, Martelli V, Catalano F, Nardin S, et al. The role of immunotherapy in microsatellites stable metastatic colorectal cancer: state of the art and future perspectives. *Front Oncol.* 2023;13:1161048.
77. Zhang X, Wu T, Cai X, Dong J, Xia C, Zhou Y, et al. Neoadjuvant Immunotherapy for MSI-H/dMMR Locally Advanced Colorectal Cancer: New Strategies and Unveiled Opportunities. *Front Immunol.* 2022;13:795972.
78. Liu C, Wang X, Qin W, Tu J, Li C, Zhao W, et al. Combining radiation and the ATR inhibitor berzosertib activates STING signaling and enhances immunotherapy via inhibiting SHP1 function in colorectal cancer. *Cancer Commun (Lond).* 2023;43(4):435-54.
79. Ros J, Balconi F, Baraibar I, Saoudi Gonzalez N, Salva F, Tabernero J, Elez E. Advances in immune checkpoint inhibitor combination strategies for microsatellite stable colorectal cancer. *Front Oncol.* 2023;13:1112276.
80. Barnieh FM, Loadman PM, Falconer RA. Progress towards a clinically-successful ATR inhibitor for cancer therapy. *Curr Res Pharmacol Drug Discov.* 2021;2:100017.
81. Eek Mariampillai A, Hauge S, Kongsrud K, Syljuasen RG. Immunogenic cell death after combined treatment with radiation and ATR inhibitors is dually regulated by apoptotic caspases. *Front Immunol.* 2023;14:1138920.
82. Sheng H, Huang Y, Xiao Y, Zhu Z, Shen M, Zhou P, et al. ATR inhibitor AZD6738 enhances the antitumor activity of radiotherapy and immune checkpoint inhibitors by potentiating the tumor immune microenvironment in hepatocellular carcinoma. *J Immunother Cancer.* 2020;8(1).
83. Dennison L, Mohan AA, Yarchoan M. Tumor and Systemic Immunomodulatory Effects of MEK Inhibition. *Curr Oncol Rep.* 2021;23(2):23.
84. Wang W, Wu L, Zhang J, Wu H, Han E, Guo Q. Chemoimmunotherapy by combining oxaliplatin with immune checkpoint blockades reduced tumor burden in colorectal cancer animal model. *Biochem Biophys Res Commun.* 2017;487(1):1-7.
85. Aldrich S. CRC cell lines Mutations (30.01.2024) [<https://www.sigmaaldrich.com/CH/de/technical-documents/technical-article/research-and-disease-areas/cancer-research/colorectal-cancer-cell-lines>].
86. Berg KCG, Eide PW, Eilertsen IA, Johannessen B, Bruun J, Danielsen SA, et al. Multi-omics of 34 colorectal cancer cell lines - a resource for biomedical studies. *Mol Cancer.* 2017;16(1):116.
87. Cellosaurus. Characterization of LS1034 (30.01.2024) [https://www.cellosaurus.org/CVCL_1382].

8. Acknowledgements

First, I would like to express my deep gratitude to PD Dr. Anurag Gupta for his immense support, the guidance, the patience and being by my side through all up and downs in the past 4 years. You not only taught me how to critically evaluate my scientific work, but also to enjoy successful steps along this journey. I will nostalgically remember all the time spent together inside and outside the lab.

Then my deepest appreciation goes to Dr. med. Kuno Lehmann for the opportunity to pursue my doctoral studies in his lab. During the past 4 years, I experienced great support and encouragement from his side. I am grateful for all the inputs from a more clinical/medical side that perfectly completed my studies in the lab.

Moreover, I would like to acknowledge my thesis committee, Prof. Dr. Maries van den Broek, Prof. Dr. Lubor Borsig and Prof. Dr. med. Michael Scharl for the thoughtful advices, right guidance and support during the course of this PhD thesis.

Special thanks goes also to Lilian Roth, Sabrina Steiner, Laura Heeb and Sara Da Silva Guerra for the immense support in every possible work and life situation. You truly are the good souls of the lab, I am incredibly happy to have done my PhD in a lab with such a familiar support and I will never forget our long working days in Schlieren. I am looking forward to have you as friend for the rest of my life.

Another special thanks goes to Lea Scherrer and Sima Ulugöl. Thank you, from the bottom of my heart that you have been such fantastic students. You contributed a lot to this project, supported me while I was in Schlieren and it was just a pleasure to work with highly motivated co-workers.

I also want to say thank you to all past and present liver, pancreas and uterus Lab members: Eva, Keyue, Catherine, Leandro, Udo, Ursi, Hemma, Kirstin, Rafael, Severin, Kendra, Matthias, Bostijan, Richard, Daniela, Dominique. It was truly a pleasure to work with you. I will miss our lunch times and exciting discussions.

Furthermore, I would also like to thank Prof. Dr.med. Chantal Pauli for her support to generate and donate patient-derived organoids.

The completion of this project would have not been possible without my wonderful family and friends. I profoundly appreciate my husband Kok Sue Huynh for his support and encouragement during my whole PhD. Without him I am sure, I would not have achieved my goals. Thanks to my family, who was always there to pick me up in difficult times and provide me with an amazing support and food. Thank you for always believing in me.

9. Curriculum vitae

Name: Linda Huynh-Russo

Date of birth: 22.02.1993

Nationality: Swiss

Education:

07.2019 – today	PhD in Cancer Biology Life Science Zurich Graduate School, UZH University Hospital Zurich, Surgery- und Transplantation Department
09.2017 – 04.2019	Master of Science in Cancer Biology University Zurich, Switzerland
09.2014 – 09.2017	Bachelor of Science in Biology University Zurich, Switzerland
09.2016 – 02.2017	Erasmus , semester abroad University of Aberdeen, Scotland
08.2011 – 07.2014	KME (Kantonale Maturitätsschule für Erwachsene) Zurich
08.2008 – 07.2011	Apprenticeship as Pharma-Assistant Bahnhof Apotheke Schaffhausen, Switzerland

Scientific Activities:

2023:	20th Hepatobiliary and Gastrointestinal Research Retreat Grindelwald, Switzerland (oral presentation) 18th Day of clinical research Zurich, Switzerland (poster presentation) 10th Cancer Biology PhD Program Student's Retreat Locarno, Switzerland (oral presentation)
2022:	Cell Symposia: Hallmarks of Cancer Elsevier Conference, San Diego, USA (poster presentation) 9th Cancer Biology PhD Program Student's Retreat Interlaken, Switzerland (poster presentation)
2021:	8th Cancer Biology PhD Program Student's Retreat online, Switzerland (poster presentation)
2020:	19th Hepatobiliary and Gastrointestinal Research Retreat Pontresina, Switzerland (oral presentation)

Publications:

Roth L, **Russo L**, Ulugoel S, Freire Dos Santos R, Breuer E, Gupta A, Lehmann K. Peritoneal Metastasis: Current Status and Treatment Options. *Cancers (Basel)*. 2021 Dec 23;14(1):60. doi: 10.3390/cancers14010060. PMID: 35008221

Capdeville C, **Russo L**, Penton D, Migliavacca J, Zecevic M, Gries A, Neuhauss SC, Grotzer MA, Baumgartner M. Spatial proteomics finds CD155 and Endophilin-A1 as mediators of growth and invasion in medulloblastoma. *Life Sci Alliance*. 2022 Mar 16;5(6):e202201380. doi: 10.26508/lsa.202201380. PMID: 35296518

Roth L, Eshmuminov D, **Russo L**, Laminger F, Kober F, Roka S, Lehmann K. Serum procalcitonin improves diagnosis of infectious complications after CRS/HIPEC. *World J Surg Oncol*. 2023 Jan 12;21(1):5. doi: 10.1186/s12957-022-02884-9. PMID: 36631814; PMCID: PMC9835368.

Roth L., **Russo L.**, Heeb L., Ulugöl S., Freire Dos Santos R., Breuer E., Ungethüm U., Haberecker M., Paul C., Clavien P., Koelzer V., Gupta A., Lehmann K. CD8+ T-cells restrict the development of peritoneal metastasis and support the efficacy of hyperthermic intraperitoneal chemotherapy (HIPEC). (In revision Nature Communications)